CHARACTERIZATION OF CROSSLINKED ARTIFICIAL PROTEIN FILMS

Thesis by

Paul Nowatzki

In partial fulfillment of the requirements

for the degree of

Doctor of Philosophy

CALIFORNIA INSTITUTE OF TECHNOLOGY

Pasadena, California

2006

(Defended January 10, 2006)

Acknowledgements

I would foremost like to thank my advisor, Professor David Tirrell, for giving me the opportunity to work in his laboratory, and for his direction and mentorship. His breadth of knowledge, depth of insight, and impeccable character are truly remarkable; I like to think a little of each has rubbed off on me.

Thanks also to the members of my thesis committee, Professors Mark Davis, Julie Kornfield, and G. Ravichandran, for their time, comments, and advice. Ravi has been particularly helpful in focusing our thoughts in the thin film studies.

I am grateful to Christian Franck, whose optimism and persistence on the AFM project was crucial to its success. I also very much appreciate Sarah Heilshorn's spearheading the elastase degradation project.

I want to acknowledge the support of my parents and their dedication to my education. My awesome wife Courtney helped me keep things in perspective. Finally, I thank Tirrell lab members past and present for their help; the positive environment in the group has helped make Caltech a very pleasant place to be.

CHARACTERIZATION OF CROSSLINKED ARTIFICIAL PROTEIN FILMS

January 2006

Paul Nowatzki, B.Ch.E., University of Minnesota—Twin Cities

Ph.D., California Institute of Technology

Supervised by David Tirrell

Abstract

Genetically engineered artificial proteins are promising candidates for new biomaterials because their amino acid sequences can be precisely controlled. This work describes the characterization of crosslinked films of biomimetic artificial extracellular matrix (aECM) proteins with hybrid functions designed to meet materials needs in applications such as small diameter vascular grafts and corneal tissue implants. Elastin-derived polypeptides give the proteins flexibility, while RGD and CS5 peptide domains from fibronectin serve to adhere cells.

Techniques were sought to crosslink aECM proteins in ways that resulted in tunable mechanical properties. Hexamethylene diisocyanate was used to crosslink aECM proteins into uniform, transparent, highly-extensible hydrogel films with low water contents characteristic of native elastin. Their elastic moduli, 0.1 – 1.1 MPa, depended on crosslinker concentration and aECM protein length, and spanned the observed range of elastin fibers.

The suitability of biomaterials implants depends strongly on their susceptibility to proteolytic degradation *in vivo*. It was shown that small sequence changes in the elastin-like portion of aECM proteins were sufficient to decrease their rate of degradation by elastase sevenfold, illustrating a simple method to tune the protease sensitivity of designed proteins. The effects were seen in both soluble proteins and crosslinked films analyzed by measuring their decrease in elastic modulus during degradation.

An aECM protein was examined for its effectiveness as a corneal onlay, or permanent contact lens. The protein was crosslinked into transparent, elastic, water-rich lenses and was implanted into rabbit corneas. The onlays were stable and well-tolerated, and full re-epithelialization occurred within 4-7 days. Histological examination revealed normal regenerating epithelial cell morphology on the anterior surface, good interfaces between the onlay and surrounding tissue, and only minimal inflammation.

To create substrates for studying the coordinating effects of mechanical and biological signals on cell behavior, thin films were made from a photoreactive aECM protein containing the non-canonical amino acid *para*-azidophenylalanine. Atomic force microscopy (AFM) nanoindentation was used to calculate elastic modulus, and the technique was confirmed by bulk tensile measurements and finite element simulations. Film modulus could be tuned either by differential irradiation or variable incorporation of *para*-azidophenylalanine.

Table of Contents

List of Figures and Tables

1 INTRODUCTION

1.1 Artificial proteins: definition and background

Genetic engineering technologies have proven extremely useful to biologists. The development of recombinant DNA techniques in the 1970s[1] made it possible to copy genetic material from one organism and insert it into another. While a valuable tool for studying fundamental biology, this also had immediate commercial applications, allowing human proteins like insulin and erythropoietin to be synthesized in large quantities in bacterial cells, improving the shelf-life and pest resistance of crops, and facilitating the production of new vaccines.[2]

Combined with the ability to sequence long pieces of DNA base-pair by base-pair, genetic engineering is even more powerful, since it allows peptides and proteins of nearly any imaginable sequence of natural amino acids to be synthesized in a host organism, such as *E. coli*. These a*rtificial proteins* (also *designed* or *engineered proteins*), made by genetic engineering to include non-natural amino acid sequences, are attractive candidates for creating new materials.[3] Their sequences can be controlled completely, a distinct advantage over synthetic polymers where control is restricted to block, random, or alternating copolymers. Another advantage is their uniformity of chain length, compared with traditional polymer materials that always display some diversity of molecular weight.

The incorporation of modular, repeating structures in artificial proteins can be used to achieve the desirable physical properties characteristic of synthetic polymers, or entirely new features. Early examples of distinctive architectures enabled by protein polymers include β-sheet structures in which the lamellar thickness was controlled by the sequence periodicity,[4] smectic liquid crystal phases of stiff helical rods with uniform molecular weight,[5] and hydrogels that reversibly converted to viscous liquids with pH and temperature changes.[6] Alternatively, artificial proteins may be based on structural proteins like silk.[7] While the scope of properties displayed by natural proteins is large, ranging from collagenous gels of vitreous humor with storage shear modulus of less than 30 Pa[8] to spider silks with elastic modulus 16 GPa,[9] all use the same amide-bond backbone and must be composed from the set of 20 natural amino acid monomers. The chemical diversity of artificial proteins, on the other hand, may be increased with techniques to incorporate non-canonical amino acids.[10,11]

1.2 Artificial proteins as biomaterials

Artificial proteins seem particularly well suited to be used as implantable biomaterials, where the magnitude of potential benefits is large and the amount of material required is often modest. Proteins have the potential to interact intimately with surrounding tissue and promote normal wound healing, whereas metals or synthetic polymers elicit a foreign body reaction when implanted, in which the material is isolated from the body by a fibrous capsule and inflammation persists in the surrounding tissue.[12,13]

More importantly, artificial proteins can be *bioactive*, containing peptide domains from natural proteins that are known to elicit specific biological reactions, such as promoting the adhesion of a particular cell type. In principle, chimeric and engineered artificial proteins could exhibit any combination of the diverse functions of natural proteins including catalysis, binding, signaling, and transport. The ability to hybridize multiple functions in a single protein is a distinct advantage over traditional techniques that require chemical modifications to make materials biocompatible or bioactive. A disadvantage is that certain artificial protein sequences may be immunogenic or may be expressed in low yield in host organisms.

1.3 Applications

Artificial proteins can be made to have both desirable mechanical and biological properties, so they may be attractive candidates for use in the full range of biomaterials applications, from rigid and permanent, like bone implants,[14,15] to soft and degradable, like hydrogels that promote wound healing.[16] For the promise of artificial proteins to be fulfilled, the effects of sequence and architecture on their physical properties must be better understood.

The original and primary focus of our group's research into bioactive artificial proteins has been in devising new materials for vascular grafts. The quest for an effective synthetic blood vessel reaches back decades, but success has been limited.[17,18] Especially challenging from a clinical perspective are small

diameter (< 5 mm) vascular grafts that are indicated, for example, to replace the major peripheral arteries that supply the legs and arms. The preferred surgical approach to replace an occluded or diseased peripheral artery is to use a similar-diameter vein harvested from the same patient, but the supply and quality of appropriate veins is limited. Commonly used synthetics, expanded polytetrafluoroethylene (ePTFE / "Gore-Tex") and woven poly-ethylene terephthalate ("Dacron"), work reasonably well for large diameter vascular grafts (> 5 mm), but fail at small diameters.[18-20]

The reasons synthetic polymer grafts fail are thought to be twofold. One, they do not support the regeneration or maintenance of endothelial cells, which coat all mammalian blood vessels and are essential for their health.[21] Two, the rigidity of synthetic polymer grafts, which distend roughly 1% during a blood pressure cycle versus ~10% for native vessels, causes abnormal shear stresses and consequent abnormal cellular function. Specifically, smooth muscle cells react by over-proliferation (intimal hyperplasia) and block the synthetic blood vessel over time.[17,22]

Many groups have attempted to design functional small diameter vascular grafts, typically addressing either the mechanical or biological needs of such materials.[18,23] Compliant grafts have been made from elastomeric synthetic polymers like polyurethane,[24,25] while efforts to support an endothelial cell monolayer have included pre-seeding of existing synthetic grafts,[26,27] modifying the surface properties by plasma treatment,[28] or adsorption of bioadhesive molecules like fibronectin.[29] Several biofunctionalized polyurethane graft

designs have been made[30-32] in an attempt to address both biological and mechanical requirements. Tissue engineering may eventually produce working blood vessels,[33-35] although the techniques are costly, and matching the mechanical properties of native tissue will require considerable development. Our group envisions hybrid artificial proteins that effect both blood vessel-like flexibility and the ability to adhere endothelial cells in a single material.

More recently, we have investigated using artificial proteins of the type originally designed for vascular grafts in other biomaterials applications. One possibility is to use flexible, signal-bearing artificial proteins to direct stem cell fate in neurorestorative implants.[36] Synthetic corneal onlays, a reversible alternative to ablative refractive vision surgeries such as LASIK, are another possible application. While this is a more recent challenge in biomaterials engineering, similar issues have arisen as with polymeric vascular grafts. Synthetic materials do not promote the adhesion of the epithelial cells necessary to maintain the biology of the cornea,[37] while the complexity of adapted biological materials like collagen lead to immune reactions and abnormal cell growth.[38] There is a need for transparent, stable, elastic materials that adhere epithelial cells, and artificial proteins of the type designed for use in vascular grafts appear well-suited to this application.

1.4 Design strategy

The research described in this thesis is based on a family of artificial proteins with a common design. Their architecture is analogous to block

copolymers, with cell-binding peptide domains alternating with larger flexible domains that govern the mechanical properties (Figure 1). Both domains are biomimetic: the cell-binding domains are cloned from portions of the human protein fibronectin, which adheres to a wide range of integrin cell-surface receptors and extracellular matrix molecules, and the flexible domain is derived from mammalian elastin, which is a large component of mechanically responsive tissues like skin, tendons, and blood vessels. Because these proteins capture key features of the extracellular matrix, we refer to them as artificial extracellular matrix proteins ("aECM" or "aE").

One cell-binding domain engineered into the artificial proteins is RGD (Arg-Gly-Asp), from the tenth type III module of fibronectin, which mediates adhesion to a variety of cell types through several integrin receptors.[39] Its prolific ability to adhere cells has brought about its use in dozens of biomaterials.[16,40,41] The other cell-binding domain used here is CS5, from the alternatively spliced type III connecting segment region of fibronectin, which is known to adhere to the integrin $\alpha_4\beta_1$.[42] It was observed that human endothelial cells attach and proliferate on immobilized GREDVY peptides (a portion of the CS5 sequence), while human fibroblasts, smooth muscle cells, and platelets do not,[43] so CS5-bearing proteins may be useful in vascular grafts.[44]

The elastin-like domains contain multimers of pentapetides with sequence $(VPGXG)_n$, where X is any amino acid, extensively studied by Urry et al.[45] These peptides are derived from hydrophobic repeating sequences in mammalian elastin, rich in valine, glycine, proline, and alanine. Crosslinked peptides of this

type replicate many of the mechanical properties of native elastin.[45,46] They display what is known as a lower critical solution temperature (LCST) in water, in which the proteins are soluble at low temperatures, but separate into an aggregated phase when the temperature is raised above their characteristic LSCT.[45]

Despite their ability to aggregate, elastin and elastin-like peptides do not have a well-defined folded three dimensional structure either above or below the LCST; they are rich in β-turn or β-sheet-like secondary structure,[47,48] but are extraordinarily mobile.[49,50] The structure-function relationship of elastin has long been a contentious issue and a subject of considerable research. The classical view is that elastin is like a solvent-swollen rubbery network whose elasticity derives from the architecture of its crosslinks.[49,51,52] However, models of elastin based on crystallographic evidence of closely related molecules[53,54] have induced others to suggest extended secondary-structural motifs which provide an entropic restoring force when distorted under strain.[45,55,56] Neither model can account for all of elastin's observed properties,[57] but recent experiments that examine elastin-like peptides using solid-state NMR[58,59] describe the distribution of torsional angles, while molecular simulations[57,60] have pointed out the importance of hydration in controlling elasticity.

Because of their unique thermosensitive behavior, elastin-based peptides have been incorporated into artificial proteins designed for a wide range of materials applications,[61] including soft tissue augmentation,[62] drug delivery,[63,64] immunosorbent assays,[65] tumor cell targeting,[66] nanoporous materials,[67]

switchable-permeability membranes,[68] protein purification,[69] and heavy metal remediation.[70] The well-characterized peptide VPGVG has been shown to be broadly biocompatible in toxicity, antigenicity, pyrogenicity, thrombogenicity, and mutagenicity tests, and does not result in fibrous capsule formation when implanted.[71] In light of these encouraging mechanical and biological properties, our laboratory chose $(VPGIG)_n$ as a structural basis for artificial extracellular matrix proteins. The substitution of isoleucine (I) for valine (V) in the native-like sequence lowers the LCST to near 10 °C[72] and allows the resulting protein to be easily purified by temperature cycling at laboratory conditions.[73]

1.5 Previous results

The first artificial extracellular matrix proteins designed and synthesized by our laboratory (Figure 1.1A) contained alternating CS5 and $(VPGIG)_n$ domains, which promoted the adhesion of endothelial cells when adsorbed to glass.[73] To allow proteins of this type to be chemically crosslinked into insoluble networks, the sequence was modified to include N- and C-terminal lysine residues (Figure 1.1B). At the same time, a T7 antibody recognition tag was appended, as it facilitated identification during purification and increased protein expression levels. This material was chemically crosslinked with glutaraldehyde into stable matrices with tensile properties similar to native elastin.[74] These proteins were also crosslinked with hexamethylene diisocyanate, a less toxic[75] lysine-reactive molecule; mechanical properties and swelling of the resulting matrices are characterized in Chapter 2 of this thesis. When adsorbed

to surfaces, proteins of this type support endothelial cell adhesion at physiologically relevant shear rates.[76]

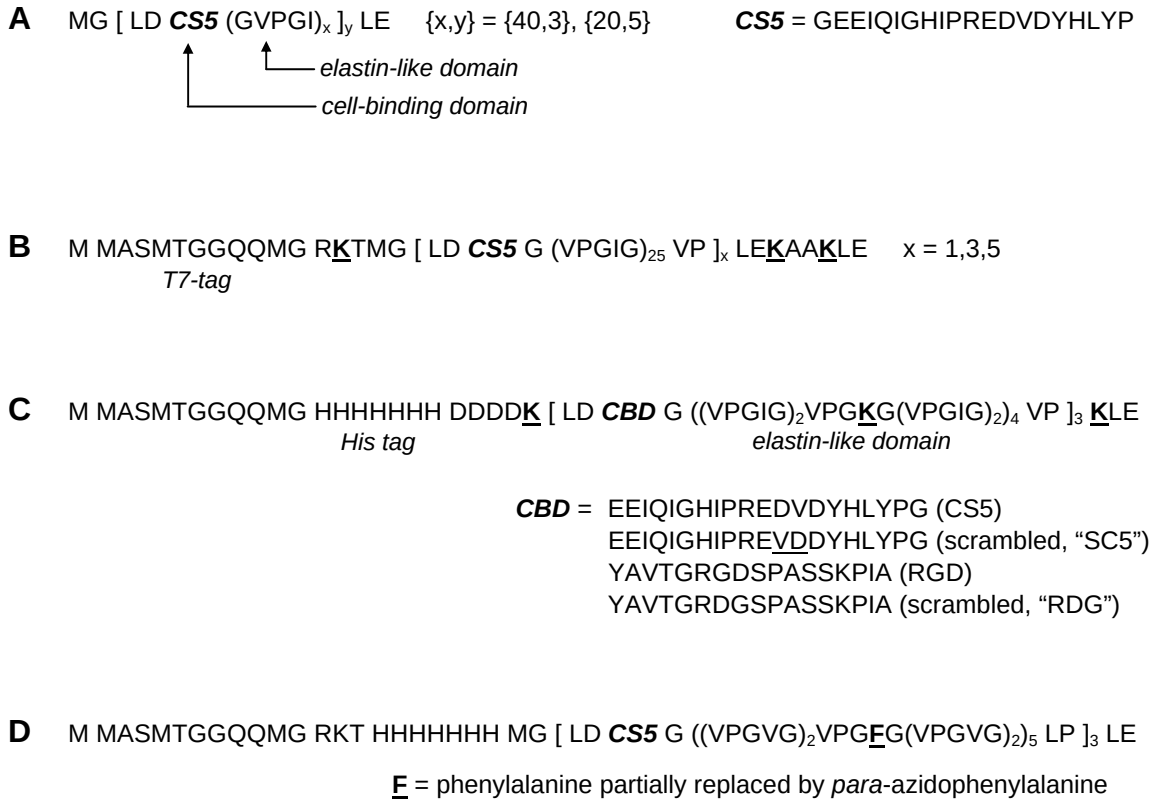

Figure 1.1 Amino acid sequences of artificial extracellular matrix (aECM) proteins, with the functions of component peptides identified. Crosslinked films of (B) are characterized in Chapter 2. Proteolytic degradation of (B) and (C) is studied in Chapter 3. Chapter 4 reports the performance of corneal onlays made from (C) with RGD cell-binding domains. The synthesis and characterization of mechanically tunable thin films of (D) are described in Chapter 5.

The next generation of aECM proteins added two features: one, an increased density of lysine side chains, spaced throughout the elastin portion of

the protein, to facilitate highly lysine-specific crosslinking with using N-hydroxysuccinimidyl esters; two, native and sequence-scrambled versions of the CS5 and RGD cell binding domains, so that the sequence-specificity of cell binding could be demonstrated (Figure 1.1C). Binding of endothelial cells to the CS5 and RGD domains was confirmed.[77] The binding to CS5 appeared to be made less robust by the lysines in the elastin-like domain.[78] Mechanical properties of crosslinked films of these third generation proteins again spanned the desired range.[79] Chapter 3 examines the sequence-dependence of proteolytic degradation of soluble and crosslinked aECM proteins of this (1.1C) and the previous (1.1B) designs. Chapter 4 describes the *in vivo* performance of corneal onlays, permanent contact lenses, made from crosslinked RGD-based aECM proteins of this third type.

A photosensitive aECM protein was also made by incorporating the non-canonical amino acid *para*-azidophenylalanine[80] into phenylalanine sites regularly placed within the elastin-like domains, as were lysines in the chemically crosslinkable protein (Figure 1.1D). The ability to photocrosslink artificial proteins may aid their application as biomaterials, but it also provides opportunities for developing cell culture substrates with patterns of mechanical properties, described in Chapter 5, which can be used to understand mechanosensitive cell behavior. This design was also used as a protein photoresist, allowing cells to be simply and controllably patterned on surfaces; this work is described in the Appendix.

1.6 Thesis organization and description of contributions

This thesis reports progress in developing biomaterials using crosslinked matrices of artificial extracellular matrix (aECM) proteins. I have focused on physical characterizations of these materials, which, along with research in our laboratory into their biological activity, has elucidated important principles for protein-based design and brought the aECM proteins from the drawing board through to implantation in mammals.

A primary objective of this work was to devise crosslinking systems to stabilize the aECM proteins into matrices with elastic properties similar to human blood vessels. Chapter 2 describes the crosslinking of aECM proteins with isocyanate-functional molecules to give highly extensible, uniform hydrogel films whose density and elastic moduli are similar to native elastin. The crosslinker concentration was observed to affect both the modulus and swelling characteristics of the matrices. I wrote this chapter and performed all the experiments.

Another key property of biomaterials implants that must be well understood is their susceptibility to degradation *in vivo*. While elastin in nature has an exceptionally long half-life of tens of years,[62] proteolytic enzymes are up-regulated when tissues are remodeled, e.g., at implantation sites, and the chemical properties of the aECM proteins may affect their degradation in other ways. The susceptibility of two types of aECM proteins, in both soluble and crosslinked form, to elastase degradation is measured in Chapter 3. Small sequence changes to the protein were observed to powerfully affect degradation

rate, a result that will inform the design of future protein-based materials to best fit the materials requirements of their applications. The paper was principally written by Dr. Sarah Heilshorn, a member of our laboratory, who began work on the project in the laboratories of Tetsuji Yamaoka at the Kyoto Institute of Technology. Sarah did all experiments involving soluble proteins, while all the work on crosslinked films was done by me. Specifically, I devised a crosslinking system to match physical properties between the two aECM architectures, characterized their degradation by mechanical testing, and analyzed the results using rubber network assumptions.

The elasticity and cell-binding capabilities of the aECM made them easily adaptable for use as corneal onlays, or permanent contact lenses. Chapter 4 reports *in vivo* testing in rabbit corneas of transparent onlay lenses made by crosslinking aECM proteins containing RGD cell-binding domains. A majority of this chapter was written by me, including the introduction, discussion, and conclusions sections, and the description of the lenses themselves. I made and characterized the lenses, although the aECM protein was originally cloned by Julie Liu and the crosslinking technique was adapted from one developed by Dr. Kathy Di Zio, members of the Tirrell laboratory. The surgeries and *in vivo* characterizations, and their descriptions for the manuscript, were performed at the University of California at San Francisco by Dr. Marsha Cheung and Dr. Daniel Schwartz. Substantial portions of the experimental and results section texts are taken from U.S. Patent Application 11/040,130, by the same authors as the manuscript.

Chapter 5 describes our attempt to fashion systems that can be used to understand cell response to biomaterials with coordinating mechanical and biological signals. Recently, cells have been observed to react to the stiffness of the substrate on which they are characterized.[81-83] We used aECM proteins that incorporate a photoreactive, non-canonical acid to make single films with patterned mechanical properties. The elastic properties of the films were determined with an AFM nanoindentation technique, the validity of which was confirmed by bulk sample measurements and finite element simulations. I wrote the chapter and performed all measurements and analysis it describes, while Christian Franck (Graduate Aeronautics Laboratories, California Institute of Technology) did the finite element modeling and provided substantial expertise and insight throughout. Chapter 5 makes reference to a yet-unpublished paper from our group, which I had a minor role in writing; it is included in an Appendix for convenience.

1.7 References

(1) Watson JD. *Recombinant DNA: A short course*; W. H. Freeman: New York, **1983**.

(2) Zoller M, Watson JD, Gilman M, Witkowski J. *Recombinant DNA*; W. H. Freeman: New York, **1992**.

(3) McGrath KP, Kaplan DL, Eds. *Protein-Based Materials*; Birkhauser: Boston, **1997**.

(4) Krejchi MT, Atkins EDT, Waddon AJ, Fournier MJ, Mason TL, Tirrell DA. Chemical sequence control of beta-sheet assembly in macromolecular crystals of periodic polypeptides. *Science* **1994**, *265*, 1427-1432.

(5) Yu SJM, Conticello VP, Zhang GH, Kayser C, Fournier MJ, Mason TL, Tirrell DA. Smectic ordering in solutions and films of a rod-like polymer owing to monodispersity of chain length. *Nature* **1997**, *389*, 167-170.

(6) Petka WA, Harden JL, McGrath KP, Wirtz D, Tirrell DA. Reversible hydrogels from self-assembling artificial proteins. *Science* **1998**, *281*, 389-392.

(7) Altman GH, Diaz F, Jakuba C, Calabro T, Horan RL, Chen JS, Lu H, Richmond J, Kaplan DL. Silk-based biomaterials. *Biomaterials* **2003**, *24*, 401-416.

(8) Nickerson CS, Kornfield JA. A "cleat" geometry for suppressing wall slip. *J. Rheol.* **2005**, *49*, 865-874.

(9) Perez-Rigueiro J, Viney C, Llorca J, Elices M. Mechanical properties of single-brin silkworm silk. *J. Appl. Polym. Sci.* **2000**, *75*, 1270-1277.

(10) Noren CJ, Anthonycahill SJ, Griffith MC, Schultz PG. A general method for site-specific incorporation of unnatural amino acids into proteins. *Science* **1989**, *244*, 182-188.

(11) Link AJ, Mock ML, Tirrell DA. Non-canonical amino acids in protein engineering. *Curr. Opin. Biotechnol.* **2003**, *14*, 603-609.

(12) Tang LP, Eaton JW. Inflammatory responses to biomaterials. *Am. J. Clin. Pathol.* **1995**, *103*, 466-471.

(13) Ratner BD, Bryant SJ. Biomaterials: Where we have been and where we are going. *Annu. Rev. Biomed. Eng.* **2004**, *6*, 41-75.

(14) Suchanek W, Yoshimura M. Processing and properties of hydroxyapatite-based biomaterials for use as hard tissue replacement implants. *J. Mater. Res.* **1998**, *13*, 94-117.

(15) Anselme K. Osteoblast adhesion on biomaterials. *Biomaterials* **2000**, *21*, 667-681.

(16) Hubbell JA. Biomaterials in tissue engineering. *Bio/Technology* **1995**, *13*, 565-576.

(17) Greenwald SE, Berry CL. Improving vascular grafts: the importance of mechanical and haemodynamic properties. *J. Pathol.* **2000**, *190*, 292-299.

(18) Kannan RY, Salacinski HJ, Butler PE, Hamilton G, Seifalian AM. Current status of prosthetic bypass grafts: A review. *J. Biomed. Mater. Res. B* **2005**, *74B*, 570-581.

(19) Bos GW, Poot AA, Beugeling T, van Aken WG, Feijen J. Small-diameter vascular graft prostheses: Current status. *Arch. Physiol. Biochem.* **1998**, *106*, 100-115.

(20) Nerem RM, Seliktar D. Vascular tissue engineering. *Annu. Rev. Biomed. Eng.* **2001**, *3*, 225-243.

(21) Zilla P, Vonoppell U, Deutsch M. The endothelium - a key to the future. *J. Card. Surg.* **1993**, *8*, 32-60.

(22) Salacinski HJ, Goldner S, Giudiceandrea A, Hamilton G, Seifalian AM, Edwards A, Carson RJ. The mechanical behavior of vascular grafts: A review. *J. Biomater. Appl.* **2001**, *15*, 241-278.

(23) Xue L, Greisler HP. Biomaterials in the development and future of vascular grafts. *J. Vasc. Surg.* **2003**, *37*, 472-480.

(24) Eberhart A, Zhang Z, Guidoin R, Laroche G, Guay L, De la Faye D, Batt M, King MW. A new generation of polyurethane vascular prostheses: Rara avis or ignis fatuus? *J. Biomed. Mater. Res.* **1999**, *48*, 546-558.

(25) Sonoda H, Takamizawa K, Nakayama Y, Yasui H, Matsuda T. Coaxial double-tubular compliant arterial graft prosthesis: time-dependent morphogenesis and compliance changes after implantation. *J. Biomed. Mater. Res. A* **2003**, *65A*, 170-181.

(26) Deutsch M, Meinhart J, Fischlein T, Preiss P, Zilla P. Clinical autologous in vitro endothelialization of infrainguinal ePTFE grafts in 100 patients: A 9-year experience. *Surgery* **1999**, *126*, 847-855.

(27) Bordenave L, Remy-Zolghadri M, Fernandez P, Bareille R, Midy D. Clinical performance of vascular grafts lined with endothelial cells. *Endothelium-J. Endoth.* **1999**, *6*, 267-275.

(28) Tseng DY, Edelman ER. Effects of amide and amine plasma-treated ePTFE vascular grafts on endothelial cell lining in an artificial circulatory system. *J. Biomed. Mater. Res.* **1998**, *42*, 188-198.

(29) Bhat VD, Klitzman B, Koger K, Truskey GA, Reichert WM. Improving endothelial cell adhesion to vascular graft surfaces: Clinical need and strategies. *J. Biomater. Sci. Polym. Ed.* **1998**, *9*, 1117-1135.

(30) Doi K, Matsuda T. Enhanced vascularization in a microporous polyurethane graft impregnated with basic fibroblast growth factor and heparin. *J. Biomed. Mater. Res.* **1997**, *34*, 361-370.

(31) Hsu SH, Chen WC. Improved cell adhesion by plasma-induced grafting of L-lactide onto polyurethane surface. *Biomaterials* **2000**, *21*, 359-367.

(32) Verma S, Marsden PA. Nitric oxide-eluting polyurethanes - vascular grafts of the future? *N. Engl. J. Med.* **2005**, *353*, 730-731.

(33) L'Heureux N, Paquet S, Labbe R, Germain L, Auger FA. A completely biological tissue-engineered human blood vessel. *FASEB J.* **1998**, *12*, 47-56.

(34) Niklason LE, Gao J, Abbott WM, Hirschi KK, Houser S, Marini R, Langer R. Functional arteries grown in vitro. *Science* **1999**, *284*, 489-493.

(35) Ratcliffe A. Tissue engineering of vascular grafts. *Matrix Biol.* **2000**, *19*, 353-357.

(36) Liu CY, Apuzzo MLJ, Tirrell DA. Engineering of the extracellular matrix: Working toward neural stem cell programming and neurorestoration - Concept and progress report. *Neurosurgery* **2003**, *52*, 1154-1165.

(37) Xie RZ, Stretton S, Sweeney DF. Artificial cornea: Towards a synthetic onlay for correction of refractive error. *Biosci. Rep.* **2001**, *21*, 513-536.

(38) Evans MDM, McLean KM, Hughes TC, Sweeney DF. A review of the development of a synthetic corneal onlay for refractive correction. *Biomaterials* **2001**, *22*, 3319-3328.

(39) Ruoslahti E. RGD and other recognition sequences for integrins. *Annu. Rev. Cell Dev. Biol.* **1996**, *12*, 697-715.

(40) Vandermeulen GWM, Klok HA. Peptide/protein hybrid materials: Enhanced control of structure and improved performance through conjugation of biological and synthetic polymers. *Macromol. Biosci.* **2004**, *4*, 383-398.

(41) Hersel U, Dahmen C, Kessler H. RGD modified polymers: biomaterials for stimulated cell adhesion and beyond. *Biomaterials* **2003**, *24*, 4385-4415.

(42) Mould AP, Komoriya A, Yamada KM, Humphries MJ. The CS5 Peptide Is a 2nd Site in the IIICS region of fibronectin recognized by the integrin alpha-4-beta-1 - inhibition of alpha-4-beta-1 function by RGD peptide homologs. *J. Biol. Chem.* **1991**, *266*, 3579-3585.

(43) Hubbell JA, Massia SP, Desai NP, Drumheller PD. Endothelial cell-selective materials for rissue engineering in the vascular graft via a new receptor. *Bio/Technology* **1991**, *9*, 568-572.

(44) Nicol A, Gowda DC, Parker TM, Urry DW In *Biotechnology and Bioactive Polymers*; Gebelein C, Carraher C, Eds.; Plenum Press: New York, **1994**, p 95.

(45) Urry DW. Physical chemistry of biological free energy transduction as demonstrated by elastic protein-based polymers. *J. Phys. Chem. B* **1997**, *101*, 11007-11028.

(46) Urry DW, Luan C-H, Harris CM, Parker TM In *Protein-Based Materials*; McGrath KP, Kaplan DL, Eds.; Birkhauser: Boston, **1997**, pp 133-177.

(47) Debelle L, Alix AJP, Jacob MP, Huvenne JP, Berjot M, Sombret B, Legrand P. Bovine elastin and kappa-elastin secondary structure determination by optical spectroscopies. *J. Biol. Chem.* **1995**, *270*, 26099-26103.

(48) Urry DW, Long MM, Ohnishi T, Jacobs M. Circular dichroism and absorption of polytetrapeptide of elastin - polymer model for beta-turn. *Biochem. Biophys. Res. Commun.* **1974**, *61*, 1427-1433.

(49) Hoeve CAJ, Flory PJ. Elastic properties of elastin. *Biopolymers* **1974**, *13*, 677-686.

(50) Torchia DA, Piez KA. Mobility of elastin chains as determined by C-13 nuclear magnetic resonance. *J. Mol. Biol.* **1973**, *76*, 419-424.

(51) Hoeve CAJ, Flory PJ. The elastic properties of elastin. *J. Am. Chem. Soc.* **1959**, *80*, 6523-6526.

(52) Kakivaya SR, Hoeve CAJ. Glass point of elastin. *Proc. Natl. Acad. Sci. U. S. A.* **1975**, *72*, 3505-3507.

(53) Cook WJ, Einspahr H, Trapane TL, Urry DW, Bugg CE. Crystal-structure and conformation of the cyclic trimer of a repeat pentapeptide of elastin, cyclo-(L-Valyl-L-Prolylglycyl-L-Valylglycyl)3. *J. Am. Chem. Soc.* **1980**, *102*, 5502-5505.

(54) Karle IL, Urry DW. Crystal structure of cyclic (APGVGV)(2,) an analog of elastin, and a suggested mechanism for elongation/contraction of the molecule. *Biopolymers* **2005**, *77*, 198-204.

(55) Urry DW. Entropic elastic processes in protein mechanisms. 1. Elastic structure due to an inverse temperature transition and elasticity due to internal chain dynamics. *J. Protein Chem.* **1988**, *7*, 1-34.

(56) Urry DW, Hugel T, Seitz M, Gaub HE, Sheiba L, Dea J, Xu J, Parker T. Elastin: a representative ideal protein elastomer. *Philos. Trans. R. Soc. Lond. B Biol. Sci.* **2002**, *357*, 169-184.

(57) Li B, Alonso DOV, Daggett V. The molecular basis for the inverse temperature transition of elastin. *J. Mol. Biol.* **2001**, *305*, 581-592.

(58) Yao XL, Hong M. Structure distribution in an elastin-mimetic peptide (VPGVG)(3) investigated by solid-state NMR. *J. Am. Chem. Soc.* **2004**, *126*, 4199-4210.

(59) Ohgo K, Ashida J, Kumashiro KK, Asakura T. Structural determination of an elastin-mimetic model peptide, (Val-Pro-Gly-Val-Gly)(6), studied by C-13 CP/MAS NMR chemical shifts, two-dimensional off magic angle spinning spin-diffusion NMR, rotational echo double resonance, and statistical distribution of torsion angles from protein data bank. *Macromolecules* **2005**, *38*, 6038-6047.

(60) Li B, Alonso DOV, Bennion BJ, Daggett V. Hydrophobic hydration is an important source of elasticity in elastin-based biopolymers. *J. Am. Chem. Soc.* **2001**, *123*, 11991-11998.

(61) Rodriguez-Cabello JC, Reguera J, Girotti A, Alonso M, Testera AM. Developing functionality in elastin-like polymers by increasing their molecular complexity: the power of the genetic engineering approach. *Prog. Polym. Sci.* **2005**, *30*, 1119-1145.

(62) Urry DW, Pattanaik A, Xu J, Woods TC, McPherson DT, Parker TM. Elastic protein-based polymers in soft tissue augmentation and generation. *Journal of Biomaterials Science-Polymer Edition* **1998**, *9*, 1015-1048.

(63) Chilkoti A, Dreher MR, Meyer DE, Raucher D. Targeted drug delivery by thermally responsive polymers. *Adv. Drug Delivery Rev.* **2002**, *54*, 613-630.

(64) Kopecek J. Smart and genetically engineered biomaterials and drug delivery systems. *Eur. J. Pharm. Sci.* **2003**, *20*, 1-16.

(65) Kim JY, Mulchandani A, Chen W. An immunoassay for atrazine using tunable immunosorbent. *Anal. Biochem.* **2003**, *322*, 251-256.

(66) Meyer DE, Kong GA, Dewhirst MW, Zalutsky MR, Chilkoti A. Targeting a genetically engineered elastin-like polypeptide to solid tumors by local hyperthermia. *Cancer Res.* **2001**, *61*, 1548-1554.

(67) Reguera J, Fahmi A, Moriarty P, Girotti A, Rodriguez-Cabello JC. Nanopore formation by self-assembly of the model genetically engineered elastin-like polymer (VPGVG)(2)(VPGEG)(VPGVG)(2) (15). *J. Am. Chem. Soc.* **2004**, *126*, 13212-13213.

(68) Rao GVR, Balamurugan S, Meyer DE, Chilkoti A, Lopez GP. Hybrid bioinorganic smart membranes that incorporate protein-based molecular switches. *Langmuir* **2002**, *18*, 1819-1824.

(69) Stiborova H, Kostal J, Mulchandani A, Chen W. One-step metal-affinity purification of histidine-tagged proteins by temperature-triggered precipitation. *Biotechnol. Bioeng.* **2003**, *82*, 605-611.

(70) Kostal J, Mulchandani A, Chen W. Tunable biopolymers for heavy metal removal. *Macromolecules* **2001**, *34*, 2257-2261.

(71) Urry DW, Parker TM, Reid MC, Gowda DC. Biocompatibility of the bioelastic materials, poly(GVGVP) and its gamma-irradiation cross-linked matrix - summary of generic biological test-results. *J. Bioactive and Compatible Polym.* **1991**, *6*, 263-282.

(72) Urry DW. Molecular machines - How motion and other functions of living organisms can result from reversible chemical changes. *Angewandte Chemie-International Edition in English* **1993**, *32*, 819-841.

(73) Panitch A, Yamaoka T, Fournier MJ, Mason TL, Tirrell DA. Design and biosynthesis of elastin-like artificial extracellular matrix proteins containing periodically spaced fibronectin CS5 domains. *Macromolecules* **1999**, *32*, 1701-1703.

(74) Welsh ER, Tirrell DA. Engineering the extracellular matrix: A novel approach to polymeric biomaterials. I. Control of the physical properties of artificial protein matrices designed to support adhesion of vascular endothelial cells. *Biomacromolecules* **2000**, *1*, 23-30.

(75) Van Luyn MJA, Van Wachem PB, Olde Damink LHH, Dijkstra PJ, Feijen J, Nieuwenhuis P. Relations between in vitro cytotoxicity and cross-linked dermal sheep collagens. *J. Biomed. Mater. Res.* **1992**, *26*, 1091-1110.

(76) Heilshorn SC, DiZio KA, Welsh ER, Tirrell DA. Endothelial cell adhesion to the fibronectin CS5 domain in artificial extracellular matrix proteins. *Biomaterials* **2003**, *24*, 4245-4252.

(77) Liu JC, Heilshorn SC, Tirrell DA. Comparative cell response to artificial extracellular matrix proteins containing the RGD and CS5 cell-binding domains. *Biomacromolecules* **2004**, *5*, 497-504.

(78) Heilshorn SC, Liu JC, Tirrell DA. Cell-binding domain context affects cell behavior on engineered proteins. *Biomacromolecules* **2005**, *6*, 318-323.

(79) Di Zio K, Tirrell DA. Mechanical properties of artificial protein matrices engineered for control of cell and tissue behavior. *Macromolecules* **2003**, *36*, 1553-1558.

(80) Kirshenbaum K, Carrico IS, Tirrell DA. Biosynthesis of proteins incorporating a versatile set of phenylalanine analogues. *Chembiochem* **2002**, *3*, 235-237.

(81) Pelham RJ, Wang YL. Cell locomotion and focal adhesions are regulated by substrate flexibility. *Proc. Natl. Acad. Sci. U. S. A.* **1997**, *94*, 13661-13665.

(82) Lo CM, Wang HB, Dembo M, Wang YL. Cell movement is guided by the rigidity of the substrate. *Biophys. J.* **2000**, *79*, 144-152.

(83) Discher DE, Janmey P, Wang YL. Tissue cells feel and respond to the stiffness of their substrate. *Science* **2005**, *310*, 1139-1143.

2 PHYSICAL PROPERTIES OF ARTIFICIAL EXTRACELLULAR MATRIX PROTEIN FILMS PREPARED BY ISOCYANATE CROSSLINKING

2.1 Abstract

Artificial extracellular matrix proteins, genetically engineered from elastin- and fibronectin-derived repeating units, were crosslinked with hexamethylene diisocyanate in dimethylsulfoxide. The resulting hydrogel films were transparent, uniform, and highly extensible. Their tensile moduli depended on crosslinker concentration and spanned the range characteristic of native elastin. The water content of the films was low (~27%), but the temperature-dependent swelling behavior of the crosslinked materials was reminiscent of the lower critical solution temperature (LCST) property of the soluble polymers.

Reprinted from: Nowatzki, P.J., Tirrell D.A. *Biomaterials* vol. 25, no. 7-8 (Mar-Apr 2004), p1261-1267, *with permission from Elsevier*.

2.2 Introduction

Artificial proteins, because their architectures can be precisely controlled, are potentially useful for a variety of biomaterials applications. Here we describe artificial extracellular matrix proteins to address the long-standing problem of high failure rates in small- and medium-diameter vascular grafts. Both the autologous and synthetic (polytetrafluoroethylene and polyethylene terephthalate) grafts currently used have unacceptably low long-term patency.[1,2] The primary causes of graft failure are thrombosis and intimal hyperplasia, the latter associated with a proliferation of smooth muscle cells in blood vessels that eventually blocks circulation.[3,4] Intimal hyperplasia is widely thought to be caused by the unnatural stresses induced by the mismatch in mechanical properties between the graft and the natural vessel,[4,5] or by the inability of the graft to sustain an endothelial cell monolayer, which is critical in the maintenance of vascular health.[6,7] Thus, recent efforts to develop vascular grafts have focused on compliance matching, and on promoting the growth of, or sustaining, a monolayer of endothelial cells on the graft surface.[1,8-10]

We and others have reported artificial proteins designed to mimic the essential mechanical and biological properties of the extracellular matrix.[11-13] In the proteins described here, elastin-based polypentapeptide sequences [$(VPGIG)_x$] provide elasticity, and periodic CS5 cell-binding domains, derived from fibronectin, impart biological function. Lysine residues were incorporated into the protein design to allow amine-specific crosslinking: one N-terminal and two C-terminal lysines were added.[12] The three artificial extracellular matrix (aECM) proteins examined in this work are designated by their molecular

weights (aE16 = 16,117; aE43 = 42,974; aE70 = 69,832); their sequences are listed below in Figure 2.1.[14]

MMASMTGGQQMGRKTMG[LD**"CS5"**G(VPGIG)$_{25}$VP]$_1$LEKAAKLE aE16

MMASMTGGQQMGRKTMG[LD**"CS5"**G(VPGIG)$_{25}$VP]$_3$LEKAAKLE aE43

MMASMTGGQQMGRKTMG[LD**"CS5"**G(VPGIG)$_{25}$VP]$_5$LEKAAKLE aE70

"CS5" = GEEIQIGHIPREDVDYHLYP

Figure 2.1 Amino acid sequences of artificial ECM proteins.

Elastin-like polypeptides $(VPGZG)_x$, where Z is any amino acid, in aqueous solution undergo an aggregative inverse temperature transition upon heating. This entropy-driven transition occurs at a "lower critical solution temperature" (LCST) unique to the polymer. Urry and coworkers studied these polymers in detail.[15,16] The $(VPGIG)_x$ motif was chosen here as the structural basis of the aECM proteins, because it results in proteins with sub-ambient LCST (12 to 16 ºC).[11,12] The sub-ambient LCST limits protein solubility at physiological temperatures and facilitates purification of proteins expressed in bacterial hosts.

The CS5 region, an element of the alternatively spliced type III connecting segment of fibronectin, contains the minimal cell-binding ligand REDV, which targets the $\alpha_4\beta_1$ integrin, a cell-surface receptor.[17] In particular, $\alpha_4\beta_1$ has been demonstrated to mediate endothelial cell adhesion to REDV peptides.[18] Peptides that contain the REDV sequence, when grafted to glycophase glass, have been shown to support the attachment and spreading of endothelial cells, but not of smooth muscle cells and platelets.[19] Artificial extracellular matrix proteins

constructed from alternating CS5 and $(VPGIG)_x$ domains, adsorbed on glass, also support endothelial cell attachment and spreading.[11]

Since the primary amine functional groups are located only at the ends of the protein, amine-selective reagents should be capable of crosslinking the proteins without disrupting the CS5 domains. Welsh et al. crosslinked these proteins with glutaraldehyde and found that the tensile moduli of the resulting films approached that of native elastin, and, as expected, varied inversely with protein molecular weight.[12] However, the results of endothelial cell culture on glutaraldehyde crosslinked films were variable,[20] perhaps because of non-specific interactions between the proteins and endothelial cells or because of the cytotoxicity of glutaraldehyde.[21,22]

Here, hexamethylene diisocyanate (HMDI) was employed as an alternative lysine-targeted crosslinker. HMDI has been employed previously in biomaterials fixation, and its cytotoxicity is considerably lower than that of glutaraldehyde.[22] Films prepared from aECM proteins with HMDI crosslinking were transparent, had low water contents, and were viscoelastic and highly extensible. The films retained the temperature-dependent swelling behavior of the component proteins. Their initial tensile moduli were observed to be similar to that of native elastin, and should be advantageous with respect to application in vascular grafts.

2.3 Experimental

2.3.1 Materials and methods.

Hexamethylene diisocyanate (HMDI) was purchased from Aldrich; dimethylsulfoxide (DMSO) was from Mallinckrodt. Amino acid analysis was performed at the University of California, Davis Molecular Structure Facility via HCl hydrolysis, cation exchange chromatography, and post-column ninhydrin derivatization for quantitation. Bacterial fermentations were performed in a New Brunswick Scientific BioFlo 3000 bioreactor. An Instron model 5542 tensile tester with a 5 N load cell and accompanying software was used to collect tensile data.

2.3.2 Protein expression and purification.

Details of gene construction and expression were reported previously.[12] Artificial genes encoding each of the three proteins were constructed in pET28 vectors; expression was controlled by a bacteriophage T7 promoter inducible by isopropyl β-thiogalactopyranoside (IPTG). Fermentations were performed at 37 °C under antibiotic selection; here, expression was induced by 2.5 mM IPTG when the OD_{600} reached ~8, and cells were harvested 2-4 hours later. The purification scheme, which takes advantage of the inverse temperature transition of the proteins, matches that of Welsh.[12] Briefly, the target proteins partitioned into the pellet of the whole-cell lysate after centrifugation (20,100 × g, 60 min, 24 °C), were resuspended in 4M urea and centrifuged (20,100 × g, 60 min, 4 °C) to remove non-protein cellular debris, dialyzed against water (5 days, 4 °C), and

separated from the precipitated proteins by centrifugation (20,100 × g, 60 min, 4 °C). The supernatant was decanted and warmed to 30 °C to aggregate the target protein, which was then separated by centrifugation (20,100 × g, 60 min, 30 °C), resuspended in cold water, and lyophilized. The purity of the proteins and uniformity of molecular weight was previously established[12] and confirmed here by SDS-PAGE. The yields of aE16, aE43, and aE70 were 1.6, 9.1, and 6.0 g, respectively, for 10 L fermentations.

2.3.3 Crosslinked films.

The protein of interest (500 mg) was dissolved in 5 mL of dimethylsulfoxide (DMSO); the appropriate amount of hexamethylene diisocyanate (12-39 mg) was added, and the solution was mixed rapidly with a pipet. The solution was poured into an open-faced, 6.3 × 6.3 cm, polished aluminum mold and reacted in a desiccator for 8 h. To remove the DMSO, the mold was placed on a hotplate at 50-60 °C overnight. The dried film was hydrated and rinsed with distilled water, removed from the mold, and stored in water at 4 °C. When hydrated, the films were transparent, had a uniform thickness of about 0.15 mm, and were characterized by a water content of about 27%. Smaller (1.0 × 1.5 mm) films, used to obtain results in Figures 2.3 and 2.5, were made in PTFE molds by the same procedure.

2.3.4 Uniaxial tensile testing.

Films were tested in phosphate-buffered saline (PBS: 137 mM NaCl, 2.7 mM KCl, 4.3 mM Na_2HPO_4, 1.4 mM KH_2PO_4, pH adjusted to 7.40 with NaOH) using a specially designed sample chamber, in which the temperature was kept at 37 ± 1 °C by a water jacket. Rectangular test films were pressure-cut from the large cast films with a new razor blade to minimize nicks; extensions-to-break (E_b) were measured on ~2 × 18 mm samples, while moduli were measured on ~5 × 50 mm samples; all samples had a length-to-width aspect ratio of 8 or greater to minimize end effects.[23] Samples were equilibrated in the PBS bath for 30 min prior to testing. Extensions were performed at a rate of 10 % of the gauge length per minute (0.00167 / sec), a standard test rate for polymeric films.[23] Extension-to-break samples consistently broke at one of the grips, where stress concentration is highest; thus the reported E_b are artificially low.

2.3.5 Temperature-dependent length changes.

A film was mounted in the tensile tester, and the PBS bath temperature was controlled by a water jacket and monitored by a thermometer adjacent to the sample. As the temperature changed, the sample length was measured by manually adjusting the distance between the grips to keep the film taut but at zero-stress. Starting from room temperature, the sample was twice cycled between 2 °C and 50 °C; the data presented are from the second cycle. The cooling and heating rates, although not precisely controlled, were approximately 0.2 °C / min.

2.4 Results and discussion

2.4.1 Tensile properties of crosslinked films.

Films used for mechanical testing were made with isocyanate-to-primary amine ratios of 5.0 (5× HMDI) or greater; these films were uniformly insoluble, visually defect-free, and transparent both in the dried and hydrated states. At temperatures above the LCST, the films had water contents, based on weight fraction, of around 27% (Table 2.1). This water content is similar to the 32% reported for hydrated purified elastin at 36 °C.[24] Despite the low water content of these hydrogels, the water is essential to their elasticity; when dried, the films were brittle and their elastic moduli were roughly 1000 times higher than in the hydrated state. Dehydration of the films appeared completely reversible, as the water content was unchanged through five cycles of drying and wetting the films.

Table 2.1 Physical properties (37 °C) of aECM films crosslinked with HMDI. Standard deviations indicated, n = 3. 5× and 10× refer to the molar ratio of isocyanate to primary amines used in preparing the films.

Film	Weight fraction polymer	E (MPa)	G (MPa)	E_b (%)	Pred. M_c
aE16-5×	0.742 ± 0.012	0.71 ± 0.04	0.24 ± 0.01	340 ± 20	11,000
aE43-5×	0.731 ± 0.003	0.58 ± 0.02	0.19 ± 0.02	480 ± 40	13,000
aE70-5×	0.719 ± 0.005	0.40 ± 0.09	0.13 ± 0.03	570 ± 30	19,000
aE43-10×	0.752 ± 0.001	0.93 ± 0.11	0.31 ± 0.06	420 ± 30	8,000

Representative stress-strain curves for the three proteins crosslinked with isocyanate-to-primary amine ratios of 5:1 (designated "aEMW-5×") are shown in Figure 2.2. Each of the crosslinked films was highly extensible and did not break until well into the non-ideal, non-entropic range of the stress-strain curve. While the E_b are artificially low, owing to breakage at the sample ends, the films made from longer proteins were reproducibly more extensible to break. The effect of increasing the crosslinker concentration on aE43 was to stiffen the film and reduce the measured extension to break. A summary of the mechanical testing results is given in Table 2.1 above.

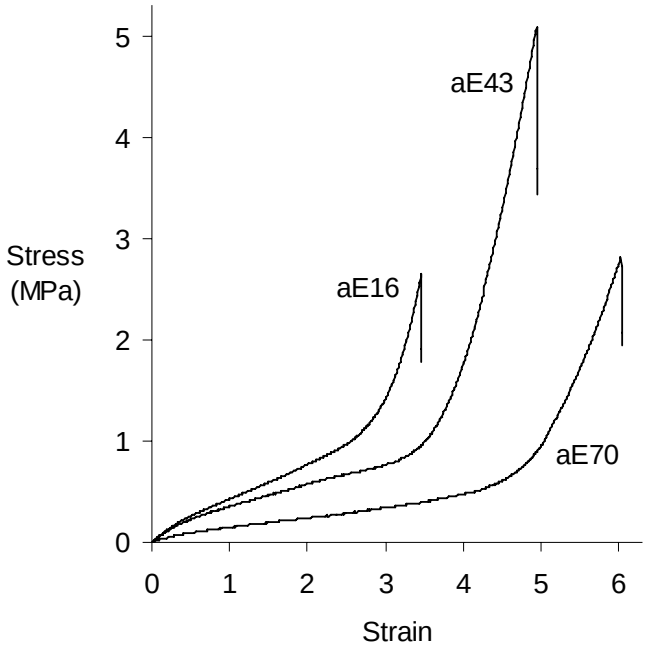

Figure 2.2 Representative tensile behavior of aE16-5×, aE43-5×, and aE70-5× films (each crosslinked with a 5:1 molar ratio of isocyanate to primary amines).

The stress-strain curves are typical of rubbers; at low strain (< 0.5) the slope decreases slightly with increasing strain, an effect associated with the statistical mechanics of chain deformation.[25] At the slow extension rate employed, 10% per minute (.00167 / sec), viscoelastic effects are minimal, and the films are considered to behave as ideal rubbers. This allows details about the molecular architecture to be extracted from the stress-strain behavior. In an ideal network, a plot of σ versus $(\lambda - 1/\lambda^2)$, where σ is the stress and λ is the elongation ratio, is linear. The slope is the shear modulus, G, which in ideal rubbers is equal to one third of the elastic modulus, E.[25] Here, the elastic moduli, E, were calculated from the linear portions of the stress-strain curves, at strain < 0.05, and the shear moduli, G, were obtained from plots of σ versus $(\lambda - 1/\lambda^2)$, up to strains of 0.25 ($\lambda = 1.25$). The shear modulus plots were indeed linear, and the resulting values of G were near one third the values of E, justifying the approximation of these materials as ideal. The elastic moduli span the range of natural elastic fibers, 0.3 to 0.6 MPa.[26]

From a statistical treatment of the ideal network, the shear modulus is inversely proportional to the average molecular weight between crosslinks, M_c, by $G = \rho RT/M_c$.[25] The ideal network treatment assumes Gaussian distribution statistics and freely jointed, non-interacting chains, whereas protein polymers are conformationally restricted and are characterized by strong inter- and intra-molecular interactions. In this case, however, the elastin units appear sufficiently mobile to resolve molecular entanglements at the test rate used, and the films behave nearly ideally. Values of M_c calculated from the equation above, then,

provide an estimate of the chain length between crosslinks. Since the lysine residues are only at the ends of the protein, the M_c should equal the molecular weight of the protein if only lysines react. To calculate ρ, the effective polymer density for each film, a protein density of 1.3 g/cm^3, commonly used for elastin,[27] and the measured water contents of the films were used. The resulting M_c, shown in Table 1, are considerably smaller than expected, especially for films made from high molecular weight proteins (aE70-5×) and high isocyanate ratios (aE43-10×). Slow-resolving entanglements may account for some of the discrepancies between the calculated M_c and the known molecular weight,[28] but the magnitude of the difference may imply that the side chains of residues other than lysine react with the isocyanate, forming additional crosslinks.

The minimum isocyanate-to-primary amine ratio required to crosslink the proteins into films was about 2.0 for aE43 and 3.0 for aE70. At and above these ratios of isocyanate, the dried protein films swelled, but were insoluble in good solvents for the protein such as cold water or DMSO. At slightly lower ratios, such as 1.5 for aE43 and 2.5 for aE70, films appeared to gel and were partially intact when hydrated, but were not completely insolubilized, suggesting partial crosslinking. Larger ratios of isocyanate are required to crosslink aE70, in which the reactive amines are more dilute and intramolecular crosslinking is thought to be more prevalent.

The concentration of diisocyanate used to crosslink the films strongly affected film stiffness. Various stoichiometric ratios of isocyanate to primary amine were used in crosslinking aE43 with HMDI, and the elastic moduli of the

resulting films are plotted in Figure 2.3. Film modulus increases with increasing isocyanate-to-amine ratio, from near-zero in minimally crosslinked films, through the 0.3-0.6 MPa range of native elastin. Above a ratio of ca. 10, the modulus appears to plateau. The fact that the modulus continues to increase at isocyanate:amine ratios greater than 1 may indicate non-productive (intramolecular) crosslinking. Furthermore, if amino acid side chains other than those of lysine react with HMDI, the calculated ratios of isocyanate to reactive groups would be artificially high.

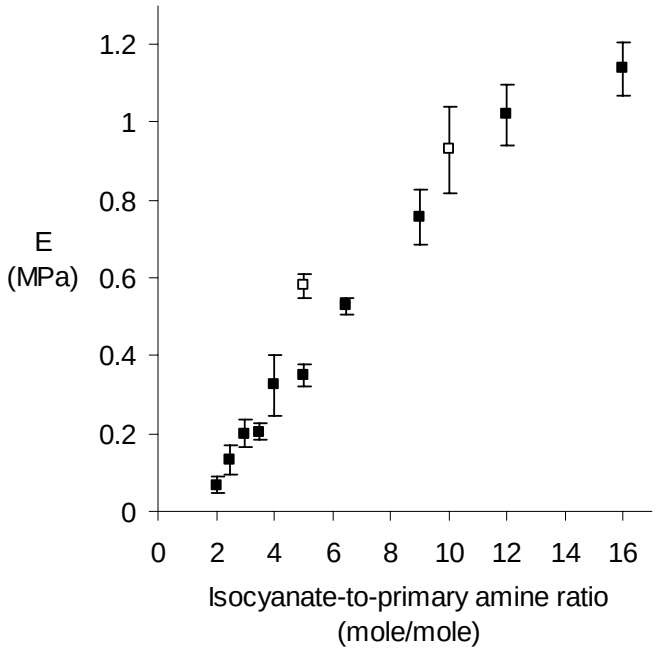

Figure 2.3 Elastic moduli of aE43 films crosslinked with various molar ratios of HMDI-to-protein. The open squares are data reported in Table 1 for large aE43 films cast in aluminum molds. The filled squares are data for films cast from smaller PTFE molds. Errors indicated as one standard deviation (n=3 films).

2.4.2 HMDI reactivity.

Amino acid analysis was used to probe the reactivity of the isocyanate toward side chains other than those of lysine. Table 2.2 indicates measured concentrations of selected amino acids before and after crosslinking for each of the three proteins; it also confirms the purity of the protein by comparing expected to measured compositions. The only significant change appears in the lysine fraction, indicating that at least 65% of lysine residues reacted with the crosslinker in each case. The other amino acid fractions, including those not shown, were experimentally indistinguishable before and after crosslinking. However, other isocyanate-side chain bonds that were formed during crosslinking may have been hydrolyzed to yield the original amino acids during the sample preparation.

Table 2.2. Amino acid analysis results comparing expected and measured mole fractions of selected amino acids in aECM proteins before and after HMDI crosslinking.

%	protein	expected	before XL	after 5×	after 10×
Arg	aE16	1.14	1.28	1.10	
	aE43	0.84	0.96	0.90	0.85
	aE70	0.77	0.93	0.92	
Asp[a]	aE16	1.71	2.08	2.10	
	aE43	1.89	2.18	2.16	2.05
	aE70	1.94	2.23	2.30	
Gly	aE16	32.6	30.3	31.6	
	aE43	34.3	32.1	31.5	32.5
	aE70	34.7	33.2	33.4	
His	aE16	1.14	1.18	1.18	
	aE43	1.26	1.21	1.23	1.30
	aE70	1.29	1.29	1.26	
Lys	aE16	1.71	1.95	**0.60**	
	aE43	0.63	0.75	**0.20**	**0.27**
	aE70	0.39	0.63	**0.14**	
Val	aE16	15.4	16.2	16.1	
	aE43	17.1	17.6	18.0	17.4
	aE70	17.4	17.6	17.5	

[a] In some preparations amino acid analysis indicated that acidic residues (Asp, Glu) partially react (< 30%)

The activity of HMDI toward lysine is apparent, but the specificity remains uncertain. In general, isocyanates may react with nucleophilic functional groups such as amines, alcohols, and protonated acids.[29] HMDI in particular was observed to react with the side-chains of backbone-protected lysine, cysteine, and histidine, and to a lesser extent tyrosine, in water,[30] but comparable studies in DMSO do not appear to have been reported. Reactions of HMDI with other residues, such as arginine or aspartic acid, are of particular concern because such reactions could alter the functionality of the CS5 cell-binding domain.

2.4.3 Unidimensional temperature swelling.

aE43-10× films swell considerably when cooled from physiological conditions to near 0 °C (Figure 2.4). The transition is centered near 10 °C, which is slightly lower than the reported LCST of 17 °C for aE70 in solution,[12] and coincides well with the LCSTs of 12 °C and 13 °C reported for similar aECM proteins lacking the lysine-containing terminal linkers[31] and with the value of 10 ± 5 °C predicted for $(VPGIG)_x$.[15] Thus, the film retains the thermal transition behavior of the soluble protein. In comparison with the transition of the protein, which at high concentrations occurs over a range of just a few degrees, the transition in the film is much broader. Apparently, crosslinking the film reduces the cooperativity of the transition, perhaps by trapping elastin-like segments of the protein in conformations that alter their tendency to undergo the phase change. Lee et al. also examined the temperature-dependent swelling behavior

of elastin-like materials, and observed a similarly broadened LCST transition in films crosslinked by γ-irradiation.[32,33]

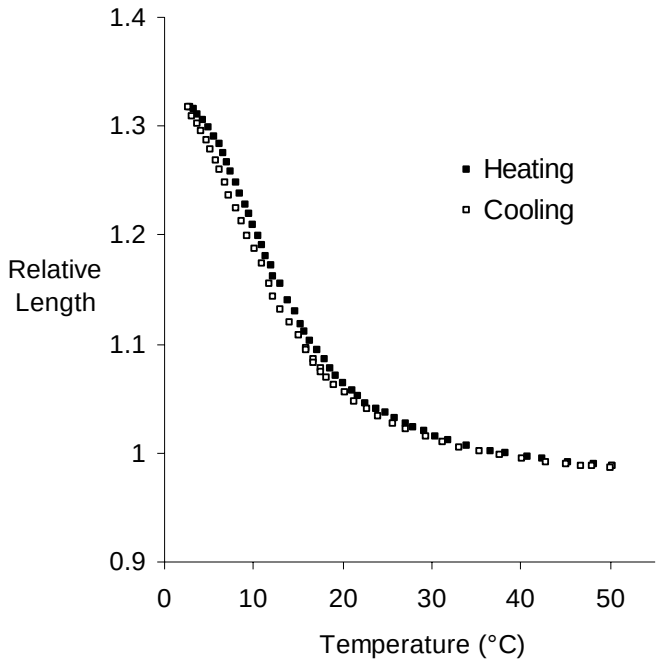

Figure 2.4 Temperature-dependent change in length of an aE43-10× film. Length plotted relative to the length at 37 °C. Hysteresis between the heating and cooling curves is minimal at the slow heating and cooling (0.2 °C / min) rates used.

The extent of swelling of aE43 and aE70 films, as the temperature is reduced from above to below the LCST (from 21 °C to 4 °C), decreased as the crosslinker concentration increased, as indicated in Figure 2.5. It is interesting to compare the length changes observed upon cooling of films in Figure 2.5, 94% for aE43-2× and 74% for aE70-3×, with the 63% increase in radius of gyration of a $(VPGVG)_{18}$ molecule (LCST = 27 ºC) between 42 and 10 ºC, calculated by Li et al. using molecular simulations of a single peptide chain surrounded by water

molecules.[34] Lee et al. observed a wide range of swelling extents upon traversing the LCST in films of $(VPGZG)_x$-based materials crosslinked chemically or with γ-irradiation; as in the present study, the degree of swelling was dependent on crosslink density.[32,33] At similar crosslink densities, however, they observed more extensive swelling than was seen here: for free-radical crosslinked $(VPGIG)_{260}$ with a calculated molecular weight between crosslinks (M_c) of 19,000, they observed a length change upon cooling from above to below the LCST of ~90% (deduced from weight swelling ratio data),[33] compared to the 46% change in length seen here for aE70-5× (M_c = 19,000).

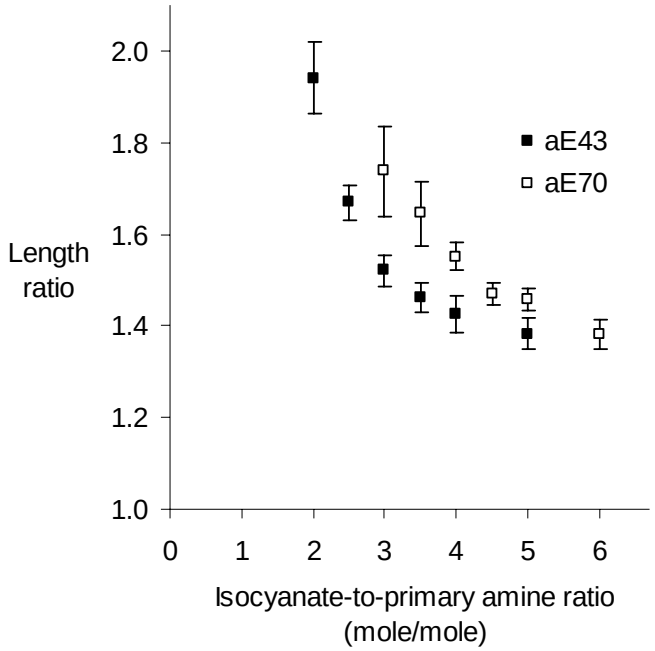

Figure 2.5 Dimensional changes from above to below the LCST in aE43 and aE70 films crosslinked with varying concentrations of HMDI. The length ratio refers to the length of the film in water at 4 °C divided by the length at 21 °C. Errors indicated as one standard deviation (n=4 films).

2.5 Conclusions

Insoluble, coherent, elastic films were made from artificial extracellular matrix proteins by crosslinking with hexamethylene diisocyanate in dimethylsulfoxide. The films were considerably more extensible than previously reported crosslinked elastin-like proteins, which is attributed to their uniformity and lack of defects. The elastic moduli of the films were larger than was observed for the same materials crosslinked with glutaraldehyde,[12] and matched the modulus of native elastin. Additionally, the moduli varied with both protein size and crosslinker concentration; thus, the elastic modulus of the films can be precisely controlled. Assessment of the reactivity of the isocyanate toward protein side chains was incomplete, but amino acid analysis confirmed a change in lysine concentrations after crosslinking. The unexpectedly high modulus of the films may indicate additional reactive side-chains. The engineering demands of the vascular graft warrant continuing characterization of the viscoelastic and biological properties of crosslinked aECM films. The transparency of the films makes them convenient substrates for cell culture studies, which are underway.

Acknowledgement: This work was supported by the National Institutes of Health (R01-HL59987) and the National Science Foundation (BES-9901648).

2.6 References

(1) Bos GW, Poot AA, Beugeling T, van Aken WG, Feijen J. Small-diameter vascular graft prostheses: Current status. *Arch. Physiol. Biochem.* **1998**, *106*, 100-115.

(2) Abbott WM, Callow A, Moore W, Rutherford R, Veith F, Weinberg S. Evaluation and performance standards for arterial prostheses. *J. Vasc. Surg.* **1993**, *17*, 746-756.

(3) Greenwald SE, Berry CL. Improving vascular grafts: the importance of mechanical and haemodynamic properties. *J. Pathol.* **2000**, *190*, 292-299.

(4) Salacinski HJ, Goldner S, Giudiceandrea A, Hamilton G, Seifalian AM, Edwards A, Carson RJ. The mechanical behavior of vascular grafts: A review. *J. Biomater. Appl.* **2001**, *15*, 241-278.

(5) Brossollet LJ. Mechanical issues in vascular grafting - a review. *Int. J. Artif. Organs* **1992**, *15*, 579-584.

(6) Zilla P, Vonoppell U, Deutsch M. The endothelium - a key to the future. *J. Card. Surg.* **1993**, *8*, 32-60.

(7) Welch M, Durrans D, Carr HM, Vohra R, Rooney OB, Walker MG. Endothelial cell seeding: a review. *Ann. Vasc. Surg.* **1992**, *6*, 473-484.

(8) Eberhart A, Zhang Z, Guidoin R, Laroche G, Guay L, De la Faye D, Batt M, King MW. A new generation of polyurethane vascular prostheses: Rara avis or ignis fatuus? *J. Biomed. Mater. Res.* **1999**, *48*, 546-558.

(9) Deutsch M, Meinhart J, Fischlein T, Preiss P, Zilla P. Clinical autologous in vitro endothelialization of infrainguinal ePTFE grafts in 100 patients: A 9-year experience. *Surgery* **1999**, *126*, 847-855.

(10) Stone D, Phaneuf M, Sivamurthy N, LoGerfo FW, Quist WC. A biologically active VEGF construct in vitro: Implications for bioengineering-improved prosthetic vascular grafts. *J. Biomed. Mater. Res.* **2002**, *59*, 160-165.

(11) Panitch A, Yamaoka T, Fournier MJ, Mason TL, Tirrell DA. Design and biosynthesis of elastin-like artificial extracellular matrix proteins containing periodically spaced fibronectin CS5 domains. *Macromolecules* **1999**, *32*, 1701-1703.

(12) Welsh ER, Tirrell DA. Engineering the extracellular matrix: A novel approach to polymeric biomaterials. I. Control of the physical properties of artificial protein matrices designed to support adhesion of vascular endothelial cells. *Biomacromolecules* **2000**, *1*, 23-30.

(13) Nicol A, Gowda DC, Parker TM, Urry DW In *Biotechnology and Bioactive Polymers*; Gebelein C, Carraher C, Eds.; Plenum Press: New York, **1994**, p 95.

(14) These proteins were originally reported[12] as containing $(VPGIG)_{20}$ instead of $(VPGIG)_{25}$; the correct sequences were determined here by DNA sequencing.

(15) Urry DW. Physical chemistry of biological free energy transduction as demonstrated by elastic protein-based polymers. *J. Phys. Chem. B* **1997**, *101*, 11007-11028.

(16) Urry DW, Luan C-H, Harris CM, Parker TM In *Protein-Based Materials*; McGrath KP, Kaplan DL, Eds.; Birkhauser: Boston, **1997**, pp 133-177.

(17) Mould AP, Komoriya A, Yamada KM, Humphries MJ. The CS5 Peptide Is a 2nd Site in the IIICS region of fibronectin recognized by the integrin alpha-4-beta-1 - inhibition of alpha-4-beta-1 function by RGD peptide homologs. *J. Biol. Chem.* **1991**, *266*, 3579-3585.

(18) Massia SP, Hubbell JA. Vascular endothelial-cell adhesion and spreading promoted by the peptide REDV of the IIICS region of plasma fibronectin is mediated by integrin alpha-4-beta-1. *J. Biol. Chem.* **1992**, *267*, 14019-14026.

(19) Hubbell JA, Massia SP, Desai NP, Drumheller PD. Endothelial cell-selective materials for rissue engineering in the vascular graft via a new receptor. *Bio/Technology* **1991**, *9*, 568-572.

(20) Welsh ER "Engineering the extracellular matrix: A novel approach to polymeric biomaterials," Ph.D. Thesis, University of Massachusetts Amherst, **1999**.

(21) Sung HW, Liang IL, Chen CN, Huang RN, Liang HF. Stability of a biological tissue fixed with a naturally occurring crosslinking agent (genipin). *J. Biomed. Mater. Res.* **2001**, *55*, 538-546.

(22) Van Luyn MJA, Van Wachem PB, Olde Damink LHH, Dijkstra PJ, Feijen J, Nieuwenhuis P. Relations between in vitro cytotoxicity and cross-linked dermal sheep collagens. *J. Biomed. Mater. Res.* **1992**, *26*, 1091-1110.

(23) "Standard Test Method for Tensile Properties of Thin Plastic Sheeting," ASTM D 882-00.

(24) Gosline JM, French CJ. Dynamic mechanical properties of elastin. *Biopolymers* **1979**, *18*, 2091-2103.

(25) Aklonis JJ *Introduction to Polymer Viscoelasticity*; Wiley-Interscience: New York, **1983**.

(26) Abbott WM, Cambria RP *Biologic and Synthetic Vascular Prostheses*; Gurne & Stratton: New York, **1982**.

(27) Gosline J, Lillie M, Carrington E, Guerette P, Ortlepp C, Savage K. Elastic proteins: biological roles and mechanical properties. *Philos. Trans. R. Soc. Lond. B Biol. Sci.* **2002**, *357*, 121-132.

(28) Riande E, Diaz-Calleja R, Prolongo MG, Masegosa RM, Salom C *Polymer Viscoelasticity: Stress and Strain in Practice*; Marcel Dekker: New York, **2000**.

(29) Ulrich H *Chemistry and Technology of Isocyanates*; Wiley: New York, **1996**.

(30) Mraz J, Bouskova S. 2,4-toluenediisocyanate and hexamethylenediisocyanate adducts with blood proteins: assessment of reactivity of amino acid residues in vitro. *Chem. Biol. Interact.* **1999**, *117*, 173-186.

(31) Panitch A "Design, synthesis and characterization of artificial extracellular matrix proteins for tissue engineering," Ph.D. Thesis, University of Massachusetts Amherst, **1997**.

(32) Lee J, Macosko CW, Urry DW. Elastomeric polypentapeptides cross-linked into matrixes and fibers. *Biomacromolecules* **2001**, *2*, 170-179.

(33) Lee J, Macosko CW, Urry DW. Swelling behavior of gamma-irradiation cross-linked elastomeric polypentapeptide-based hydrogels. *Macromolecules* **2001**, *34*, 4114-4123.

(34) Li B, Alonso DOV, Daggett V. The molecular basis for the inverse temperature transition of elastin. *J. Mol. Biol.* **2001**, *305*, 581-592.

3 CONTROLLED PROTEOLYTIC DEGRADATION OF PROTEIN-BASED BIOMATERIALS

3.1 Abstract

A new method to easily tailor the proteolytic degradation of protein-based biomaterials is presented. By introducing slight alterations into the primary amino acid sequences of cell-adhesive, elastin-like proteins, the degradation kinetics and resulting patterns of proteolytic fragments are altered. Degradation of protein-polymers containing the VPGIG elastin-like sequence was minimal after 6 h exposure to 0.22 μM elastase (k_{cat} = 0.007 s^{-1}, K_m = 504 μM), while incorporation of lysine residues within this elastin-like domain increased the degradation rate such that no intact protein was present after 6 h exposure (k_{cat} = 0.033 s^{-1}, K_m = 2451 μM). These engineered proteins were crosslinked into freestanding, implantable films with initial elastic moduli ranging from 0.12 - 0.65 MPa. Incorporation of lysine residues within the elastin-like domain resulted in a two-to-sevenfold increase in the bulk material degradation rate compared to the VPGIG elastin-like protein. These results demonstrate the usefulness of protein engineering to create new cell-adhesive biomaterials with tunable initial moduli and degradation properties.

Manuscript prepared for submission by Sarah C. Heilshorn[1], Paul J. Nowatzki[1], Tetsuji Yamaoka[2], David A. Tirrell[1]

(1) Division of Chemistry and Chemical Engineering, California Institute of Technology

(2) Department of Polymer Science and Engineering, Kyoto Institute of Technology

3.2 Introduction

The ability to tailor the degradation rate of implanted biomaterials is a necessity when designing materials for specific medical uses. In traditional synthetic biomaterials, a variety of strategies have been employed to control degradation rates. These include optimization of polymer chemistry to alter the concentration of hydrolysable bonds,[1-3] blending of polymer crosslink units to control network structure,[4] and inclusion of peptides into a synthetic polymer network to promote sequence-specific degradation by matrix metalloproteinases.[5] In this work, we employ a genetic engineering approach to design protein-based biomaterials with tailored proteolytic degradation rates.

Engineered proteins are an attractive class of biomedical materials due to their templated biosynthesis, which allows precise control of molecular architecture. This strategy has been utilized in the *de novo* design of artificial proteins exhibiting a variety of novel structural and biomimetic properties.[6-11] Artificial proteins containing elastin-like repeats are of particular interest due to their high expression levels, ease of purification,[12] biocompatibility,[13] and tunable mechanical properties.[14-16] By judicious placement of crosslinking sites, the elastic modulus of the resulting bulk biomaterial can be controlled within the range of 0.1-1.0 MPa.

To promote cell interactions with these biomaterials, various cell-binding and cell-signaling domains have been interspersed with the elastin-like structural units.[17-21] Incorporation of the CS5 domain into these elastin-like polymers promotes sequence-specific spreading and adhesion of human umbilical vein

endothelial cells (HUVEC).[18,22] These materials exhibit many of the characteristics desirable for use as small-diameter vascular grafts, including elasticity similar to natural blood vessels and adhesion of endothelial cells.

Numerous enzymes with proteolytic capabilities exist *in vivo*; however, native elastin is resistant to many of these proteases, with the notable exception of elastase.[23] Therefore, this study seeks to quantify the elastase degradation of engineered elastin-like materials and develop strategies by which this degradation rate can be altered. Two forms of elastase are commonly found in humans, pancreatic elastase and leukocyte elastase (HLE, also known as lysosomal elastase, granulocyte elastase, polymorphonuclear elastase, and neutrophil elastase), which differ in substrate specificity and inhibitor sensitivity. HLE preferentially cleaves the peptide bond directly following small, hydrophobic amino acid side chains.[24] Elastase activity is greatly affected by enzyme-substrate contacts remote from the active site.[25,26] This suggests that appropriate genetic engineering of the elastin-like repeat within engineered protein-polymers would allow tuning of HLE degradation rates. Indeed, a comparison of HLE degradation of protein-polymers containing two distinct elastin-like sequences (Figure 3.1) resulted in different patterns of proteolytic fragments and a large difference in the rate of bulk material degradation. This change in degradation was caused by insertion of lysine residues into the elastin-like sequence while maintaining the authenticity of the CS5 cell-binding domain. Therefore, a protein-design strategy has been validated as a novel method to control degradation rates of protein-based, cell-adhesive biomaterials.

Protein aE1

M MASMTGGQQMG HHHHHHH DDDDK {LD GEEIQIGHIPREDVDYHLYP G [(VPGIG)$_2$VPGKG(VPGIG)$_2$]$_4$ }$_3$ LE
T7 tag *His tag* *CS5 cell-binding domain* *elastin-like domain*

Mol Wt. = 37.1 kDa; expected fragments = multiples of 1.3, 1.7, and 3.7 kDa

Protein aE2

M MASMTGGQQMG RKTMG {LD GEEIQIGHIPREDVDYHLYP G [VPGIG]$_{25}$ VP}$_3$ LEKAAKLE
T7 tag *CS5 cell-binding domain* *elastin-like domain*

Mol. Wt. = 43.0 kDa; expected fragments = 2.6, 13.4, 16.0, 26.9, 29.5, and 38.1 kDa

Protein aE3

M MASMTGGQQMG RKTMG {LD GEEIQIGHIPREDVDYHLYP G [VPGIG]$_{25}$ VP}$_3$ LEKAAKLE
T7 tag *CS5 cell-binding domain* *elastin-like domain*

Mol. Wt. = 16.1 kDa (fragmentation not analyzed – crosslinked films only)

Figure 3.1 Amino acid sequences of the engineered elastin-like proteins. Protein aE1 has three repeats of the CS5 and lysine-containing elastin-like domains. Protein aE2 has three repeats of the CS5 and elastin-like domains with lysine residues at the C- and N-termini only. Protein aE3 is identical to aE2 except it contains only one repeat, decreasing the molecular weight between the lysine residues at the C- and N-termini. The preferred elastase cleavage sites, based on N-terminal sequencing of proteolytic fragments (Table 3.1), are identified by arrows. Cleavage at these sites would result in the listed fragment mass sizes.

3.3 Experimental

3.3.1 Protein expression and purification.

Plasmids encoding sequences aE1, aE2, and aE3 have been previously described.[14,15] Proteins were expressed in *E. coli* and purified as reported.[18] Purity was assessed by SDS-PAGE and Western blotting with anti-T7 tag-horseradish peroxidase conjugate antibody (Novagen).

3.3.2 Analysis of elastase degradation fragments.

The degradation reaction was carried out at 37°C for 3 days in sodium borate buffer, pH 8, with 0.22 μM human leukocyte elastase (HLE, Elastin Products Company, Owensville, MO) and 100 μM protein aE1 or aE2. Samples were taken at 0, 1, 3, 6, 12, 24, 48, and 72 h and diluted with an equal amount of 2X SDS-sample buffer including β-mercaptoethanol and frozen at -20°C. Samples were boiled for 5 min and run on a 12% Tris-tricine gel at 150 V for 1 h. Gels were run in triplicate and either stained with Coomassie blue, transferred to PVDF membrane for N-terminal sequencing of proteolysis fragments, or transferred to nitrocellulose for Western blot analysis using an anti-T7 tag-horseradish peroxidase conjugate antibody. Densitometry was performed on Western blots using Image J (NIH freeware image analysis program) to quantify the amount of whole-length protein remaining at each time point, as compared to known whole-length protein concentrations. N-terminal sequencing by Edman degradation was performed on proteolysis fragments at the California

Institute of Technology Protein/Peptide Micro Analytical Laboratory using a protein micro-sequencer (Applied Biosystems, model 492).

3.3.3 Kinetics of elastase degradation.

The degradation reaction was carried out at 37°C for 6 h in sodium borate buffer, pH 8, with 0.22 μM HLE and 5-108 μM protein under constant mixing. The extent of reaction was characterized using 2,4,6-trinitrobenzene sulfonic acid at 4°C to quantify the number of N-termini in solution at 0, 1, 2, 4, and 6 hours. Six replicates of each substrate concentration were performed.

3.3.4 Crosslinking of protein films.

To crosslink proteins aE1 and aE2, 30 mg of protein was dissolved in 250 μL of water at 4°C, and tris-succinimidyl aminotriacetate (TSAT) was dissolved in 50 μL of 25:75 dimethylformamide:dimethyl sulfoxide at 4°C. The two solutions were rapidly mixed and pipetted into an open-faced mold. Films were dried overnight at 55°C. To achieve similar elastic moduli between the two films, a 0.35:1 ratio of succinimidyl ester functional groups to primary amines was used to crosslink aE, while a 1:1 ratio was used for aE3.

Matching previous work, aE2 was crosslinked with hexamethylene diisocyanate (HMDI) in dimethylsulfoxide,[16] and aE1 was crosslinked with bis(sulfosuccinimidyl) suberate (BS3) in 4°C water.[15] The crosslinker concentrations were chosen such that each film had an initial elastic modulus of ~0.6 MPa, similar to that of native elastin.[27] For aE1, the ratio of succinimidyl

ester groups in BS3 to primary amines in the protein was 1:1; for aE2, a 5:1 stoichiometric ratio of isocyanates to primary amines was used.

3.3.5 Elastase degradation of crosslinked films.

Crosslinked films (~3 mg dry, approximate dimensions = 0.25 x 1.5 x 12 mm) were exposed to 0.5 mL of 0.22 μM elastase in PBS solution at 37°C. At various time points, samples were removed, equilibrated for 15 min in PBS (pH 7.4, 37°C), and tensile tested with a modified Instron instrument (model 5542). Samples were extended 20% at a rate of 10% gauge length/min; at this slow rate and minimal extension, viscoelastic effects and hysteresis were observed to be negligible. The elastic moduli were calculated over the initial portion (0-4%) of the stress-strain curves. The samples did not noticeably swell or shrink during the course of the experiment, so the initial cross-sectional area of each sample was used to calculate stress at all time points.

3.3.6 Weight fraction protein.

Protein content of the films was determined from the mass difference between wet and dry samples. Wet samples were prepared by equilibration in PBS, pH 7.4, 37°C, followed by wicking away of excess buffer with filter paper. Films were dried at 50°C for 12 hours in a vacuum oven.

3.4 Results and Discussion

3.4.1 Protein expression and purification.

The purification takes advantage of the differential solubility of elastin-like proteins above and below a lower critical solution temperature. Thermal cycling and centrifugation was used to purify proteins aE1, aE2, and aE3 in yields of 2.6, 6.6, and 2.1 g, respectively, from 10 L batch fermentations, which correspond to expression yields of 10, 22, and 7 mg/g wet cell mass.

3.4.2 Elastase degradation of engineered proteins with altered elastin-like sequences.

The pattern of proteolytic fragments formed during HLE degradation was analyzed by SDS-PAGE and is shown in Figure 3.2; the number of fragments versus time is indicated in Figure 3.3. To simulate physiologically relevant conditions, the degradation reaction was performed at 37°C, above the LCST for both proteins. As expected, the variations in amino acid sequence within the elastin-like domains altered HLE degradation of the two synthetic proteins. HLE degradation of protein aE1 resulted in many smaller bands of fragments after only 1 h of elastase exposure and complete protein degradation at 12 h. In contrast, degradation of protein aE2 resulted in six primary fragments, approximately 3, 12, 15, 27, 30, and 38 kD in mass, and complete protein degradation at 72 h. Therefore, both the time course of degradation and the resulting molecular weights of proteolytic fragments can be altered by replacing the lysine residues within the elastin-like domain of protein aE1 with isoleucine residues in protein aE2.

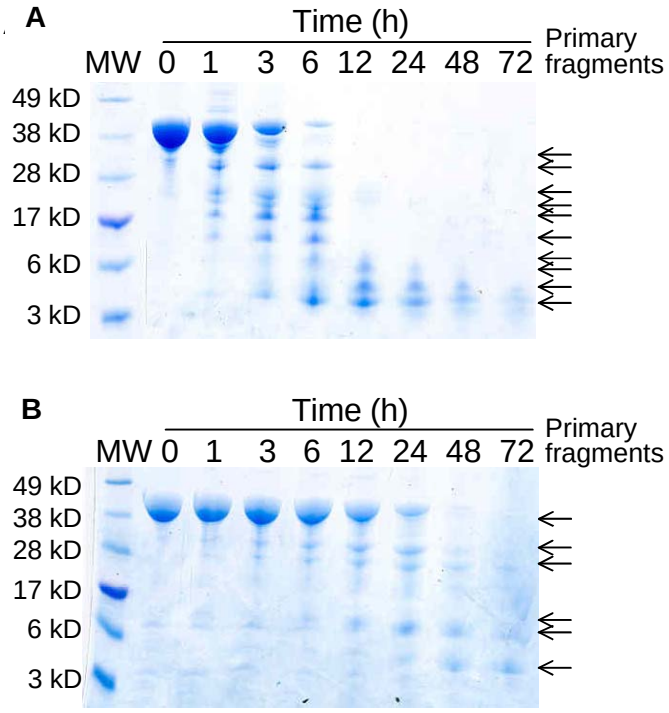

Figure 3.2 SDS-PAGE of elastase degradation fragments of proteins aE1 (A) and aE2 (B). Protein aE1 is degraded into several fragments that form a "ladder" of molecular weights, denoted by the arrows to the right. Protein aE2 degrades into six fragments with approximate molecular weights of 3, 12, 15, 27, 30, and 38 kD, again denoted by the arrows. These fragment sizes correspond to the predicted proteolytic fragment molecular weights in Figure 3.1.

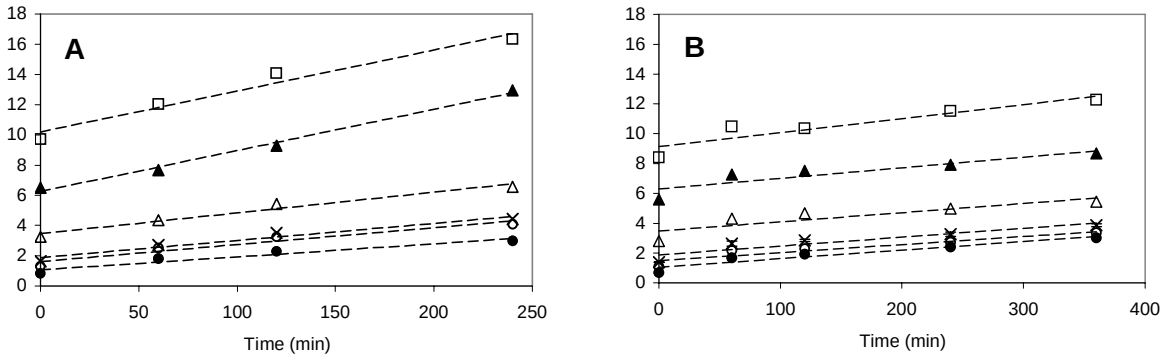

Figure 3.3 Number of N-termini detected at each time point for proteins aE1 (A) and aE2 (B). Protein concentrations for A are 108, 72, 36, 18, 14, and 9 μM (descending). Protein concentrations for B are 93, 62, 31, 16, 12, and 6 μM.

N-terminal sequencing of several degradation bands revealed that the peptide bond after isoleucine was the favored cut-site of both proteins aE1 and aE2 (Table 3.1). Although synthetic peptide studies have suggested that valine is the optimum cut-site for HLE, other side chains including alanine, methionine, leucine, isoleucine, and threonine have been reported, as have the artificial amino acids norvaline and norleucine.[26,28,29] Protein aE1 appeared to cleave preferentially at the isoleucines contained within the elastin-like sequences, resulting in many degradation fragments varying in size by one elastin-unit repeat. In contrast, protein aE2 was preferentially cleaved at the isoleucines contained within the CS5 cell-binding domains. Based on the N-terminal sequencing results, the cleavage sites and the molecular weight patterns of proteolytic fragments for proteins aE1 and aE2 were predicted (Figure 3.1).

Table 3.1 N-terminal sequencing results of selected proteolytic fragments.

Protein	Fragment size (kD)	Called sequence	Protein region of the called sequence	N-terminal cut site of the called sequence
aE1	28	GVPGIG	Elastin-like domain	Isoleucine
	28	MMASM	N-terminus	Not applicable
	21	GVPGI	Elastin-like domain	Isoleucine
	17	GVPGIG	Elastin-like domain	Isoleucine
	17	MMASM	N-terminus	Not applicable
aE2	15	MMASM	N-terminus	Not applicable
	12	GHIPRE	CS5 domain	Isoleucine

Consistent with the hypothesis that protein aE1 is cleaved at multiple sites within the elastin-like domain, Figure 3.3A contains a "ladder" of proteolytic fragment sizes. Similarly, the predicted fragment sizes of protein aE2 match well with the bands in Figure 3.3B.

It has previously been found that, owing to the high content of hydrophobic amino acids in the elastin-like domain, various protein fragments stain with Coomassie blue very differently depending on the presence or absence of the T7 tag (unpublished data). Therefore, Western analysis was used to determine the amount of full-length, intact protein remaining after HLE exposure for various times (Figure 3.4A). Densitometry was employed to quantify the percent of full-length protein remaining at each time point (Figure 3.4B). At 6 h, 0% of protein aE1 remained intact compared to over 90% of protein aE2. The reaction velocity is constant for both reactions, although protein aE2 degrades over a much longer time scale than protein aE1. This suggests that the protein concentration for each reaction is saturating, i.e., the substrate concentration is much higher than the Michaelis constant (K_m), and the reaction rates are at their maximum velocities. (This assumption is validated by more rigorous kinetic testing below; see Figure 3.5.) Therefore, the approximate degradation rate constant, k_{cat}, is 0.036 s^{-1} for protein aE1 and 0.003 s^{-1} for protein aE2.

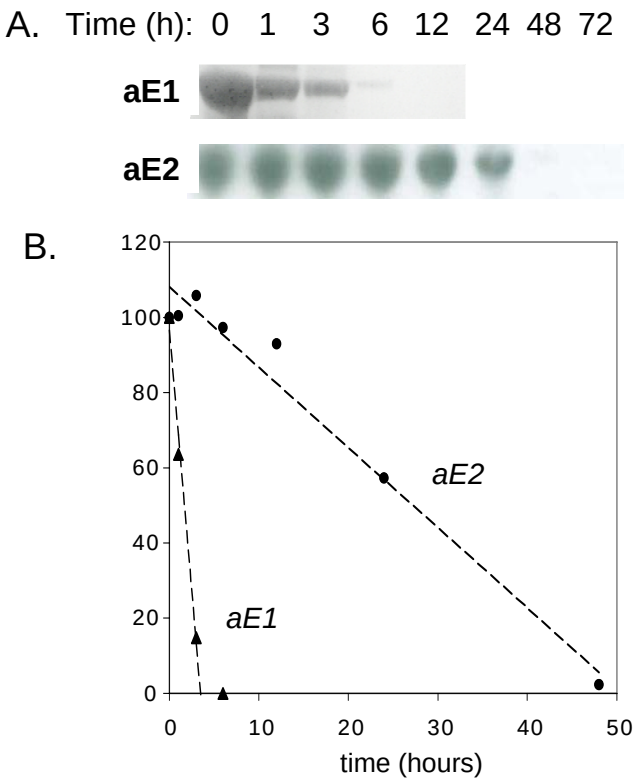

Figure 3.4 (A) Western blot of full-length, intact proteins aE1 and aE2 remaining after HLE exposure. (B) Full-length protein aE1 and aE2 remaining after HLE exposure at various time points.

A more rigorous kinetic analysis was performed using 2,4,6-trinitrobenzene sulfonic acid to determine the kinetic constants of the degradation reaction (Figure 3.5). Similar to the results above, constant initial reactions rates were found for both proteins aE1 and aE2 at each substrate concentration tested. The relationship between initial reaction rate and substrate concentration for both proteins aE1 and aE2 fit the Michaelis-Menten enzyme kinetic model, yielding coefficients of determination, i.e., R-values, of 0.95 and 0.77, respectively. Because of the slow degradation of protein aE2, the data had a lower signal-to-noise ratio and thus more uncertainty was introduced into the

parameter fitting. Nevertheless, the determined k_{cat} values of 0.033 s^{-1} and 0.007 s^{-1} for proteins aE1 and aE2, respectively, are in good agreement with the degradation rate constants calculated using the densitometry method described above.

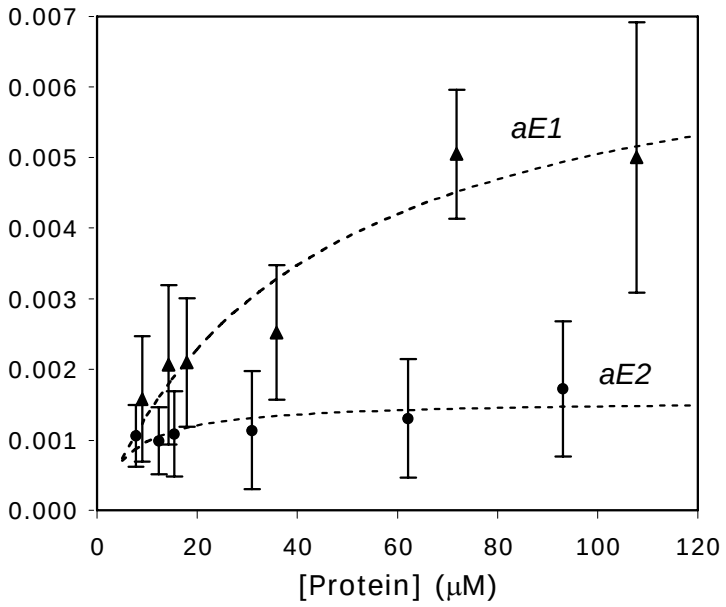

Figure 3.5 Kinetic analysis of elastase degradation of proteins aE1 and aE2. Error bars represent a 90% confidence interval. Dashed lines represent best fits of the observed data to the Michaelis-Menten model.

Because the molecular weight (aE1=37,100 Da, aE2=43,000 Da) and isoleucine content (aE1=57 residues/chain, aE2=84 residues/chain) of each protein are different, Michaelis constant (K_m) values were determined both as a function of total protein concentration ($K_{m,bulk}$), which is relevant for bulk material degradation, and isoleucine concentration ($K_{m,Ile}$), which is relevant for comparison of reaction rates. For protein aE1, $K_{m,bulk}$ is 43 μM and $K_{m,Ile}$ is

2.45 mM. For the slower degrading protein aE2, $K_{m,bulk}$ is 6 μM and $K_{m,Ile}$ is 0.50 mM. Interestingly, $k_{cat}/K_{m,Ile}$, a measure of the enzyme's "kinetic perfection,"[30] is similar for both reactions (aE1=13.5 $s^{-1}M^{-1}$, aE2=13.9 $s^{-1}M^{-1}$). Therefore, at substrate concentrations much lower than $K_{m,bulk}$, the two proteins will degrade at similar rates; however, at higher substrate concentrations, which are required for freestanding, implantable films as described later (Figure 3.6), the maximal degradation velocities of the two proteins are markedly different.

The time required for the reaction to occur was qualitatively similar to those published in the literature for elastase degradation of elastin and much longer than the times required for the synthetic peptide substrate reactions.[28,31-33] However, these reports did not analyze the kinetic constants of the degradation of insoluble elastin. Kinetic constants for HLE degradation of plasmin have been reported using an indirect competitive reaction method to measure K_m and a direct turbidimetric method to measure k_{cat}. These data report a K_m value (0.442 μM) much lower than that of proteins aE1 and aE2 and a k_{cat} value (0.022 s^{-1}) similar to protein aE1.[34] Meanwhile, the K_m and k_{cat} values reported for HLE degradation of soluble synthetic peptide substrates vary from 140-160,000 μM and 0.01-37 s^{-1}, respectively, depending on amino acid sequence.[25,28]

3.4.3 Elastase degradation of crosslinked protein films.

Next, freestanding films of the crosslinked proteins were exposed to HLE to determine if the degradation rates of bulk protein-based biomaterials were similarly altered by changes in the primary amino acid sequence. Use of the trifunctional crosslinker molecule tris-succinimidyl aminotriacetate (TSAT) allowed at different ratios for aE1 and aE3 allowed the initial elastic moduli (and thus the molecular weight between crosslinks), water content, and dimensions of the films being compared to be similar; physical properties of the films are listed below in Table 3.2. By substituting the lower-molecular weight protein aE3 for the architecturally identical protein aE2 in the films, a smaller molecular weight between crosslinks (M_c), and thus a higher elastic modulus (E) similar to protein aE1 could be achieved.

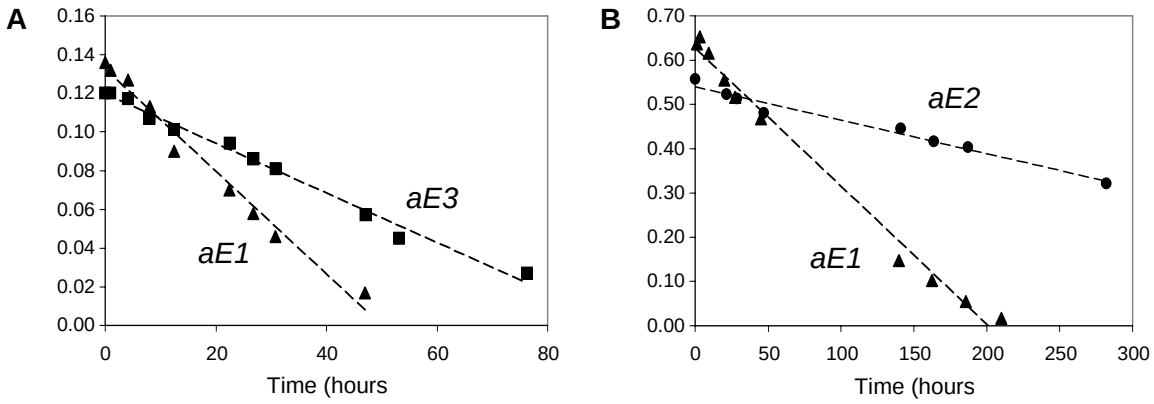

Figure 3.6 (A) Decrease in elastic modulus after HLE exposure of protein films aE1 (triangles) and aE3 (squares) formed with TSAT crosslinking chemistry. (B) Decrease in elastic modulus after HLE exposure of crosslinked protein films aE1 (triangles) and aE2 (circles) formed with differing crosslinking chemistries to yield high initial moduli.

Table 3.2 Properties and degradation rates of crosslinked elastin-like protein films.

Protein	Crosslinker / stoichiometry	Weight fraction polymer	Sample polymer mass (mg)	E_o (MPa)	M_c initial (kDa/mol)	Degradation rate constant (s^{-1})
aE1	TSAT 0.35×	0.35	2.8	0.136	25.9	0.0058
aE3	TSAT 1.0×	0.37	2.6	0.120	31.0	0.0022
aE1	BS3 1×	0.52	4.0	0.65	8.0	0.0110
aE2	HMDI 5×	0.73	2.6	0.56	13.1	0.0015

As expected, films of protein aE3 degraded significantly faster than did films of protein aE1 (Figure 3.6A), reflecting the results for the soluble proteins. If it is assumed that these films behave like ideal networks and that the substrate concentration is saturating, an approximate first-order rate constant of degradation can be determined. The substrate concentration for each film listed in Table 3.2 is greater than 10 mM, which is about three orders of magnitude larger than the $K_{m,bulk}$ values determined from Figure 3.5. Similarly, the protein concentration required for a variety of biomedical applications such as tissue engineering scaffolds, drug-delivery vehicles, or implanted materials for tissue reconstruction would presumably be much larger than $K_{m,bulk}$. Therefore, the degradation reaction will proceed at maximal velocity. HLE is assumed to diffuse freely into the water-rich, highly mobile elastin-like networks; the observed uniformity of degradation throughout the film cross-section, as opposed to degradation only at the film surfaces, supports this assumption. Prior work with these [14-16] and other elastin-like proteins[35] have shown that the ideal network assumption is a reasonable one. For an ideal rubber network,

$E=3\rho RT/M_c$, where E is the elastic modulus, ρ is the polymer density (taken to be 1.3 g/ml,[36] multiplied by the appropriate volume fraction polymer from Table 3.2), T is the temperature, and M_c is the molecular weight between effective crosslinks.[37] The molar concentration of effective crosslinks can then be calculated from the total dry film mass divided by M_c. As the film is degraded, the concentration of effective crosslinks is reduced; therefore, the maximal degradation velocity is defined as the loss in effective crosslinks over time. The effective degradation rate constants are listed in Table 3.2 above. Because some peptide cleavages will not result in loss of an effective crosslink, the degradation rate constants calculated from this analysis are smaller than the k_{cat} values determined above. Analogously to the degradation rates of uncrosslinked proteins, the insertion of lysine residues into the elastin-like domains resulted in quicker bulk film degradation.

The difference in degradation rates is also apparent when comparing films of much higher initial elastic moduli (Figure 3.6B), although the comparison is less straightforward because the crosslinker and water content are different. Films of protein aE1 and protein aE2, crosslinked with bis(sulfosuccinimidyl suberate) (BS3) and hexamethylene diisocyanate (HMDI), respectively, were previously characterized as having initial elastic moduli near 0.6 MPa, typical of native elastin.[15,16,27] Film aE1 displayed an effective degradation rate constant 7.3 times larger than film aE2 (Table 1). Taken together, these results demonstrate that crosslinked films of elastin-like engineered proteins can be designed to have a variety of initial moduli and HLE degradation rates.

3.4.4 Elastase concentration considerations.

It is important to note that the HLE concentration used in these experiments was chosen somewhat arbitrarily based on previous studies analyzing degradation kinetics of synthetic substrates. The HLE level chosen, 6.3 μg/ml or 0.22 μM, resulted in degradation rates easily quantified over short time scales, i.e., hours and days. This allowed the facile comparison of elastase degradation through design of the elastin-like sequence. Clinical studies cite HLE levels of 53.3 ± 9.3 ng/ml in human plasma.[38] Furthermore, HLE activity is tightly regulated *in vivo* by natural inhibitors; therefore, the same concentration of purified HLE will display much higher activity *in vitro*.[39] Further complicating this matter, serum levels of HLE are thought to increase in response to sepsis and procedures requiring cardiopulmonary bypass.[40,41] For these reasons, future analyses of degradation rates of engineered proteins for specific medical applications will be most instructive if evaluated *in vivo*. This work represents a first step in establishing the kinetics and time-scales of elastase degradation and validates the genetic engineering approach as a novel method to tailor substrate degradability.

3.5 Conclusions

This study demonstrates the usefulness of a novel genetic engineering method to synthesize biomaterials with controlled degradation rates for potential medical applications. Two synthetic proteins containing identical cell-binding domains were shown to exhibit altered patterns of HLE degradation based on the amino acid sequence engineered within the elastin-like domain. Insertion of lysine residues into the elastin-like domain resulted in a bulk, crosslinked film with an effective degradation rate constant 2.6 to 7.3 times larger than films without lysines in the elastin-like domains. Through variation in the conditions of crosslinking and genetic engineering of the molecular weight between crosslinks, the moduli of elastin-like synthetic protein films can also be tailored. Control over the initial modulus and degradation rate along with the ability to include cell-recognition domains within the synthetic proteins suggest these materials may be useful in designing tissue engineering scaffolds, drug-delivery vehicles, or implanted materials for tissue reconstruction.

Acknowledgments

This work was supported by NIH Grant 5 ROI HL59987-03, NSF Grant BES-9901648, and the NSF East Asia Summer Institute. N-terminal sequencing was performed by the Caltech Protein/Peptide Microanalytical Laboratory and supported by The Beckman Institute at Caltech.

3.6 References

(1) Elbert DL, Hubbell JA. Conjugate addition reactions combined with free-radical cross-linking for the design of materials for tissue engineering. *Biomacromolecules* **2001**, *2*, 430-441.

(2) Davis KA, Burdick JA, Anseth KS. Photoinitiated crosslinked degradable copolymer networks for tissue engineering applications. *Biomaterials* **2003**, *24*, 2485-2495.

(3) Kim BS, Hrkach JS, Langer R. Biodegradable photo-crosslinked poly(ether-ester) networks for lubricious coatings. *Biomaterials* **2000**, *21*, 259-265.

(4) Rydholm AE, Bowman CN, Anseth KS. Degradable thiol-acrylate photopolymers: polymerization and degradation behavior of an in situ forming biomaterial. *Biomaterials* **2005**, *26*, 4495-4506.

(5) Lutolf MP, Lauer-Fields JL, Schmoekel HG, Metters AT, Weber FE, Fields GB, Hubbell JA. Synthetic matrix metalloproteinase-sensitive hydrogels for the conduction of tissue regeneration: Engineering cell-invasion characteristics. *Proc. Natl. Acad. Sci. U. S. A.* **2003**, *100*, 5413-5418.

(6) McPherson DT, Xu J, Urry DW. Product purification by reversible phase transition following Escherichia coli expression of genes encoding up to 251 repeats of the elastomeric pentapeptide GVGVP. *Protein Expr. Purif.* **1996**, *7*, 51-57.

(7) Petka WA, Harden JL, McGrath KP, Wirtz D, Tirrell DA. Reversible hydrogels from self-assembling artificial proteins. *Science* **1998**, *281*, 389-392.

(8) Krejchi MT, Atkins EDT, Waddon AJ, Fournier MJ, Mason TL, Tirrell DA. Chemical sequence control of beta-sheet assembly in macromolecular crystals of periodic polypeptides. *Science* **1994**, *265*, 1427-1432.

(9) Szela S, Avtges P, Valluzzi R, Winkler S, Wilson D, Kirschner D, Kaplan DL. Reduction-oxidation control of beta-sheet assembly in genetically engineered silk. *Biomacromolecules* **2000**, *1*, 534-542.

(10) O'Brien JP, Fahnestock SR, Termonia Y, Gardner KCH. Nylons from nature: Synthetic analogs to spider silk. *Adv. Mater.* **1998**, *10*, 1185-1195.

(11) Meyer DE, Chilkoti A. Genetically encoded synthesis of protein-based polymers with precisely specified molecular weight and sequence by recursive directional

ligation: Examples from the elastin-like polypeptide system. *Biomacromolecules* **2002**, *3*, 357-367.

(12) Urry DW, Gowda DC, Parker TM, Luan CH, Reid MC, Harris CM, Pattanaik A, Harris RD. Hydrophobicity scale for proteins based on inverse temperature transitions. *Biopolymers* **1992**, *32*, 1243-1250.

(13) Urry DW, Parker TM, Reid MC, Gowda DC. Biocompatibility of the bioelastic materials, poly(GVGVP) and its gamma-irradiation cross-linked matrix - summary of generic biological test-results. *J. Bioactive and Compatible Polym.* **1991**, *6*, 263-282.

(14) Welsh ER, Tirrell DA. Engineering the extracellular matrix: A novel approach to polymeric biomaterials. I. Control of the physical properties of artificial protein matrices designed to support adhesion of vascular endothelial cells. *Biomacromolecules* **2000**, *1*, 23-30.

(15) Di Zio K, Tirrell DA. Mechanical properties of artificial protein matrices engineered for control of cell and tissue behavior. *Macromolecules* **2003**, *36*, 1553-1558.

(16) Nowatzki PJ, Tirrell DA. Physical properties of artificial extracellular matrix protein films prepared by isocyanate crosslinking. *Biomaterials* **2004**, *25*, 1261-1267.

(17) Nicol A, Gowda DC, Urry DW. Cell-adhesion and growth on synthetic elastomeric matrices containing Arg-Gly-Asp-Ser-3. *J. Biomed. Mater. Res.* **1992**, *26*, 393-413.

(18) Heilshorn SC, DiZio KA, Welsh ER, Tirrell DA. Endothelial cell adhesion to the fibronectin CS5 domain in artificial extracellular matrix proteins. *Biomaterials* **2003**, *24*, 4245-4252.

(19) Panitch A, Yamaoka T, Fournier MJ, Mason TL, Tirrell DA. Design and biosynthesis of elastin-like artificial extracellular matrix proteins containing periodically spaced fibronectin CS5 domains. *Macromolecules* **1999**, *32*, 1701-1703.

(20) Liu CY, Apuzzo MLJ, Tirrell DA. Engineering of the extracellular matrix: Working toward neural stem cell programming and neurorestoration - Concept and progress report. *Neurosurgery* **2003**, *52*, 1154-1165.

(21) Liu JC, Heilshorn SC, Tirrell DA. Comparative cell response to artificial extracellular matrix proteins containing the RGD and CS5 cell-binding domains. *Biomacromolecules* **2004**, *5*, 497-504.

(22) Heilshorn SC, Liu JC, Tirrell DA. Cell-binding domain context affects cell behavior on engineered proteins. *Biomacromolecules* **2005**, *6*, 318-323.

(23) Robert L, Robert AM, Jacotot B. Elastin-elastase-atherosclerosis revisited. *Atherosclerosis* **1998**, *140*, 281-295.

(24) Geneste P, Bender ML. Esterolytic activity of elastase. *Proc. Natl. Acad. Sci. U. S. A.* **1969**, *64*, 683-685.

(25) Thompson RC, Blout ER. Dependence of kinetic parameters for elastase-catalyzed amide hydrolysis on length of peptide substrates. *Biochemistry* **1973**, *12*, 57-65.

(26) Harper JW, Cook RR, Roberts CJ, McLaughlin BJ, Powers JC. Active-site mapping of the serine proteases human leukocyte elastase, cathepsin G, porcine pancreatic elastase, rat mast-cell protease-I and protease-II, bovine chymotrypsin-A-alpha, and staphylococcus-aureus protease V-8 using tripeptide thiobenzyl ester substrates. *Biochemistry* **1984**, *23*, 2995-3002.

(27) Abbott WM, Cambria RP *Biologic and Synthetic Vascular Prostheses*; Gurne & Stratton: New York, **1982**.

(28) Nakajima K, Powers JC, Ashe BM, Zimmerman M. Mapping the extended substrate binding-site of cathepsin-G and human-leukocyte elastase - studies with peptide substrates related to the alpha-1-protease inhibitor reactive site. *J. Biol. Chem.* **1979**, *254*, 4027-4032.

(29) McBride JD, Freeman HNM, Leatherbarrow RJ. Selection of human elastase inhibitors from a conformationally-constrained combinatorial peptide library. *Eur. J. Biochem.* **1999**, *266*, 403-412.

(30) Stryer L *Biochemistry*; 4 ed.; W. H. Freeman and Company: New York, **1995**.

(31) Rao SK, Mathrubutham M, Karteron A, Sorensen K, Cohen JR. A versatile microassay for elastase using succinylated elastin. *Anal. Biochem.* **1997**, *250*, 222-227.

(32) Reilly CF, Travis J. Degradation of human-lung elastin by neutrophil proteinases. *Biochim. Biophys. Acta* **1980**, *621*, 147-157.

(33) Morrison HM, Welgus HG, Owen CA, Stockley RA, Campbell EJ. Interaction between leukocyte elastase and elastin: quantitative and catalytic analyses. *Biochim. Biophys. Acta - Prot. Struct. Mol. Enzymol.* **1999**, *1430*, 179-190.

(34) Kolev K, Komorowicz E, Owen WG, Machovich R. Quantitative comparison of fibrin degradation with plasmin, miniplasmin, neurophil leukocyte elastase and cathepsin G. *Thromb. Haemost.* **1996**, *75*, 140-146.

(35) Aaron BB, Gosline JM. Elastin as a random network elastomer - a mechanical and optical analysis of single elastin fibers. *Biopolymers* **1981**, *20*, 1247-1260.

(36) Gosline J, Lillie M, Carrington E, Guerette P, Ortlepp C, Savage K. Elastic proteins: biological roles and mechanical properties. *Philos. Trans. R. Soc. Lond. B Biol. Sci.* **2002**, *357*, 121-132.

(37) Aklonis JJ *Introduction to Polymer Viscoelasticity*; Wiley-Interscience: New York, **1983**.

(38) Oudijk EJD, Nieuwenhuis HK, Bos R, Fijnheer R. Elastase mediated fibrinolysis in acute promyelocytic leukemia. *Thromb. Haemost.* **2000**, *83*, 906-908.

(39) Hornebeck W, Potazman JP, Decremoux H, Bellon G, Robert L. Elastase-type activity of human serum - its variation in chronic obstructive lung diseases and atherosclerosis. *Clin. Physiol. Biochem.* **1983**, *1*, 285-292.

(40) Mojcik CF, Levy JH. Aprotinin and the systemic inflammatory response after cardiopulmonary bypass. *Ann. Thorac. Surg.* **2001**, *71*, 745-754.

(41) Gohra H, Mikamo A, Okada H, Hamano KI, Zempo N, Esato K. Granulocyte elastase release and pulmonary hemodynamics in patients with mitral valvular disease. *World J. Surg.* **2002**, *26*, 643-647.

4 CORNEAL ONLAYS FROM CROSSLINKED ARTIFICIAL EXTRACELLULAR MATRIX PROTEINS

4.1 Abstract

An artificial protein designed to mimic key features of the extracellular matrix is proposed for use in corneal onlays. The protein contains an elastin-like repeating sequence to confer flexibility and a fibronectin-derived cell binding domain containing the peptide RGD (Arg-Gly-Asp) to promote adhesion of corneal epithelial cells. The protein was crosslinked through its lysine side chains with bis(sulfosuccinimidyl) suberate (BS3). The resulting onlay lenses were highly extensible (>350% strain) and had a Young's modulus of 0.17 ± 0.02 MPa. Implantation of the crosslinked lenses in rabbits (n=12) for one week indicated that the onlays were well-tolerated in the cornea. The onlays had fully re-epithelialized within 4-7 days of implantation, compared to 2-4 days for native corneal stroma. The cell morphology on the onlay implant was typical of regenerating epithelium, and only minimal inflammation was observed.

Manuscript prepared for submission by Paul J. Nowatzki[1], Daniel M. Schwartz[2], Marsha Cheung[2], Shiao Chang[3], Robert H. Grubbs[1], and David A. Tirrell[1]

(1) Division of Chemistry and Chemical Engineering, California Institute of Technology
(2) Department of Ophthalmology, University of California, San Francisco
(3) Calhoun Vision, Pasadena, CA

Portions of the Experimental and Results sections appear in U.S. Patent Application No. 11/040,130 (filed 1/23/2005). "Engineered Proteins and Methods of Making and Using." inventors David A. Tirrell, Daniel M. Schwartz, Paul J. Nowatzki, Robert H. Grubbs.

4.2 Introduction

Surgical procedures to correct refractive error, especially laser in situ keratomileusis (LASIK) and photorefractive keratectomy (PRK), have proven effective in the correction of myopia, astigmatism, and low to moderate hyperopia. However, these procedures have limited efficacy in the correction of high hyperopia and very high myopia.[1] Furthermore, the lack of reversibility of these procedures is a major drawback, because the refractive power of the cornea may change over time. In this work we describe the implantation of corneal onlays made from an artificial protein, with the ultimate goal of achieving a reversible but stable means for surgical refractive correction.

Corneal implants have recently attracted attention as reversible alternatives to ablative surgeries.[2] An implant would be designed based on its shape and index of refraction to change the refractive properties of the cornea in a prescribed way. The implant can be placed inside a flap cut into the corneal stroma (keratoplasty), called a *corneal inlay*, or at the anterior surface of the corneal stroma, just under the corneal epithelium (epikeratoplasty), called a *corneal onlay* (see Figure 4.1). The epithelium can be scraped off, or debrided, allowing the epithelium to grow back over the surface of the onlay. Alternatively, an epithelial flap can be peeled back and replaced on top of the onlay, reducing healing time, as is done in the ablative LASEK (laser epithelial keratomileusis) technique.[3]

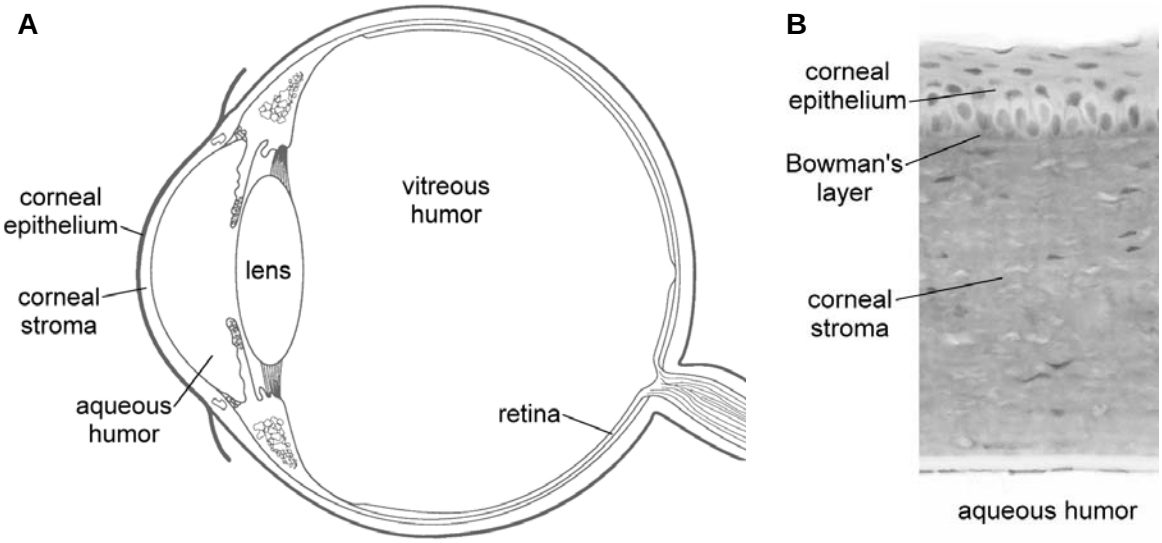

Figure 4.1 (A) Structure of the eye. (B) Histological cross-section of the cornea. A corneal onlay resides between the cellular corneal epithelium and collagenous stroma; an inlay is placed inside the stroma. The human cornea is 550 μm thick.

(B adapted from http://www.webmed.unibo.it/didattica/pezzetti/Connettivi/cornea20he.jpg)

The implantation of corneal onlays is particularly appealing because of its surgical simplicity, which, unlike LASIK or placing a corneal inlay, does not require use of a microkeratome to cut a corneal flap. Obviating this incision may prevent certain surgical complications of LASIK, which include corneal flap abnormalities,[4,5] epithelial ingrowth,[5] night vision disturbances,[6] and microbial keratitis.[7] The forward positioning of an onlay in the cornea is also preferable both optically and in minimizing its disruption to nutrient flow.[2] Because an onlay is not held in place by a corneal flap, there must be a means of adhering an onlay to the sub-epithelial layer (Bowman's layer) of the cornea.

Materials of both biologic and synthetic origins have been tested as corneal onlays. Human corneal tissue grafts resulted in abnormalities in epithelial cell physiology and extracellular matrix.[8-10] Because collagen is the primary component of corneal stroma, onlay lenses were made from collagen type IV, but these degraded over time.[11] This lack of stability due to proteolysis was seen in other collagen-based and collagen-hybrid lenses.[2] A consistent problem for synthetic corneal implants such as those made from poly(ethylene terephthalate), poly(methyl methacrylate), or polytetrafluoroethylene, on the other hand, is their inability to adhere an epithelium.[12,13] Synthetic materials designed for use as onlays that have been reported to support growth of epithelial cells include plasma-treated polyvinylalcohol copolymer hydrogels[14] and perfluoropolyethers, which were more effective when coated with collagen I.[2,15]

Based on these studies, the ideal properties of an effective corneal onlay material can be identified.[2,16] First, the material needs to be optically clear, dimensionally stable, and surgically handleable. A key requirement is its ability to adhere and permit migration and proliferation of epithelial cells. It must also be biocompatible over the long term, integrate closely with the surrounding tissue, not induce abnormal epithelial cell physiology, and be stable to proteases in the cornea. Ideally, its mechanical properties will be compatible with surrounding tissue and resistant to environmental stresses placed on the eye.

Biomimetic artificial proteins represent a new materials approach for corneal onlays. Genetic engineering has enabled the synthesis of proteins with

precisely controlled sequences and architectures.[17,18] These proteins should prove especially useful as biomaterials for several reasons. Their innate biocompatibility allows close interaction with surrounding tissue, potentially circumventing the foreign body reaction, which results in a fibrous capsule being formed around most synthetic polymer implants.[19] In particular, artificial proteins can include active peptide domains from natural proteins that promote cell adhesion[20] or direct cell differentiation.[21] Hybrid proteins containing modular combinations of structural, bioactive, and designed peptide sequences have been constructed,[18,22,23] with the idea of effecting multiple functionalities in a single material.

The work described here adapts an artificial protein, originally designed as a cell-adhesive material for use in vascular grafts, whose sequence is based on two naturally occurring extracellular matrix proteins, fibronectin and elastin. The amino acid sequence of the protein is shown in Figure 4.2. A 17-amino acid sequence taken from the tenth type III module of fibronectin including the RGD (Arg-Gly-Asp) sequence serves to support the adhesion and growth of an overlying epithelial cell layer. RGD is well-known to mediate adhesion through integrin cell-surface receptors to many cell types, thereby influencing morphology, migration, growth, and differentiation.[24] The RGD cell-binding domains are alternated with long sequences of elastin-like polypentapeptides that impart flexibility and resiliency. Elastin-like peptides of this type have been shown to be broadly biocompatible[25] and resistant to degradation,[26] and the highly dynamic, mobile structure of elastin[27] and elastin-like peptides[28] is

expected to facilitate diffusion through elastin-based matrices. Lysines are periodically spaced through the protein and serve as sites for crosslinking into stable matrices. This *artificial extracellular matrix protein* has been shown to attach endothelial cells specifically through the RGD cell binding domain,[23] and chemical crosslinking of similar materials resulted in transparent hydrogels with elastic moduli of 0.2 MPa.[29]

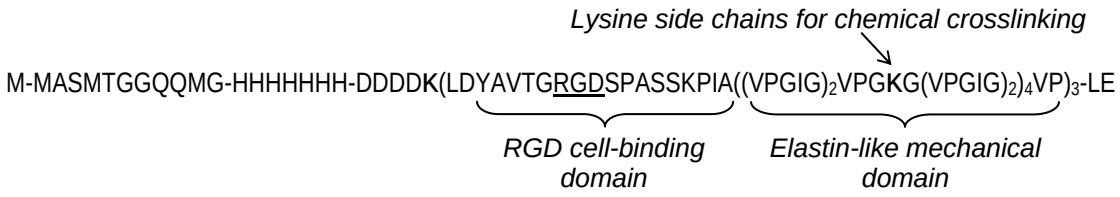

Figure 4.2 Amino acid sequence of the artificial extracellular matrix protein aE-RGD. The functions of key peptide elements are indicated.

It was hypothesized that this artificial extracellular matrix protein could be successful in corneal onlays because of its transparency, flexibility, resistance to degradation, permeability, and ability to adhere cells. Here, the artificial extracellular matrix protein was crosslinked into lens-shaped onlays, which were implanted into rabbit corneas using a corneal pocket model[30] and evaluated over the one week required for epithelialization. The results are sufficiently encouraging to merit longer-term implantation studies.

4.3 Experimental

4.3.1 Protein expression.

Protein aE-RGD, Figure 4.2, was cloned into *E. coli* by Liu et al.[23] The corresponding gene is under control of a T7 bacteriophage promoter: plasmid pET28RW-(RGD-EL4)$_3$.10a, expression host strain BL21 (DE3)pLysS. Its molecular weight is 34.8 kDa. The sequence contains three repeats of cell binding and elastin-like cassettes, with an N-terminal T7 tag for antibody identification, a 7-His tag for alternative purification, and an enterokinase cleavage site which can be used to remove the N-terminal portion.

Protein expression was performed as previously reported,[23] using standard methods. Briefly, host cells were grown in a 10 L fermenter (New Brunswick Scientific BioFlo 3000) using Terrific Broth medium at pH 7.4. At an optical density of ~6, protein expression was induced with 1 mM isopropyl-1-β-D-thiogalactosidase (IPTG); cells were harvested 1.25-1.75 hours after induction by centrifugation at 4°C.

4.3.2 Protein purification.

Cells containing the expressed aE-RGD protein were resuspended in TEN buffer (10 mM Tris-HC1, pH 7.5, 1 mM EDTA, 100 mM NaCl) at a concentration of 0.5 g/mL and frozen at -20°C. The suspension was defrosted, lysing the cells, and shaken with 10 μg/mL of deoxyribonuclease I, 10 μg/mL of ribonuclease A, 5 mM magnesium chloride, and 1 mM phenylmethylsulfonyl fluoride to inhibit

proteolysis, at 37 °C for 3 h. The lower critical solution temperature (LCST) of aE-RGD at 35 °C,[23] where the protein separates from an aqueous solution as the temperature is raised,[31] allows the protein to be purified by temperature cycling. The pH of the cell lysate was adjusted to 9.0, to ensure protein solubility, and the solution was centrifuged below the LCST (~1 h, ≥28,000×g, 4°C). To the supernatant (containing the protein), 1 M NaCl was added, and centrifugation was repeated above the LCST (~1 h, ≥28,000×g, 37°C). The pellet was redispersed in water to a concentration of 50-100 mg/mL. The temperature cycling was repeated twice more to increase protein purity. The solution containing the aE-RGD protein was dialyzed at 4°C for 3 days, to remove salts and contaminants, and lyophilized. The purity and molecular weights of the protein were verified by SDS-PAGE gels and Western blot, using standard methods, and confirmed previous[23] amino acid analysis and matrix-assisted laser desorption ionization-mass spectrometry (MALDI-MS) observations. Typical 10 L fermentations using these procedures yielded ~300 grams wet cell mass and 1 to 2 grams pure aE-RGD.

4.3.3 Cross-linking aE-RGD to form corneal onlays.

Two-piece poly(methylmethacrylate) contact lens molds of 6 mm optic diameter and 7.5 mm radius (Ocular Technology Inc., Goleta, CA) were used for forming corneal onlays. The molds created onlay lenses ~135 μm thick. The crosslinking procedure was adapted from Di Zio et al.[29] All crosslinking steps were performed in a cold room at 4 °C, below the LCST of aE-RGD,[23] to ensure

transparency of the lenses. aE-RGD (20 mg) was dissolved in water (55 μL). Bis(sulfosuccinimidyl) suberate (BS3), a lysine-specific crosslinking molecule, was dissolved in water (2.3 mg in 20 μL). The two solutions were rapidly mixed (10 sec) in a microcentrifuge tube by pipet tip and were quickly spun (10 sec) on a tabletop centrifuge to remove bubbles introduced in mixing. Into each of five molds, 12 μL of the mixture was pipetted; the molds were stacked under a weight (300g) and crosslinking proceeded overnight at 4 °C. Lenses were removed from the molds at room temperature, rinsed in excess water, and stored in a sealed humidified container until use.

4.3.4 Mechanical testing.

Rectangular pieces of lenses (~2 × 5 × 0.115 mm) were tested in an Instron 5542 uniaxial tensile tester, modified to house the sample in phosphate buffered saline at 37 °C, using a strain rate of 10% of the original length per minute.[32]

4.3.5 Surgical implantation of lenses.

The technique to implant the onlays was adapted from Evans et al.[30] The rabbits used in the study (n = 12, adult albino) were anesthetized using inhaled 3% isoflurane and topical proparacaine. Throughout the surgery, the vital signs of the animals were carefully monitored, including the corneal reflex, heart rate, respiration, and oxygen saturation.

To hold the lenses in place on the surface of the cornea, a pocket was created surgically, as shown in Figure 4.3. The right eye of each animal was

irrigated with betadine solution, and a wire lid speculum was placed into the eye. A 3.0 mm trephine was used to create a partial thickness keratotomy, approximately 100-200 μm in depth in the central cornea. The 0.12 forceps and the 69 blade were used to remove the stromal lamella within the trephined area from the base of the keratotomy. This left a circular keratectomy of 3.0 mm in diameter. A sharp pocket blade was used to make a 3 mm wide circular intralamellar pocket at the base of the keratotomy extending circumferentially outward toward the corneal limbus.

Three groups of corneas were prepared. In group 1 (n = 3), the wounds were created but no implants were placed. In group 2 (n = 12), the same wounds were constructed, and then the 5.0 mm diameter corneal onlay implant was carefully placed on the corneal surface. The implant was tucked 360 degrees into the grooved pocket using a blunt cyclodialysis spatula. No sutures were placed in this group. In group 3 (n= 3), the same wound was constructed, the implants were placed in the pocket, and then 9-0 Nylon sutures were placed over the implant to keep it into place. After implantation, the eyes were irrigated with BSS solution. The rabbits were given an injection of Carprofen analgesic (5 mg/kg IM) postoperatively.

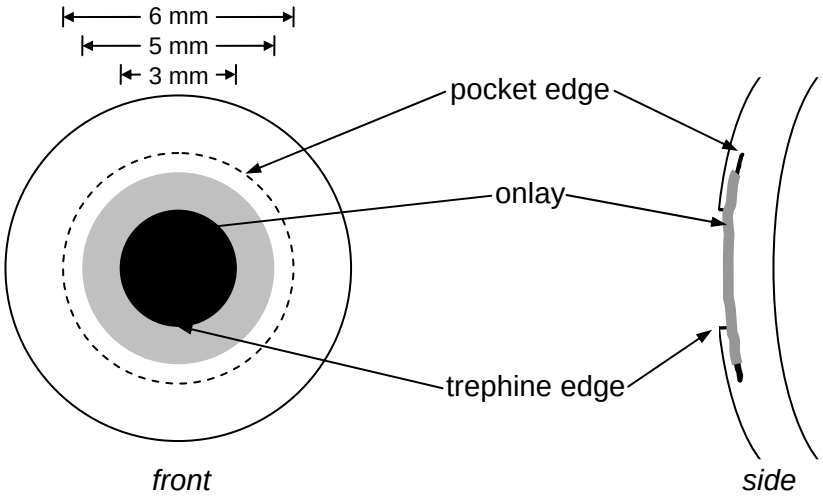

Figure 4.3 Schematic representation of the corneal pocket and implanted onlay lens.

4.3.6 Clinical evaluation.

Daily evaluation was performed for one week after implantation. The animals were closely followed for any signs of discomfort or wound infection. At any sign of discomfort, the animal was given one drop of topical 0.03% flurbiprofen and Carprofen 5 mg/kg IM q24 hours. The animals' weights were monitored. Slit lamp biomicroscopy was performed every 2-4 days following the initial procedure. Fluorescein staining with blue light was used to assess the speed and extent of epithelial cell growth on the onlays. Any signs of inflammation were noted.

4.3.7 Histology.

Rabbits were euthanized using standard guidelines for large animals, consisting of intramuscular ketamine 35-50 mg/kg and xylazine 5-10 mg/kg.

Each animal also received an intracardiac injection of sodium pentobarbital and underwent bilateral thoracotomy.

The eyes were fixed in glutaraldehyde solution and examined histologically at different time points. The slides were stained with hematoxylin-eosin (H&E), periodic acid-Schiff (PAS), Mason trichrome for collagen, and staining for mucopolysaccharides. Stained sections were mounted and viewed by light microscopy. The pattern of epithelial growth over the corneal implant was assessed histologically. The degree of inflammation both within the corneal stroma as well as within the implant was evaluated.

4.4 Results

4.4.1 Protein aE-RGD.

As shown in Figure 4.4A, the 35 kDa aE-RGD protein migrated as the predominant band on an SDS-PAGE Gel. Two minor bands are visible, indicating bacterial protein contaminants not fully removed during purification. T7-tag Western blotting, Figure 4.4B, confirmed the 35 kDa band as the aE-RGD protein.

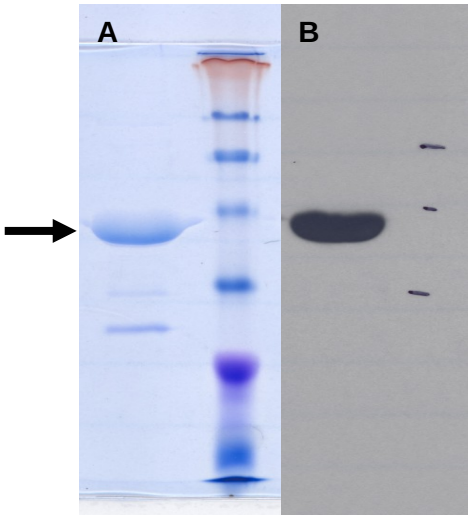

Figure 4.4 (A) SDS-PAGE and (B) Western blot analysis of aE-RGD. Minor impurity bands appear in the SDS-PAGE gel.

4.4.2 Mechanical characterization of lenses.

The crosslinked lenses remained transparent both during crosslinking at 4 °C, and when raised to 37 °C for mechanical testing. Because of the temperature-sensitive behavior of elastin-like protein films,[32,33] the onlays shrink from the 6.0 mm diameter × 0.135 mm thick mold dimensions to 5.0 mm diameter × 0.115 mm thick at 37 °C.

The tensile behavior of the lenses, shown in Figure 4.5, is characteristic of rubbery materials, consistent with previous tests of similarly designed artificial extracellular matrix proteins.[22,29,32] The elastic modulus, E, was measured to be 0.17 ± 0.02 MPa (n=3, from different batches), and each lens was extensible to at least 380% of its original length. Compared to BS3-crosslinked aECM proteins of similar design but different cell binding domain,[29] the lenses showed a similar elastic modulus but greater extensibility.

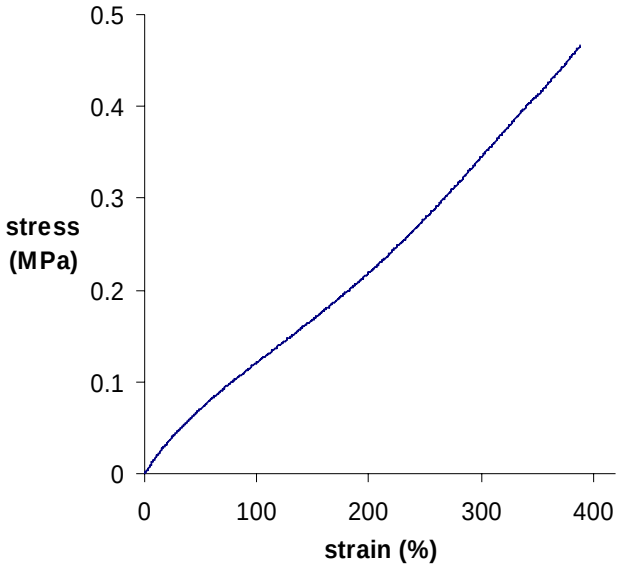

Figure 4.5 Representative uniaxial stress-strain behavior of a corneal onlay lens, tested at 37 °C in phosphate-buffered saline. E = 0.17 MPa.

The ability of the lenses to deform to high strains without failing is an advantage in their application as corneal onlays, which must withstand both surgical implantation and environmental forces once in place. The measured elastic modulus is similar to the 1 MPa suggested as an ideal compromise between the dual needs of compliance and wearer comfort, and sufficient stiffness for surgical handling.[2] If necessary, the modulus of the lenses could be decreased by reducing the crosslinker concentration. It could be increased by switching from a bi-functional to a tri-functional crosslinker (tris-succinimidyl aminotriacetate,[34] Pierce, Rockford, IL), or by re-engineering the protein sequence to contain more lysine side chains within the elastin-like domain. The range of elastic moduli observed in elastin-based artificial proteins, 0.03-35 MPa,[35] suggests that the basic design framework employed here could be adaptable to many materials needs.

4.4.3 Surgical implantation and observations.

The animals tolerated the procedure well and there were no surgical complications. The implants also tolerated the procedure well, as they were relatively easy to manipulate and durable during the surgery as long as they were well hydrated. Immediately postoperatively, the onlays remained intact and well positioned within the circular stromal pocket. There was a small difference in maintenance of the onlay in the proper position depending on whether sutures were placed or not, as three of the unsutured onlays fell out within the first 2-3 days of surgery. In the eyes where sutures were placed, the implants showed some surface wrinkling due to the tension that the sutures placed on the implant.

Compared to the controls, initial mild to moderate inflammation was observed in all the eyes with the implants, as shown by mild hyperemia of the bulbar conjunctiva and mild corneal stromal edema. There was no significant mucoid or purulent discharge noted in any of the animals.

4.4.4 Clinical evaluation.

Epithelialization, as visualized by fluorescein staining (Figure 4.6), in all cases initiated at the periphery of the exposed surface of the corneal onlays and progressed inward toward the center. The time required for full epithelialization varied somewhat between individual animals. The control eyes (sham surgery) showed commencement of epithelialization by day 1 and full epithelialization

within 2-4 days (not shown). All of the onlay animals (groups 2 and 3) showed epithelial cells on the periphery of the onlay by day 2 and full epithelialization within 4-7 days (Figure 4.6C). Results are summarized in Table 4.1.

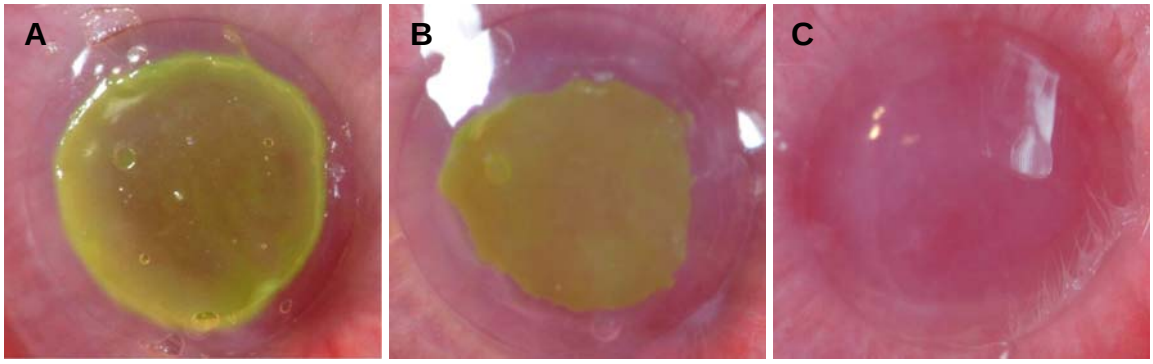

Figure 4.6 Fluorescein staining indicates the extent of re-epithelialization over the onlay surface. (A) Post-implantation, fluorescein stains the onlay up to the surgical defect edge. (B) At 2 days, re-epithelialization has begun to progress inward from the periphery. (C) At 7 days, the onlay is completely re-epithelialized.

Table 4.1 One week rabbit implantation study results

	Group 1 **Control: no onlay** n=5	Group 2 **Onlay** n=12	Group 3 **Onlay + sutures** n=3
Epithelial growth onto the debrided zone	Day 1	Day 2	Day 2
Full re-epithelialization	Day 2-4	Day 4-7	Day 4-7
Exam findings	Eyes quiet	Mild inflammation*	Mild inflammation**
Maintenance	-	9 of 12 remained in place at day 7	2 of 3 remained in place at day 7

* Mild signs of inflammation noted included mild corneal edema and ciliary flush.

** One eye was noted to have a large hypopyon and was sacrificed early.

4.4.5 Histology.

Epithelial cells had covered the entire implant at the time of examination one week after the surgery. The epithelium overlying the onlay appeared normal and consisted of 1-2 cell layers, typical for regenerating epithelium (Figure 4.7B). The interface between the corneal stroma and the implant was unremarkable, with some epithelial growth under the edges of the onlays (Figure 4.7A). The corneal stroma posterior to the onlay appeared normal. In a few cases, the corneal stroma and the corneal implant showed a moderate amount of inflammatory cells, including lymphocytes and neutrophils. In other cases, the stroma and implant appeared normal and free of inflammation.

At low magnification, Mason trichrome staining showed no staining of the novel onlay material compared to the natural cornea, indicating that no collagen was present in the onlay.

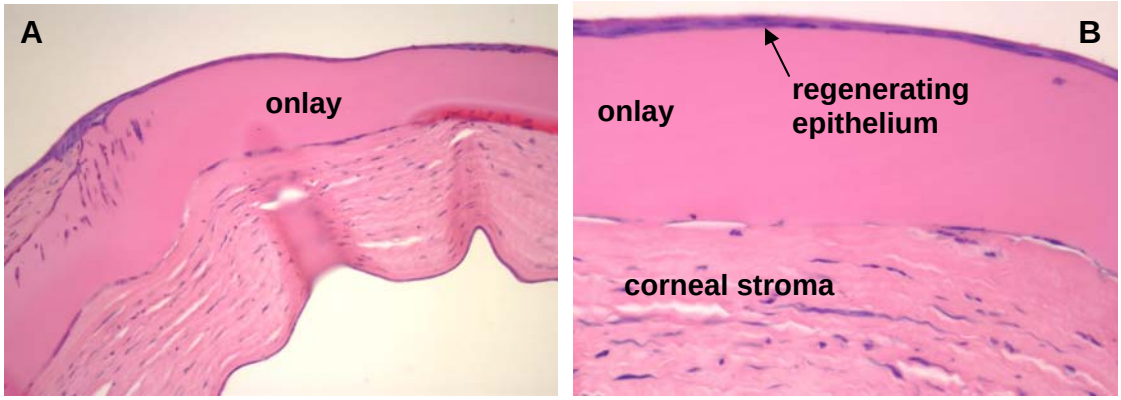

Figure 4.7 Cross-sections of implanted corneal onlays at 7 days post-implantation. Histological sections of low (A) and high (B) magnification are shown; the onlay is 115 μm thick. Epithelium 1-2 layers thick covers the anterior onlay surface. Evidence of the corneal pocket used to hold the onlay can be seen in the left of (A).

4.5 Discussion

The ability of the artificial extracellular matrix protein onlays to support complete re-epithelialization is encouraging, as are the good interface with surrounding tissue and the absence of degradation. The time-course for re-epithelialization, 4-7 days, is faster than the 5-11 days previously reported for collagen I-coated perfluoropolyethers, among the most successful synthetic onlays to date, although the size of the defect here is smaller (3 mm versus 6 mm).[15] The aE-RGD protein films were far more successful in promoting epithelium growth than previously reported synthetic polymer hydrogel lenses coated or tethered with various adhesive peptides and proteins, including fibronectin and RGD; in the best case these required 15 days for randomly seeded rabbit epithelial cells to grow to confluence in culture.[36]

Longer implantation studies using the same implantation technique, for example on a 3-month time scale with periodic sacrifices for evaluation, will be useful in characterizing the patency of the onlays. This time period will give better evidence of onlay degradation and remodeling if it occurs. Electron microscopy can be used to examine the onlay-epithelial interface to establish the presence of adhesion complexes including hemidesmosomes and anchoring fibrils.

To maximize the likelihood of success in these longer studies, the lenses should be sterilized prior to implantation. Because radiation (γ-irradiation) or chemical (ethylene oxide) treatments may change the biochemical or mechanical properties of the aE-RGD protein, heat-based methods such as autoclave

treatment are indicated. Furthermore, extractable bacterial endotoxin should be minimized in future preparations; eliminating the mild immune response to the lenses may simply require more stringent purification techniques to remove this contaminant. Alternatively, two-phase extraction, ion-exchange chromatography, and affinity-based techniques have been used to remove endotoxin from protein solutions.[37]

Depending on the performance of the onlay lenses on longer time scales, it may be necessary to modify the sequence of the aE-RGD protein through recombinant DNA techniques. Easily implemented minor sequence modifications can affect the stiffness[29] or degradation[34] of artificial protein films. The areal density of the RGD cell binding domain on the anterior surface of the onlay may affect epithelial cell adhesion. Alternative cell binding domains might be used to promote adhesion through different integrin receptors.

While artificial proteins or other approaches may solve the issue of epithelial cell adhesion to onlay materials, the significant challenge of devising an optically transparent method to attach the onlay to the anterior surface of the corneal stroma remains. The corneal pocket model is effective for initial evaluation of onlay materials, but the promise of onlays relies on their ability be placed without surgical incisions. Based on histological evaluation, the onlays seem to integrate well into surrounding tissue at 7 days, but a short-term means of securing the onlays is required for the application. Controlled application of tissue adhesives may be a straightforward solution. A photocrosslinking approach, made possible by incorporation of non-canonical amino acids,[38] may

be simpler to implement. The ability to re-engineer the artificial protein sequence may enable still other means of adhesion.

4.6 Conclusions

This preliminary study shows that artificial proteins, designed to mimic key features of the natural extracellular matrix, can be fashioned in the form of contact lenses and successfully implanted into a rabbit cornea. Rabbit corneal epithelial cells adhere to and proliferate over these implanted onlays, which are fairly well tolerated by the rabbit eye despite sterility and contaminant concerns.

Future work in developing the onlay lenses for the application will include more strenuous purification and sterilization procedures. Subsequently, long-term implantation studies will be performed to assess biocompatibility, stability, immune response, and to confirm the ability of the onlays to support mature corneal epithelium. A reliable means of ensuring adhesion between the onlays and the underlying corneal stroma must also be devised.

Acknowledgements.

Keith Duncan aided the surgical implantation studies. Calhoun Vision (Pasadena, CA) is continuing development of the onlays.

4.7 References

(1) Sugar A, Rapuano CJ, Culbertson WW, Huang D, Varley GA, Agapitos PJ, de Luise VP, Koch DD. Laser in situ keratomileusis for myopia and astigmatism: Safety and efficacy - A report by the American Academy of Ophthalmology. *Ophthalmology* **2002**, *109*, 175-187.

(2) Evans MDM, McLean KM, Hughes TC, Sweeney DF. A review of the development of a synthetic corneal onlay for refractive correction. *Biomaterials* **2001**, *22*, 3319-3328.

(3) Lee JB, Seong GJ, Lee JH, Seo KY, Lee YG, Kim EK. Comparison of laser epithelial keratomileusis and photorefractive keratectomy for low to moderate myopia. *J. Cataract Refract. Surg.* **2001**, *27*, 565-570.

(4) Vesaluoma M, Perez-Santonja J, Petroll WM, Linna T, Alio J, Tervo T. Corneal stromal changes induced by myopic LASIK. *Invest. Ophth. Vis. Sci.* **2000**, *41*, 369-376.

(5) Melki SA, Azar DT. LASIK complications: Etiology, management, and prevention. *Surv. Ophthalmol.* **2001**, *46*, 95-116.

(6) Fan-Paul NI, Li J, Miller JS, Florakis GJ. Night vision disturbances after corneal refractive surgery. *Surv. Ophthalmol.* **2002**, *47*, 533-546.

(7) Pushker N, Dada T, Sony P, Ray M, Agarwal T, Vajpayee RB. Microbial keratitis after laser in situ keratomileusis. *J. Refract. Surg.* **2002**, *18*, 280-286.

(8) Lass JH, Stocker EG, Fritz ME, Collie DM. Epikeratoplasty - the surgical correction of aphakia, myopia, and keratoconus. *Ophthalmology* **1987**, *94*, 912-923.

(9) Rao GN, Ganti S, Aquavella JV. Specular microscopy of corneal epithelium after epikeratophakia. *Am. J. Ophthalmol.* **1987**, *103*, 392-396.

(10) Rodrigues M, Nirankari V, Rajagopalan S, Jones K, Funderburgh J. Clinical and histopathologic changes in the host cornea after epikeratoplasty for keratoconus. *Am. J. Ophthalmol.* **1992**, *114*, 161-170.

(11) Thompson KP, Hanna KD, Gipson IK, Gravagna P, Waring GO, Johnsonwint B. Synthetic epikeratoplasty in rhesus-monkeys with human type-IV collagen. *Cornea* **1993**, *12*, 35-45.

(12) Xie RZ, Stretton S, Sweeney DF. Artificial cornea: Towards a synthetic onlay for correction of refractive error. *Biosci. Rep.* **2001**, *21*, 513-536.

(13) Hicks CR, Fitton JH, Chirila TV, Crawford GJ, Constable IJ. Keratoprostheses: Advancing toward a true artificial cornea. *Surv. Ophthalmol.* **1997**, *42*, 175-189.

(14) Latkany R, Tsuk A, Sheu MS, Loh IH, TrinkausRandall V. Plasma surface modification of artificial corneas for optimal epithelialization. *J. Biomed. Mater. Res.* **1997**, *36*, 29-37.

(15) Evans MDM, Xie RZ, Fabbri M, Bojarski B, Chaouk H, Wilkie JS, McLean KM, Cheng HY, Vannas A, Sweeney DF. Progress in the development of a synthetic corneal onlay. *Invest. Ophth. Vis. Sci.* **2002**, *43*, 3196-3201.

(16) Thompson KP, Hanna K, Waring GO, Gipson I, Liu Y, Gailitis RP, Johnson-Wint B, Green K. Current status of synthetic epikeratoplasty. *Refract. Corneal Surg.* **1991**, *7*, 240-248.

(17) Krejchi MT, Atkins EDT, Waddon AJ, Fournier MJ, Mason TL, Tirrell DA. Chemical sequence control of beta-sheet assembly in macromolecular crystals of periodic polypeptides. *Science* **1994**, *265*, 1427-1432.

(18) Petka WA, Harden JL, McGrath KP, Wirtz D, Tirrell DA. Reversible hydrogels from self-assembling artificial proteins. *Science* **1998**, *281*, 389-392.

(19) Ratner BD, Bryant SJ. Biomaterials: Where we have been and where we are going. *Annu. Rev. Biomed. Eng.* **2004**, *6*, 41-75.

(20) Panitch A, Yamaoka T, Fournier MJ, Mason TL, Tirrell DA. Design and biosynthesis of elastin-like artificial extracellular matrix proteins containing periodically spaced fibronectin CS5 domains. *Macromolecules* **1999**, *32*, 1701-1703.

(21) Liu CY, Apuzzo MLJ, Tirrell DA. Engineering of the extracellular matrix: Working toward neural stem cell programming and neurorestoration - Concept and progress report. *Neurosurgery* **2003**, *52*, 1154-1165.

(22) Welsh ER, Tirrell DA. Engineering the extracellular matrix: A novel approach to polymeric biomaterials. I. Control of the physical properties of artificial protein matrices designed to support adhesion of vascular endothelial cells. *Biomacromolecules* **2000**, *1*, 23-30.

(23) Liu JC, Heilshorn SC, Tirrell DA. Comparative cell response to artificial extracellular matrix proteins containing the RGD and CS5 cell-binding domains. *Biomacromolecules* **2004**, *5*, 497-504.

(24) Ruoslahti E. RGD and other recognition sequences for integrins. *Annu. Rev. Cell Dev. Biol.* **1996**, *12*, 697-715.

(25) Urry DW, Parker TM, Reid MC, Gowda DC. Biocompatibility of the bioelastic materials, poly(GVGVP) and its gamma-irradiation cross-linked matrix - summary of generic biological test-results. *J. Bioactive and Compatible Polym.* **1991**, *6*, 263-282.

(26) Chapman HA, Riese RJ, Shi GP. Emerging roles for cysteine proteases in human biology. *Annu. Rev. Physiol.* **1997**, *59*, 63-88.

(27) Torchia DA, Piez KA. Mobility of elastin chains as determined by C-13 nuclear magnetic resonance. *J. Mol. Biol.* **1973**, *76*, 419-424.

(28) Li B, Alonso DOV, Daggett V. The molecular basis for the inverse temperature transition of elastin. *J. Mol. Biol.* **2001**, *305*, 581-592.

(29) Di Zio K, Tirrell DA. Mechanical properties of artificial protein matrices engineered for control of cell and tissue behavior. *Macromolecules* **2003**, *36*, 1553-1558.

(30) Evans MDM, Xie RZ, Fabbri M, Madigan MC, Chaouk H, Beumer GJ, Meijs GF, Griesser HJ, Steele JG, Sweeney DF. Epithelialization of a synthetic polymer in the feline cornea: A preliminary study. *Invest. Ophth. Vis. Sci.* **2000**, *41*, 1674-1680.

(31) Urry DW. Physical chemistry of biological free energy transduction as demonstrated by elastic protein-based polymers. *J. Phys. Chem. B* **1997**, *101*, 11007-11028.

(32) Nowatzki PJ, Tirrell DA. Physical properties of artificial extracellular matrix protein films prepared by isocyanate crosslinking. *Biomaterials* **2004**, *25*, 1261-1267.

(33) Lee J, Macosko CW, Urry DW. Swelling behavior of gamma-irradiation cross-linked elastomeric polypentapeptide-based hydrogels. *Macromolecules* **2001**, *34*, 4114-4123.

(34) (Chapter 3) Heilshorn SC, Nowatzki PJ, Yamaoka T, Tirrell DA. Controlled proteolytic degradation of protein-based biomaterials. *Prepared for submission.*

(35) Nagapudi K, Brinkman WT, Leisen J, Thomas BS, Wright ER, Haller C, Wu XY, Apkarian RP, Conticello VP, Chaikof EL. Protein-based thermoplastic elastomers. *Macromolecules* **2005**, *38*, 345-354.

(36) Jacob JT, Rochefort JR, Bi JJ, Gebhardt BM. Corneal epithelial cell growth over tethered-protein/peptide surface-modified hydrogels. *J. Biomed. Mater. Res. B* **2005**, *72B*, 198-205.

(37) Petsch D, Anspach FB. Endotoxin removal from protein solutions. *J. Biotechnol.* **2000**, *76*, 97-119.

(38) (Appendix) Carrico IS, Heilshorn SC, Mock ML, Liu JC, Nowatzki PJ, Maskarinec SA, Franck C, Ravichandran G, Tirrell DA. Lithographic patterning of intrinsically photoreactive cell-adhesive proteins. *Prepared for submission.*

5 MECHANICALLY TUNABLE THIN FILMS OF PHOTOSENSITIVE ARTIFICIAL PROTEINS CHARACTERIZED BY AFM NANOINDENTATION

5.1 Abstract

Thin films with tunable stiffness were made by photocrosslinking an artificial extracellular matrix protein that was biosynthesized to contain *para*-azidophenylalanine (*p*N_3Phe). The elastic moduli of the films were calculated from nanoindentation data collected by atomic force microscopy (AFM) using a thin-film Hertz model. Film elastic modulus was shown to be tunable in the range of 0.3 to 1.0 MPa either by differential irradiation or by varying the level of *p*N_3Phe in the protein. Tensile measurements on bulk films of the same proteins and finite-element simulation of the indentation agreed with the thin-film modulus calculations. Single substrates with patterns of mechanical properties were created; these have potential use in studying mechanically dependent cell behavior, particularly in the context of coordinating biological signals.

Manuscript prepared for submission by Paul J. Nowatzki[1], Christian Franck[2], Guruswami Ravichandran[2], and David A. Tirrell[1].

(1) Division of Chemistry and Chemical Engineering, California Institute of Technology

(2) Graduate Aeronautics Laboratories, California Institute of Technology

5.2 Introduction

5.2.1 Mechanical sensitivity of cell behavior.

Although cells are known to respond to chemical signals, the mechanical properties of their environment are increasingly being recognized as an additional important determinant of cell behavior. Differences in substrate stiffness have been shown to affect cell adhesion,[1,2] spread area and shape,[1,3,4] traction forces and migration rate,[1,5,6] growth,[7] and differentiation.[2,8] Mechanical effects are thus postulated to play an important role in aspects of biology ranging from cell morphology to embryonic development.[9]

Cell-culture substrates with adjustable mechanical properties are essential tools for studying these phenomena. Stiffness-dependent cell behavior reported to date has most frequently been characterized on chemically crosslinked synthetic gels such as polyacrylamide.[1,5,10] Because biological and mechanical signals are expected to have coordinating effects,[9,11] in some cases it will be preferable to study cells on substrates that more closely mimic the extracellular matrix; for example, collagen-coated gels have been used.[3,8] The ability to vary mechanical properties on a single substrate would be useful in probing many conditions at once and reducing experimental variability. Moreover, films with stiffness patterns can elucidate cell behavior at mechanical interfaces,[5] and stiffness gradients allow research into what is termed mechanotaxis or durotaxis.[6,12,13]

5.2.2 Artificial protein.

We use a photosensitive artificial protein to make substrates in which the coordinating effects of stiffness and extracellular matrix biology can be studied directly. It is based on a family of previously reported artificial proteins intended for use as implantable biomaterials, which were designed to mimic key features of the extracellular matrix.[14-17] The design contains cell binding domains periodically spaced between elastin-like repeating peptides that confer flexibility; the amino acid sequence is shown in Figure 5.1. The CS5 cell binding domain, taken from the alternatively spliced type III connecting segment region of human fibronectin, serves as a means of attaching cells that express the $\alpha_4\beta_1$ integrin cell surface receptor.[18] The basis for the elasticity of the artificial protein is the repeating peptide VPGVG (Val-Pro-Gly-Val-Gly), derived from mammalian elastin and known to reproduce many of its properties.[19]

MMASMTGGQQMGRKTHHHHHHMG-
{LDGEEIQIGHIPREDVDYHLYPG[(VPGVG)$_2$(VPG**F**G)(VPGVG)$_2$]$_5$LP}$_3$LE

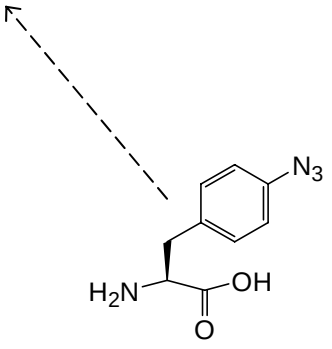

pN$_3$Phe

Figure 5.1 Amino acid sequence of the artificial extracellular matrix protein. The cell-binding sequence CS5 is underlined. The fifteen phenylalanines, **F**, are partially replaced by *para*-azidophenylalanine (right) in synthesis; protein containing this photosensitive amino acid is designated aE-*p*N$_3$Phe. In the notation aE-n%-*p*N$_3$Phe, n% indicates the fraction of Phe that is replaced with *p*N$_3$Phe.

The phenylalanine (Phe) sites dispersed throughout the elastin-like portion serve as sites for the incorporation of the non-canonical amino acid *para*-azidophenylalanine (*p*N_3Phe, Figure 5.1), which is accomplished by using a bacterial clone that expresses a mutant phenylalanyl-tRNA synthetase (PheRS) with an enlarged binding pocket.[20,21] The azide group of *p*N_3Phe is UV-photolysable, generating a nitrene that yields non-specific crosslinks to surrounding protein molecules. By varying the concentration of *p*N_3Phe during bacterial synthesis, the level of substitution for Phe in the protein can be tuned, thereby altering the crosslink density and elastic modulus of UV-irradiated protein films.[22] The photocrosslinking technique has already been used with a photomask to selectively pattern protein on substrates, demonstrating that a cell-adhesive protein can be presented to cells in predetermined geometries.[22] Herein we report the creation and characterization of thin films of this protein; their elastic moduli are tunable by variable *p*N_3Phe incorporation, in parallel to results on bulk films. Furthermore, variable irradiation of a protein with high *p*N_3Phe content allowed patterns (step-gradients) of mechanical properties to be made on a single film.

5.2.3 AFM characterization.

Mechanical properties of thin, substrate-bound films are typically measured by nanoindentation, and atomic force microscopy (AFM)-based nanoindentation in particular offers significant advantages in spatial and force resolution over conventional nanoindenters. It is therefore appropriate for

analyzing soft samples and materials whose stiffness varies on short length scales.[23-25] Here, AFM nanoindentation with a microspherical tip (600 nm diameter) was used to obtain accurate measurements of film elastic modulus.[26,27] The use of a spherical tip allows a spherical indentation model to be correctly applied, since the classical Hertz spherical model is known to cause distortions when used to analyze AFM data collected with conventional sharp, pyramidal or conical tips.[28] A film-height dependent physical model[29] accounts for the mechanical coupling of the film to its underlying support, another known source of distortion in AFM nanoindentation.[30,31] Bulk tensile tests of the same materials confirm the nanoindentation calculations made with this model.

Finite element simulations of the indentations were also performed to verify the modulus calculations and to explore the possibility of determining a more sophisticated mechanical material model from AFM data. While the linear elasticity model[29] accurately measures initial elastic modulus of the films described herein, the finite element analysis will be appropriate for characterizations of thinner films, higher strain indentation data, and arbitrary tip geometry.

5.3 Experimental

*5.3.1 Protein aE-*p*N*$_3$*Phe.*

The amino acid sequence of the photosensitive artificial extracellular protein, aE-*p*N$_3$Phe, is shown in Figure 5.1. It is made biosynthetically in a Phe-

auxotrophic strain of *E. coli* with a plasmid bearing genes coding for both the protein and the Ala294Gly mutant of the *E. coli* phenylalanyl-tRNA synthetase (PheRS),[32] which allows incorporation of *p*N_3Phe (Bachem) in place of Phe when the protein expression is induced.[21]

The expression and purification of the protein, designated aE-*p*N_3Phe, were based on previous work.[22] To ensure that Phe was depleted from the medium during protein synthesis, the cells were centrifuged and resuspended in minimal medium lacking Phe and containing *p*N_3Phe 10 minutes after expression was induced, enough time for functional copies of the PheRS to be synthesized.

The incorporation level of *p*N_3Phe was measured by 600 MHz ^{1}H NMR (Varian) at a protein concentration of 15 mg/mL in DMSO-d_6 (Cambridge Isotope Laboratories) by comparing the distinct aromatic proton peak areas assigned to *p*N_3Phe and to Phe.[22] Phe replacement levels of 28%, 31%, 48%, and 66% were achieved by using 125, 188, 250, and 250 mg/L, respectively, of *p*N_3Phe in the culture medium; the corresponding proteins are designated aE-28%-*p*N_3Phe, etc.

5.3.2 AFM – equipment.

Images and force curves were collected on a Park Scientific Instruments AutoProbe M5 atomic force microscope, with accompanying ProScan v1.51b software. Pyramidal-tipped triangular silicon nitride cantilevers with nominal spring constant 0.58 N/m were used for imaging (Veeco DNP-S). A silicon nitride cantilever of the same shape, with an attached 600 nm diameter SiO_2 particle tip (Novascan, Ames, IA), was used to indent samples for collecting force

curves. Its spring constant was calculated to be 0.37 N/m by indenting against reference cantilevers with predetermined spring constants of 1.00 N/m and 0.125 N/m (Veeco CLFC). Here, $k_{test}/k_{ref} = (\delta_{tot} - \delta_{test})/(\delta_{test} \cos\theta)$, where k_{test} and k_{ref} are the spring constants of the test and reference cantilevers, δ_{tot} and δ_{test} are slopes of the force-distance curve when the test cantilever is indented against a rigid surface and the free end of the reference cantilever, and θ is the angle between the cantilevers (15°). A glass slide was glued to the back of the cantilever mount so that the cantilever and sample could be submerged in water.

5.3.3 Bulk protein films.

aE-*p*N_3Phe (4 mg) was dissolved in dimethylsulfoxide (40 μL, Mallinckrodt). The solution was spread to cover an area approximately ~1.5 cm × 1 cm on a poly(methyl methacrylate) surface, and the solvent was evaporated at 50 °C overnight. The resulting films were ~20 μm thick (dry). Once irradiated (*vide infra*), uniaxial tension tests were performed on the samples at 22 °C using an Instron 5542 with 0.5 N load cell, modified to contain the sample in a water bath; strain rate was 10% of the original length per minute,[33] at which viscoelastic effects are negligible.

5.3.4 Thin protein films.

All film-making procedures were performed in a cold room (4 °C), below the lower critical solution temperature (LCST)[19] of the protein in water. Protein (10 mg) was dissolved in water (100 μL), and the solution was centrifuged (5 min,

16,500×*g*) to remove any aggregates or particles. Protein solution (10 μL) was pipetted onto and spread to cover an unmodified 12 mm glass slide (Hecht-Assistent, Sondheim, Germany). Films were spin-coated (Specialty Coating Systems, Inc. P6204, Indianapolis, IN) at 7,000 rpm for 30 seconds and dried overnight at 4 °C. Typical film thickness was ~200 nm (dry).

5.3.5 Irradiation of films.

Dry protein films were exposed to unfiltered UV light from a high-pressure mercury arc lamp (Oriel Q, 100 watt @ 5 amps, > 20 min warm-up time; measured intensity in irradiation plane = 1.5 mW/mm^2). Time to achieve complete conversion, ~300 sec, was determined empirically. Zones of differential crosslinking were achieved on the same substrate by placing an opaque shutter over portions of the film during irradiation. Specifically, a step-gradient of irradiation times (0, 12, 20, 30, 50, 80, 120, 180, and 300 sec) was made across a 12 mm slide by manually repositioning the shutter between exposures.

Slides were agitated in excess water, 4 °C, to remove any soluble protein. Un-irradiated protein, or protein irradiated for 12 sec or less, was completely removed during this rinsing process as evidenced by AFM imaging. No delamination of irradiated films from their glass substrates was observed.

5.3.6 AFM – film thickness.

The tip of a pair of fine forceps was lightly dragged across the surface of the protein film, tearing away the protein along the scratch and revealing the

underlying glass substrate. The edge of this scratch was imaged by AFM both dry and under water; the thickness of the film is apparent from the scan (see Figure 5.2). The surface revealed by the scratch was confirmed to be glass, based on its smoothness and linear force profile when indented. The protein film thickness was calculated by averaging the height measurements at many ($n \geq 16$) points on the film, using the revealed glass surface as a baseline.

5.3.7 AFM – indentation force curves.

The films and cantilever assembly were submerged in water under ambient conditions. The 600-nm SiO_2 microsphere tip was placed above a spot where the film thickness had been measured (identified visually from the optical microscope image using reference markers on the film) to ensure that the thickness at the point of indentation was known. Force curves were collected; the instrument records z (piezo) displacement and force, the product of measured tip deflection and cantilever spring constant.

The indentation range was set to (-150 nm, +1350 nm) relative to the contact point, effectively limiting the force to ~20-30 nN and the strain magnitude to under 20%. The indent-retract cycle time was 1 sec (tip speed 3 μm/sec). Viscoelastic effects did not appear to be a significant factor at this strain rate (~4 sec^{-1}), as evidenced by the statistical superimposability of force curves collected using 1 sec and 10 sec cycles (~0.4 sec^{-1}), Figure 5.4.

To assess the uniformity of the mechanical properties, force curves were evaluated repeatedly at the same spot and at nearby spots spaced 10-20 μm

apart. For the uniformly-irradiated *p*N$_3$Phe films this procedure was repeated at three distant (> 1 mm apart) spots of individually-measured height.

5.3.8 Calculation of elastic modulus.

The Dimitriadis model[29] for indentation of linear-elastic soft material films of finite height with a spherical indenter was applied to the loading force data. For a support-bonded film of Poisson ratio $\nu = 0.5$ (incompressible, a reasonable estimate for both for rubbery networks and biological materials):

$$F = \frac{16E}{9} R^{1/2} \delta^{3/2} [1 + 1.133\chi + 1.283\chi^2 + 0.769\chi^3 + 0.0975\chi^4] \quad (1)$$

The first term of this series is the classical Hertz indentation model of force F as a function of (Young's) elastic modulus E and indentation depth δ using a rigid sphere of radius R. Additional terms were added[29] to correct for the finite height of the film, where χ is given by:

$$\chi = \sqrt{R\delta} / h \quad (2)$$

and h is the thickness of the film. As the film gets thinner, or as the indentation depth increases, the indenting sphere (AFM tip) experiences a higher force than it would for an infinitely-thick film of the same material, owing to mechanical effects of film confinement to the stiff underlying substrate. The film indentation δ was calculated by subtracting the tip displacement from the total (z) displacement.

The contact point of the force-distance curves, where the indentation and force were set to zero in the analysis, was determined by visual inspection.

While this can be difficult in some experiments,[29] it is straightforward for the force curves collected here, because we observe a distinct snap-in when the tip touches the surface (see Figure 5.3 for examples). The apparent elastic modulus was calculated by evaluating equations (1) and (2) at each recorded force-indentation point between 15 nm and 10% film indentation and averaging over the range. Below 15 nm, the scatter in the data is magnified in the calculations and distortions are common; the 10% maximum indentation is to constrain the data to the near-linear response range.[29] In this strain range, the finite-height correction factor was as large as 1.78 ($\chi = 0.395$) for the films analyzed here.

5.3.9 Finite element simulation.

A simulation of the indentation was constructed in the program ABAQUS (ABAQUS, Inc., Providence, RI). The system was represented by 2D axisymmetric elements (CAX4R) using the known protein film height and indenting tip geometry (R = 300 nm). From tensile data collected for bulk samples of aE-*p*N_3Phe, material model parameters for each material were calculated and entered into the simulation. The Yeoh model[34] was found to best describe the material response of aE-*p*N3Phe as determined through numerous uniaxial tension and compression tests. The output of force versus film indentation was compared to the AFM data collected experimentally.

5.4 Results and Discussion

5.4.1 Thin films.

The spin-coated thin films of aECM protein appeared smooth (RMS roughness = 1.3 nm, versus 0.9 nm for the revealed glass) when imaged by AFM, Figure 5.2. The film thickness was uniform over the surface of a given 12 mm glass slide substrate, varying no more than ± 10% from the average. The local thickness was much more uniform, with < 2% variation in a 30 μm scan. The hydrated thicknesses of the protein films ranged from 191 to 418 nm. Two thicker films, made using a higher concentration of aE-66%-*p*N_3Phe, were ~1500 nm thick (Table 5.1).

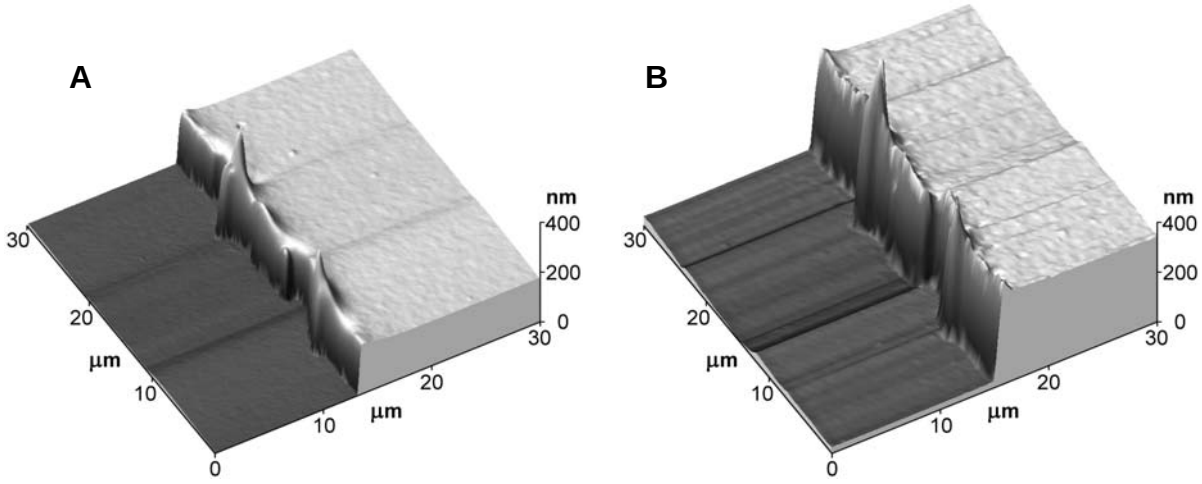

Figure 5.2 AFM topography scans of an aE-48%-*p*N_3Phe film, dry (A) and in water (B). The z scales (height) are exaggerated 22× relative to the x and y scales. The film (right side of images) was scratched to reveal the underlying glass substrate (left), indicating the height of the film; the spikes at the edge are artifacts of the scratching procedure. This film was 178 nm thick dry and 328 nm thick wet.

5.4.2 AFM force curves.

Representative loading force curves are shown in Figure 5.3; these display the parabolic shape typical of soft materials. Since the assembly is submerged in water, the attractive force between the tip and the surface is screened; nevertheless, a distinct snap-in is seen for each force curve, which allows a contact point to be confidently assigned. In cases where the snap-in appeared to occur over a few nanometers, the contact point was assigned to the middle of the snap-in rather than the bottom (at minimum force), as this was found to give the best reproducibility between repeated indentations at the same spot.

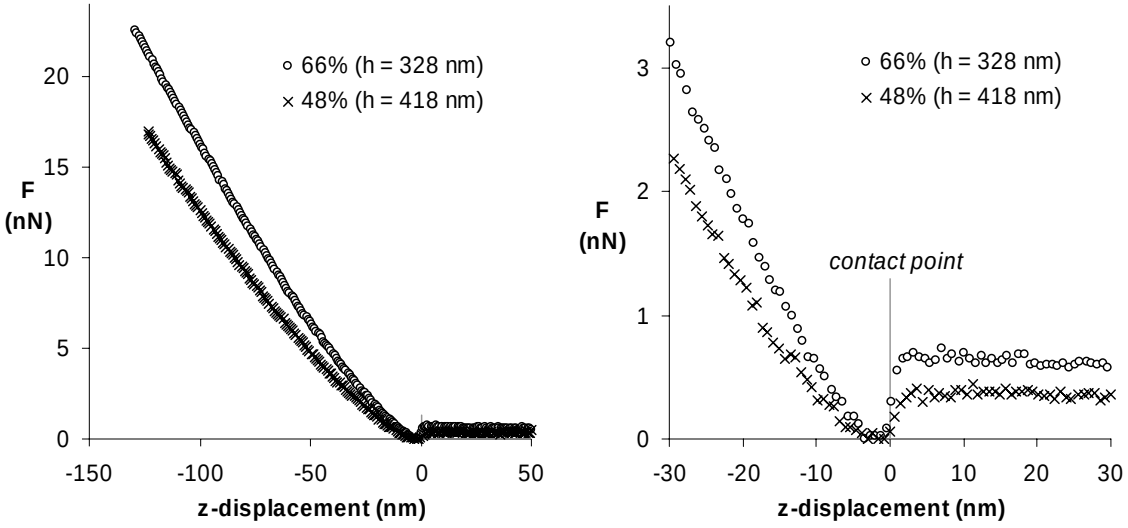

Figure 5.3 Representative loading indentation profiles for thin protein films of aE-66%-*p*N$_3$Phe and aE-48%-*p*N$_3$Phe, showing force versus z-displacement (equal to cantilever deflection plus film indentation). The raw force and displacement data have been zeroed using the snap-in to establish the contact point. The figure on the right is magnified to show the contact point assignment.

When the strain rate was reduced by a factor of 10 from the experimental rate (1 sec indent cycle, ~4 sec^{-1}), the resulting force curves appeared indistinguishable from the originals, an indication that viscoelastic effects did not significantly influence the results (Figure 5.4). Faster indentation cycles allow increased throughput and minimize the deleterious effects of sensor drift.

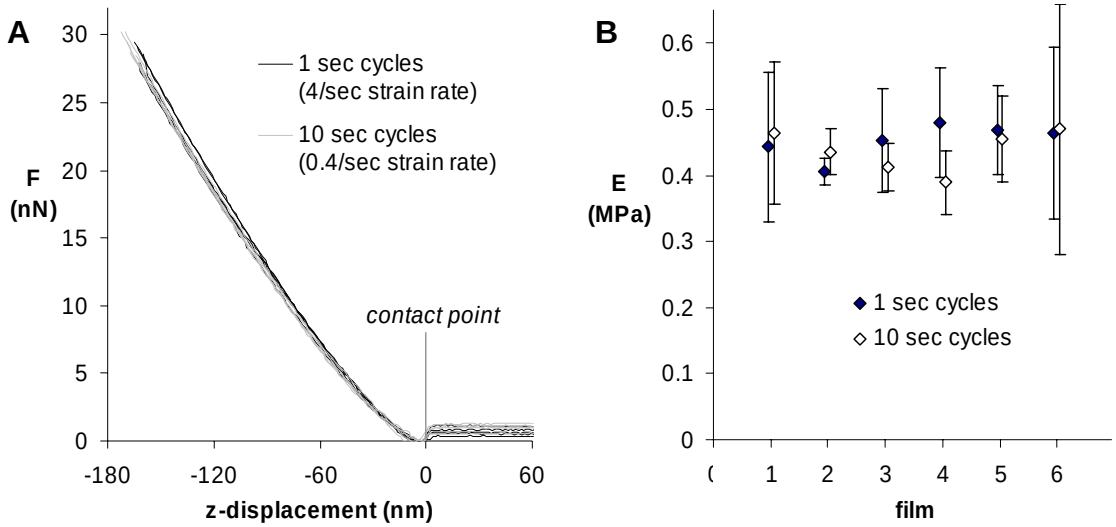

Figure 5.4 (A) Superimposed force profiles for multiple indentations (n=5) of a single aE-48%-*p*N_3Phe film using 1 sec (used herein) and 10 sec indent cycles. (B) Elastic moduli, E, calculated (see 5.4.3) using 1 sec and 10 sec indent cycles on five different aE-48%-*p*N_3Phe films (h = 217-293 nm, n≥4). No significant differences are seen based on cycle time. 1 sec indent cycles (~4 sec^{-1} strain rate) were used for all modulus data reported in this work.

Repeated indentations (up to 100) of the same spot did not cause any change in the force curves, likely because the hydrated protein films are highly elastic and the indentation depth was controlled. When surfaces on which the indentations had been performed were subsequently imaged by AFM, no

evidence of indentation was seen on either hydrated or dry films. This supports the conclusion that the collection of force curves here does not permanently deform or otherwise alter the mechanical properties of the samples.

5.4.3 Analysis of AFM force curves.

Once a force curve is collected, all variables in the equations (1) and (2) except E are known, so each point on the force-distance curve can be used to calculate an elastic modulus for the material. If the model describes the system correctly, the calculated modulus should be the same at each indentation depth. The Hertz and Dimitriadis[29] models were evaluated using this criterion for a representative data set in Figure 5.5. Because the films were less than a micron in thickness and the indentation depth represented a significant portion of the film height, the infinite-height Hertz model was inappropriate for elastic modulus calculation. The elastic properties of the protein films were significantly influenced by the underlying glass substrate, as has been observed previously for soft thin films.[29,30] Because it accounted for the finite sample thickness and coupling to a rigid substrate, the Dimitriadis model was much more effective, resulting in consistent predictions of modulus for each force curve in the indentation range of 15 nm to 10% or more of the film thickness.

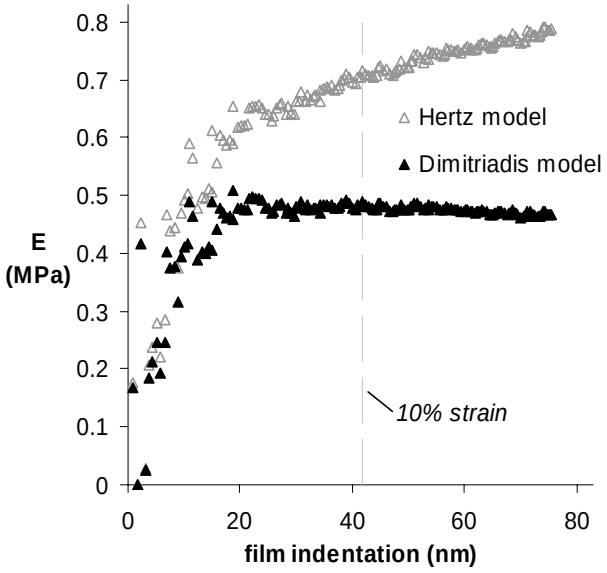

Figure 5.5 The elastic modulus (E) calculated at each point in the AFM indentation using Hertz and Dimitriadis models is shown for an aE-48%-*p*N_3Phe film (height 418 nm, same film as Figure 5.3). The height-dependent Dimitriadis model gives a consistent modulus in the > 15 nm range, while the Hertz model overestimates E and is indentation-dependent. Distortions caused by applying the Hertz model increase rapidly for thinner films.

A single value of Young's modulus (E) was assigned to each surface by averaging the model-predicted moduli from 15 nm to 10% strain; the standard deviation in E over this range averaged 3.4% and was <10% for all curves, indicating that the Dimitriadis model gives uniform predictions of E. In general, the model-calculated value of E is sensitive to the placement of the contact point,[29] but since contact is observed directly and the sub-15 nm data are excluded, the fits are robust. Illustrations of the fit of the Dimitriadis model to the experimental AFM data are shown in Figure 5.6.

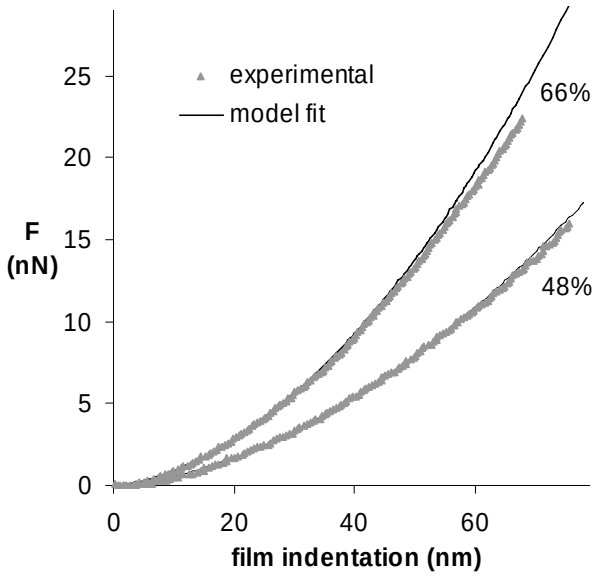

Figure 5.6 Experimental AFM indentation data compared to Dimitriadis model fits for thin films of aE-66%-*p*N_3Phe and aE-48%-*p*N_3Phe (same as in Figures 5.3 & 5.5). To constrain the analysis to the linear elastic range, the model was fit to data between 15 nm and 10% of the film height (33 nm for aE-66%-*p*N_3Phe, 42 nm for aE-48%-*p*N_3Phe), although it fits the experimental data at higher extensions nearly as well, owing to the elasticity of the protein.

Standard deviation in *E* from repeated indentation of the same spot (n=3-4 indents, 51 spots) averaged 5.1%. There was no tendency of the film to become more or less stiff with repeated indentation. Standard deviation in *E* between different spots on the same film (n=3-4 spots, ≥10 μm apart, 13 films) averaged 7.2%, nearly as small as the same-spot variance, indicating that *E* was uniform over the films. The uniformity of modulus is important for the application of these films as probes of mechanosensitive cell behavior.

In principle, raw AFM data could be used to estimate a film thickness, by iterating the height parameter in equation (2) to minimize the variation in

predicted modulus over the selected strain range, since over- or underestimated thickness will result in less consistent modulus predictions. For this technique to be applied, the linear model would need to completely describe the material mechanics in the analyzed strain range. However, experimental error makes it likely that decreases in film thickness could be mistaken for increases in stiffness, or vice-versa. The determination of modulus is more accurate when the exact film thickness is known, as it is here.

5.4.4 Finite element simulation of indentation.

All bulk tensile data were well-described by a Yeoh hyperelastic model.[34] When the Yeoh parameters calculated from the tensile data (*vide infra; see Figure 5.8*) were used to model indentation using a finite element simulation, the predicted force curves were very similar to those obtained experimentally; representative data are presented in Figure 5.7. Because of the experimental error in measuring quantities like the bulk film thickness or AFM cantilever spring constant, some differences in scalar magnitude between these two plots can be expected, although their shapes should be similar, as is seen here. The similarity between experimental AFM indentation data and simulations of the indentation using only bulk tensile properties is encouraging since it implies that the physical properties of thin and bulk films are similar, and it confirms the physical validity of the finite element analysis technique.

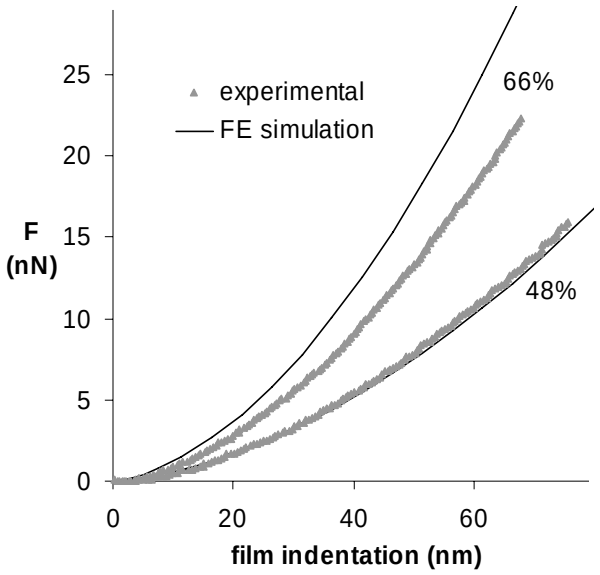

Figure 5.7 Superposition of experimental AFM data (from Figure 5.6) and finite element simulations of indentation based on bulk tensile data for protein films of aE-66%-*p*N_3Phe and aE-48%-*p*N_3Phe.

The samples investigated here are thick relative to the indentation depth and are highly elastic, so the deviations from linearity are small, as can be seen by comparing the linear model fit with experimental AFM data in Figure 5.6. However, the simulation approach should be applicable to thinner films (e.g., <100 nm) and to non-linear strain data as well, where a limited amount of data can be collected in the linear deformation range. While the Dimitriadis model is restricted to spherical tips, the simulation can be easily changed to describe conical or pyramidal tips, the type more commonly used because of their robustness and lower cost. These sharp tips have the additional advantage of being usable for imaging as well as indentation.

Inverting the technique of predicting the AFM response from the tensile data, the AFM data was used to calculate a modulus for the material using the

simulation. To accomplish this, coefficients of the Yeoh model were iterated in the finite element simulation to minimize the difference between the simulated and experimental AFM data using the entire force curve (including data past 10% indentation). The calculated *E* using this technique were indistinguishable from the *E* calculated with the Dimitriadis model. If high-strain data are collected, this technique can provide a full strain function for the material being tested in addition to the elastic modulus. While the finite element technique provides more flexibility, the simplicity of the Dimitriadis model is preferable when the geometry of the tip is known and when the linear elastic modulus *E* is the only value required.

5.4.5 Modulus control by variable incorporation of p*N*$_3$*Phe – bulk films.*

The incorporation of *p*N$_3$Phe in place of Phe in the artificial extracellular matrix protein can be tuned by varying its concentration during bacterial fermentation.[22] Here, the effects of the variable incorporation are shown for both bulk samples tested in uniaxial tension and thin-film samples tested with AFM nanoindentation. The tensile behavior of the bulk samples, in Figure 5.8 below, is typical of rubbery materials, and all aE-*p*N$_3$Phe films were extensible to 150% strain or greater.

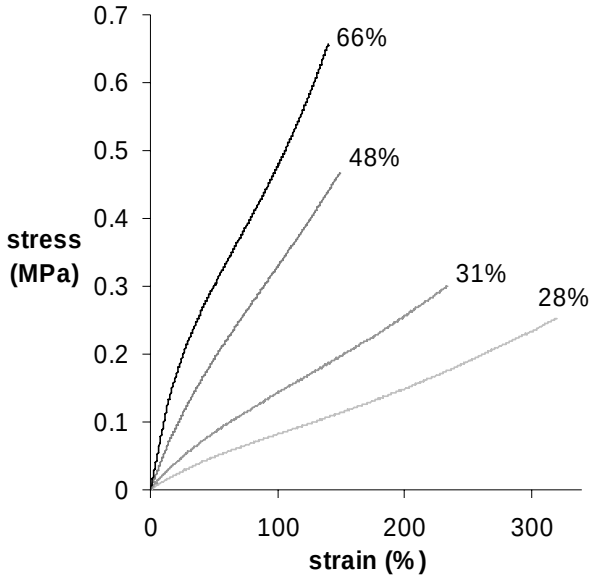

Figure 5.8 Sample tensile data for bulk films of aE-*p*N$_3$Phe, where the replacement of *p*N$_3$Phe for Phe was 28%, 31%, 48%, and 66%.

Higher moduli are seen for films made from protein with higher *p*N$_3$Phe concentrations, a result of increased crosslink densities after irradiation. If the materials are assumed to behave as ideal rubber networks, an approximation shown to be roughly valid for similar elastin-like hydrogels,[15,33] $G=(\rho RT/M_c)(1-2M_c/M)$.[35] G is the shear modulus, equal to one third the elastic modulus *E* for an incompressible material ($\nu=0.5$), a good approximation for the rubbery hydrogel protein films. The chain mass density ρ is found by multiplying the density of elastin,[36] 1.32 g/cm^3, by the measured polymer volume fraction in the films, 0.56. RT, the absolute temperature, is 22 °C = 2454 J/°K/mol. M_c is the average molecular weight between crosslinks, and the term $(1-2M_c/M)$ represents the fraction of elastically active crosslinks, where M is the molecular weight of the protein, 42.9 kDa. The M_c calculated for these films are listed in Table 5.1 A.

Table 5.1 (A) Physical properties of bulk aE-*p*N$_3$Phe films tested in uniaxial tension (n=2). (B) Physical properties of thin aE-*p*N$_3$Phe films tested by AFM (n≥6 spots, n≥24 total indents). The elastic moduli are indicated graphically in Figure 5.9.

A bulk

protein	thickness (μm)	avg. elastic modulus *E* (MPa)	mol. wt. between crosslinks M_c (kDa)	reaction efficiency
aE-66%-*p*N$_3$Phe	20	1.01 ± 0.07	4.3 ± 0.2	50 ± 3%
aE-48%-*p*N$_3$Phe	21	0.52 ± 0.04	7.0 ± 0.4	42 ± 2%
aE-31%-*p*N$_3$Phe	19	0.20 ± 0.04	11.9 ± 1.0	39 ± 3%
aE-28%-*p*N$_3$Phe	20	0.14 ± 0.02	13.8 ± 0.6	37 ± 2%

B AFM

protein	avg. thicknesses (nm)	avg. elastic modulus *E* (MPa)	mol. wt. between crosslinks M_c (kDa)	reaction efficiency
aE-66%-*p*N$_3$Phe	312, 322, 328, 1682, 1466	0.91 ± 0.16	4.9 ± 0.7	45 ± 7%
aE-48%-*p*N$_3$Phe	293, 368	0.44 ± 0.04	7.8 ± 0.4	38 ± 2%
aE-31%-*p*N$_3$Phe	223, 252	0.30 ± 0.02	9.8 ± 0.4	47 ± 2%
aE-28%-*p*N$_3$Phe	206, 206	0.29 ± 0.03	10.0 ± 0.5	51 ± 3%

Using M_c and the measured *p*N$_3$Phe incorporation, a crosslinking reaction efficiency can be calculated. For example, M_c = 4.3 kDa for aE-66%-*p*N$_3$Phe corresponds to 42.9/4.3 = 10 crosslinks per protein molecule, assuming random crosslinking, which is reasonable given the periodic Phe spacing in the protein and the statistical nature of its replacement by *p*N$_3$Phe. A 66% replacement of the 15 Phe sites in aE implies an average of 9.9 *p*N$_3$Phe side chains per molecule;

since each insertion crosslinks two molecules, this implies a reaction efficiency of 10/9.9/2 = 50%. The other films suggest efficiencies of 37-42% (Table 5.1 A). The efficiencies may be overestimated somewhat because entanglements may serve as additional effective crosslinks. In any case, the efficiency of photocrosslinking is high; the density of the protein phase (dry films) during photocrosslinking is likely one reason.

5.4.6 Modulus control by variable incorporation of pN_3*Phe – thin films.*

Figure 5.9 compares the elastic moduli, *E*, calculated from AFM data for thin films of variable *p*N_3Phe concentration to the values from uniaxial tension. For aE-48%-*p*N_3Phe and aE-66%-*p*N_3Phe, the values match within experimental error, indicating that the mechanical properties of the bulk films can be reproduced in films 200-400 nm thick, and supporting the validity of the Dimitriadis model for measuring *E*. The bulk and thin films, although cast from different solvents, are both crosslinked in the dry state, and are thus expected to have similar structures and elastic moduli.

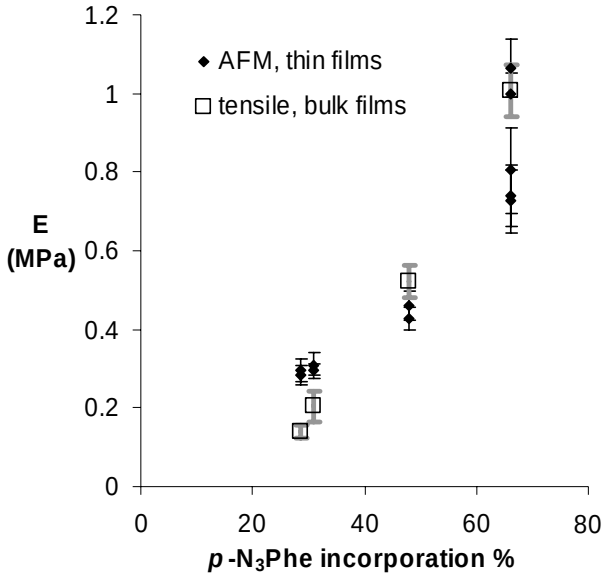

Figure 5.9 Measured elastic moduli of thin films of aE-*p*N3Phe versus fraction replacement of *p*N3Phe for Phe. Results from AFM nanoindentation of thin films and tensile testing of bulk films are compared. Separate data points are plotted for each film tested by AFM, with error bars indicating the standard deviation in *E* in a given film (n≥3 spots; n≥11 total indents). Standard deviation for tensile samples are also shown (n=2).

At low pN3Phe incorporation levels, the AFM seems to have yielded moduli slightly higher than those obtained from the tensile measurements; it is unclear whether this is due to unaccounted-for experimental error or some other factor. The analysis of reaction performed on the bulk films was repeated using the thin film moduli, and the resulting efficiencies were between 38 and 51% (Table 5.1 B).

The ability to tune the modulus of the thin films by variable *p*N3Phe incorporation should prove useful in cell-culture experiments designed to study mechanosensitive cell behavior on materials with coordinating biological signals

like the CS5 domain in protein aE. Cell behavior can be compared on substrates with systematic variations in modulus, although for certain studies, patterns of stiffness on a single film may be preferred. For example, a microfluidic mixer[13,37] may allow gradient formation from these proteins. aE-*p*N_3Phe with high and low *p*N_3Phe incorporation levels could be introduced to either side of a gradient generator and uniformly crosslinked once deposited on a surface.

5.4.7 Modulus control by variable irradiation of p*N₃Phe*

Controlling mechanical properties by differential irradiation allows films with patterns of stiffness to be made. A film containing a step gradient of stiffness was created here by UV-irradiating successive portions of the same film, made from aE-66%-*p*N_3Phe, for increasing lengths of time. The calculated elastic modulus, *E*, versus irradiation is shown in Figure 5.10 below; a greater-than-twofold variation in modulus is seen between 20 sec and 300 sec irradiation. The majority of the rise in stiffness occurs over the first minute of UV exposure, with a gradual plateau thereafter. The time required for *p*N_3Phe depletion is similar to that reported previously under similar irradiation conditions.[22]

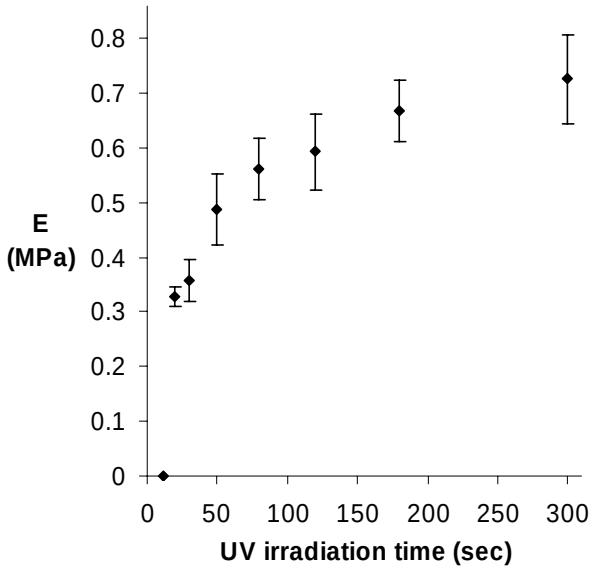

Figure 5.10 Modulus variation by variable irradiation on a single aE-66%-*p*N$_3$Phe film. Error bars indicate standard deviation in *E* within each zone of the step-gradient (n≥3 spots, n≥8 total indents per zone). Irradiation for 12 sec was not sufficient to form a crosslinked network, i.e., $E = 0$.

When washed to remove soluble protein, the thicknesses of the 20 sec and 30 sec zones along the gradient were ~35% and ~20% less than the thickness of the 80 sec and greater zones, indicating partial solubility. Taking into account the known film height, as the Dimitriadis model does, is essential for these gradients, since variable film height would make the Hertz model inaccurate even as a comparative measure of modulus.

Individual films that vary spatially in modulus on millimeter length scales, as in the step-gradient pattern created here, are useful in characterizing cell behavior. Large numbers of cells can be cultured on each zone, allowing average cell properties to be measured on several stiffness zones on a single substrate, which minimizes reagent usage and substrate preparation, and avoids

batch-to-batch variations in films and cells. Additionally, the ability to observe cell behavior at mechanical interfaces can be quite valuable on its own.[5] Films with more complex patterns of mechanical properties can also be envisioned. UV photoirradiation through a mask, which has already been used to pattern proteins into defined locations on a support,[22] could be applied to creating films with micropatterned moduli; cell behavior on micropatterned materials has been the subject of considerable recent study.[38]

While step gradients are easy to characterize with a limited number of indentations, films with continuous gradients of stiffness could also be made with the variable irradiation approach by moving an opaque shutter across the film during irradiation.[39] Gradients could be implemented over either short or long distances in the film. For steep gradients, the spatial resolution of the modulus measurement is limited only by the 300 nm-radius tip used for indentation, which should enable measurement of the variation in mechanical properties under a single spread cell. Even higher resolution may be achieved through use of conventional sharp (<20 nm) conical or pyramidal tips with finite element analysis of indentation. Gradients longer than the ~100 μm lateral piezo range of conventional AFM instruments could be characterized using translational reference points in the sample. The characterization would be facilitated by an automated technique to indent and analyze an array of spots on a sample.

5.5 Conclusions

The ability to incorporate the photosensitive amino acid *para*-azidophenylalanine into artificial proteins has made it possible to create mechanically variant thin protein films. A film height-dependent indentation model, whose results were confirmed by bulk tensile data and finite element simulation, allowed the moduli of the films to be confidently measured. These thin films are intended for use as substrates to characterize mechanosensitive cell behavior in the context of coincident biological signals. The results provide methods for making individual films with complex variations in stiffness, such as patterns and gradients, and the resolution and flexibility of the AFM technique used here should make characterizing their stiffness straightforward.

While the existing protein can be used to probe cell interactions with the CS5 binding domain, the platform for making photosensitive artificial proteins can be extended to other peptide domains of interest; we are currently characterizing RGD-containing photosensitive protein films. A better understanding of cell response to coordinating biological and mechanical signals will aid the design of functional biomaterials.

Acknowledgements

Stacey Maskarinec made proteins aE-28%-*p*N_3Phe, aE-31%-*p*N_3Phe, and aE-66%-*p*N_3Phe. Marissa Mock performed the NMR characterizations. Funding was provided by the NSF MRSEC Center for the Science and Engineering of Materials at Caltech, and by the NIH (HL 59987).

5.6 References

(1) Pelham RJ, Wang YL. Cell locomotion and focal adhesions are regulated by substrate flexibility. *Proc. Natl. Acad. Sci. U. S. A.* **1997**, *94*, 13661-13665.

(2) Cukierman E, Pankov R, Stevens DR, Yamada KM. Taking cell-matrix adhesions to the third dimension. *Science* **2001**, *294*, 1708-1712.

(3) Engler A, Bacakova L, Newman C, Hategan A, Griffin M, Discher D. Substrate compliance versus ligand density in cell on gel responses. *Biophys. J.* **2004**, *86*, 617-628.

(4) Engler AJ, Richert L, Wong JY, Picart C, Discher DE. Surface probe measurements of the elasticity of sectioned tissue, thin gels and polyelectrolyte multilayer films: Correlations between substrate stiffness and cell adhesion. *Surf. Sci.* **2004**, *570*, 142-154.

(5) Lo CM, Wang HB, Dembo M, Wang YL. Cell movement is guided by the rigidity of the substrate. *Biophys. J.* **2000**, *79*, 144-152.

(6) Gray DS, Tien J, Chen CS. Repositioning of cells by mechanotaxis on surfaces with micropatterned Young's modulus. *J. Biomed. Mater. Res. A* **2003**, *66A*, 605-614.

(7) Wang HB, Dembo M, Wang YL. Substrate flexibility regulates growth and apoptosis of normal but not transformed cells. *Am. J. Physiol. - Cell Ph.* **2000**, *279*, C1345-C1350.

(8) Engler AJ, Griffin MA, Sen S, Bonnetnann CG, Sweeney HL, Discher DE. Myotubes differentiate optimally on substrates with tissue-like stiffness: pathological implications for soft or stiff microenvironments. *J. Cell Biol.* **2004**, *166*, 877-887.

(9) Discher DE, Janmey P, Wang YL. Tissue cells feel and respond to the stiffness of their substrate. *Science* **2005**, *310*, 1139-1143.

(10) Wang YL, Pelham RJ In *Molecular Motors and the Cytoskeleton, Pt B*, **1998**; Vol. 298, pp 489-496.

(11) Maskarinec SA, Tirrell DA. Protein engineering approaches to biomaterials design. *Curr. Opin. Biotechnol.* **2005**, *16*, 422-426.

(12) Wong JY, Velasco A, Rajagopalan P, Pham Q. Directed movement of vascular smooth muscle cells on gradient-compliant hydrogels. *Langmuir* **2003**, *19*, 1908-1913.

(13) Zaari N, Rajagopalan P, Kim SK, Engler AJ, Wong JY. Photopolymerization in microfluidic gradient generators: Microscale control of substrate compliance to manipulate cell response. *Adv. Mater.* **2004**, *16*, 2133-2137.

(14) Panitch A, Yamaoka T, Fournier MJ, Mason TL, Tirrell DA. Design and biosynthesis of elastin-like artificial extracellular matrix proteins containing periodically spaced fibronectin CS5 domains. *Macromolecules* **1999**, *32*, 1701-1703.

(15) Welsh ER, Tirrell DA. Engineering the extracellular matrix: A novel approach to polymeric biomaterials. I. Control of the physical properties of artificial protein matrices designed to support adhesion of vascular endothelial cells. *Biomacromolecules* **2000**, *1*, 23-30.

(16) Di Zio K, Tirrell DA. Mechanical properties of artificial protein matrices engineered for control of cell and tissue behavior. *Macromolecules* **2003**, *36*, 1553-1558.

(17) Liu JC, Heilshorn SC, Tirrell DA. Comparative cell response to artificial extracellular matrix proteins containing the RGD and CS5 cell-binding domains. *Biomacromolecules* **2004**, *5*, 497-504.

(18) Mould AP, Komoriya A, Yamada KM, Humphries MJ. The CS5 Peptide Is a 2nd Site in the IIICS region of fibronectin recognized by the integrin alpha-4-beta-1 - inhibition of alpha-4-beta-1 function by RGD peptide homologs. *J. Biol. Chem.* **1991**, *266*, 3579-3585.

(19) Urry DW. Physical chemistry of biological free energy transduction as demonstrated by elastic protein-based polymers. *J. Phys. Chem. B* **1997**, *101*, 11007-11028.

(20) Kast P, Hennecke H. Amino-acid substrate-specificity of escherichia-coli phenylalanyl-transfer RNA-synthetase altered by distinct mutations. *J. Mol. Biol.* **1991**, *222*, 99-124.

(21) Kirshenbaum K, Carrico IS, Tirrell DA. Biosynthesis of proteins incorporating a versatile set of phenylalanine analogues. *Chembiochem* **2002**, *3*, 235-237.

(22) (Appendix) Carrico IS, Heilshorn SC, Mock ML, Liu JC, Nowatzki PJ, Maskarinec SA, Franck C, Ravichandran G, Tirrell DA. Lithographic patterning of intrinsically photoreactive cell-adhesive proteins. *Prepared for submission.*

(23) Vinckier A, Semenza G. Measuring elasticity of biological materials by atomic force microscopy. *FEBS Lett.* **1998**, *430*, 12-16.

(24) Cappella B, Dietler G. Force-distance curves by atomic force microscopy. *Surface Science Reports* **1999**, *34*, 1-103.

(25) Heinz WF, Hoh JH. Spatially resolved force spectroscopy of biological surfaces using the atomic force microscope. *Trends Biotechnol.* **1999**, *17*, 143-150.

(26) Mahaffy RE, Shih CK, MacKintosh FC, Kas J. Scanning probe-based frequency-dependent microrheology of polymer gels and biological cells. *Phys. Rev. Lett.* **2000**, *85*, 880-883.

(27) Richert L, Engler AJ, Discher DE, Picart C. Elasticity of native and cross-linked polyelectrolyte multilayer films. *Biomacromolecules* **2004**, *5*, 1908-1916.

(28) Costa KD, Yin FCP. Analysis of indentation: Implications for measuring mechanical properties with atomic force microscopy. *J. Biomech. Eng.* **1999**, *121*, 462-471.

(29) Dimitriadis EK, Horkay F, Maresca J, Kachar B, Chadwick RS. Determination of elastic moduli of thin layers of soft material using the atomic force microscope. *Biophys. J.* **2002**, *82*, 2798-2810.

(30) Domke J, Radmacher M. Measuring the elastic properties of thin polymer films with the atomic force microscope. *Langmuir* **1998**, *14*, 3320-3325.

(31) Akhremitchev BB, Walker GC. Finite sample thickness effects on elasticity determination using atomic force microscopy. *Langmuir* **1999**, *15*, 5630-5634.

(32) Sharma N "Biosynthetic introduction of aryl bromide functionality into proteins," Ph.D. Thesis, University of Massachusetts Amherst, **2001**.

(33) Nowatzki PJ, Tirrell DA. Physical properties of artificial extracellular matrix protein films prepared by isocyanate crosslinking. *Biomaterials* **2004**, *25*, 1261-1267.

(34) Yeoh OH. Some forms of the strain-energy function for rubber. *Rubber Chem. Technol.* **1993**, *66*, 754-771.

(35) Flory PJ. *Principles of Polymer Chemistry*; Cornell University Press: Ithaca, NY, **1953**.

(36) Lillie MA, Gosline JM. Unusual swelling of elastin. *Biopolymers* **2002**, *64*, 115-126.

(37) Jeon NL, Dertinger SKW, Chiu DT, Choi IS, Stroock AD, Whitesides GM. Generation of solution and surface gradients using microfluidic systems. *Langmuir* **2000**, *16*, 8311-8316.

(38) Stevens MM, George JH. Exploring and engineering the cell surface interface. *Science* **2005**, *310*, 1135-1138.

(39) Pucci V, Raggi MA, Svec F, Frechet JMJ. Monolithic columns with a gradient of functionalities prepared via photoinitiated grafting for separations using capillary electrochromatography. *J. Sep. Sci.* **2004**, *27*, 779-788.

6 CONCLUSIONS AND FUTURE WORK

There are now several examples of artificial proteins with distinctive mechanical and biological properties identified as useful for implantable biomaterials;[1-4] these illustrate the unique possibilities in architectural control and bioactivity that the engineered protein approach provides. The work presented in this thesis is an important step forward for this area of research, because it includes a successful demonstration of an artificial protein device effecting its designed function *in vivo*. Specifically, an artificial extracellular matrix (aECM) protein bearing the peptide sequence RGD in its backbone promotes the adhesion and migration of epithelial cells in a crosslinked corneal onlay film. Having been shown to epithelialize within one week, these onlay lenses will next be evaluated over several months in the same rabbit cornea model to confirm their long-term biocompatibility and their ability to support the development of mature epithelial tissue. For their ultimate application as corrective lenses, a reliable means of adhering the onlays to the corneal stroma must be engineered; this could be achieved using tissue sealants or by functionalizing their inner surface.

The success of elastin-like proteins in the ocular milieu bodes well for their use in other biomedical contexts as well. Vascular grafts are one application where there is a tremendous need for new materials, but where additional challenges are posed by dynamic mechanical stresses and direct blood contact. Here, crosslinked aECM protein films were shown to be uniform and highly-

extensible, and to mimic the elasticity of native vascular tissue. With their desirable mechanical properties and demonstrated ability to specifically and strongly adhere to endothelial cells,[5-7] the aECM materials are poised to undergo detailed *in vivo* characterizations, beginning with subdermal biocompatibility experiments and proceeding to mammalian arterial models. A requirement for these studies is the removal of the T7 tag, used for protein identification but a known antigen, from the protein. This can be accomplished enzymatically using enterokinase, or by removing the corresponding DNA from the coding sequence. The ability to control mechanical properties and degradation rates through changes in sequence and crosslinking, explored in this work, will aid the engineering of successive generations of materials to respond to the challenges of their environments.

In addition to describing promising materials for implantable devices, this thesis presents examples of how engineered artificial proteins can be used to fabricate advanced substrates to study mechanosensitive cell behavior. It was shown that incorporation of the photosensitive non-canonical amino acid *para*-azidophenylalanine (*p*N_3Phe) allowed aECM protein films of tunable modulus to be made by changes in *p*N_3Phe concentration or the degree of ultraviolet irradiation. Using variable irradiation, individual thin film substrates with patterns of mechanical properties were prepared.

Atomic force microscopy-based nanoindentation was shown to be effective in evaluating the elastic modulus of these soft thin films; the sensitivity and high resolution of this technique should make it useful for characterizing a

wide range of substrates. Automation of these or similar indentation techniques will allow the mechanical properties of finely patterned films to be rapidly mapped, facilitating their use as sophisticated cell culture substrates.

Longer photosensitive aECM proteins, of the same design as the ones described here, are expected to expand the usefulness of the materials developed in this work, since they would gel at lower *p*N_3Phe concentrations. The lower values of elastic moduli that these enable would allow a greater range of stiffness to be created in individual differentially-crosslinked films, and could soften the films from hundreds of kPa to tens of kPa, where a majority of mechanosensitive cellular responses have been observed to occur.[8]

Mechanically variant aECM protein films have an important advantage over synthetic polymer systems with the same property, because they present mechanical signals to cells in the context of biological signals. The peptide sequences need not be limited to the CS5 and RGD cell-binding domains used here. Microfluidic systems could be used to create patterns of different signal-bearing artificial proteins on a surface, which could then be subjected to variable irradiation to create films with patterns of coordinating mechanical and biological stimuli. Such substrates are likely to aid in elucidating the effects of complex environmental signals on cell behavior, which in turn will inform the future design of advanced biomaterials.

References

(1) Halstenberg S, Panitch A, Rizzi S, Hall H, Hubbell JA. Biologically engineered protein-graft-poly(ethylene glycol) hydrogels: A cell adhesive and plasmin-degradable biosynthetic material for tissue repair. *Biomacromolecules* **2002**, *3*, 710-723.

(2) Wright ER, Conticello VP. Self-assembly of block copolymers derived from elastin-mimetic polypeptide sequences. *Adv. Drug Delivery Rev.* **2002**, *54*, 1057-1073.

(3) Altman GH, Diaz F, Jakuba C, Calabro T, Horan RL, Chen JS, Lu H, Richmond J, Kaplan DL. Silk-based biomaterials. *Biomaterials* **2003**, *24*, 401-416.

(4) Shen W, Zhang KH, Kornfield JA, Tirrell DA. Tuning the erosion rate of artificial protein hydrogels through control of network topology. *Nature Materials* **2006**, *5*, 153-158.

(5) Heilshorn SC, DiZio KA, Welsh ER, Tirrell DA. Endothelial cell adhesion to the fibronectin CS5 domain in artificial extracellular matrix proteins. *Biomaterials* **2003**, *24*, 4245-4252.

(6) Liu JC, Heilshorn SC, Tirrell DA. Comparative cell response to artificial extracellular matrix proteins containing the RGD and CS5 cell-binding domains. *Biomacromolecules* **2004**, *5*, 497-504.

(7) Heilshorn SC, Liu JC, Tirrell DA. Cell-binding domain context affects cell behavior on engineered proteins. *Biomacromolecules* **2005**, *6*, 318-323.

(8) Discher DE, Janmey P, Wang YL. Tissue cells feel and respond to the stiffness of their substrate. *Science* **2005**, *310*, 1139-1143.

APPENDIX LITHOGRAPHIC PATTERNING OF INTRINSICALLY PHOTOREACTIVE CELL-ADHESIVE PROTEINS

Manuscript prepared for submission by Isaac S. Carrico,[1] Sarah C. Heilshorn,[1] Marissa L. Mock,[1] Julie C. Liu,[1] Paul J. Nowatzki,[1] Stacey Maskarinec,[1] Christian Franck,[2] Guruswami Ravichandran,[2] and David A. Tirrell[1]

(1) Division of Chemistry and Chemical Engineering, California Institute of Technology

(2) Graduate Aeronautical Laboratories, California Institute of Technology

A.1 Introduction

Control of the spatial arrangement of proteins on surfaces is essential in a number of emerging biotechnologies. Defining the location of specific proteins on the micro- or nanoscale improves the quality of protein microarrays, increases the sensitivity of biosensors,[1,2] and allows tissue engineering scaffolds to organize multiple cell types.[3] Patterning is also a powerful tool in cell biology, where cell arrays are used to elucidate key factors that mediate migration, proliferation, and cell-cell interactions.[4-6] Although photolithography holds a preeminent place as a patterning method in the microelectronics industry, optical lithography of proteins has been hampered by the need either to use traditional chemical photoresists or to modify proteins chemically by attachment of photoreactive functional groups; both methods can compromise protein function.[7]

Production of a protein "photoresist" without the need for post-translational chemical modification would require an intrinsically photoreactive

protein. Recently, the incorporation of photoreactive, non-canonical amino acids into proteins has been reported via both site-specific[8,9] and residue-specific techniques.[10] Here we describe the microbial expression of artificial proteins bearing the photosensitive non-canonical amino acid *para*-azidophenylalanine (*p*N_3Phe). The recombinant proteins, designated artificial extracellular matrix proteins with aryl azides (aE-N_3), belong to a family of engineered proteins designed to exhibit mechanical properties similar to those of native elastins[11] and to support adhesion of endothelial cells through cell-binding domains (CS5 or RGD) derived from fibronectin (Figure A.1A).[12] These proteins can be crosslinked efficiently upon irradiation at 365 nm. The physical properties of the crosslinked films can be tuned by changing the extent of *p*N_3Phe incorporation, which is accomplished simply by changing the concentration of the non-canonical amino acid in the expression medium. Thin films of aE-N_3 proteins can be patterned on surfaces via simple photolithographic techniques. We demonstrate the utility of the method by creating cell arrays through selective endothelial cell attachment to lithographically prepared protein patterns.

A.2 Results and discussion

Preparation of aE-N_3 proteins containing the CS5 cell binding domain was accomplished through residue-specific incorporation of *p*N_3Phe in *E. coli*. This method of incorporation relies on competitive activation of phenylalanine (Phe) and *p*N_3Phe by the phenylalanyl-tRNA synthetase (PheRS), the enzyme responsible for charging Phe to its cognate tRNA.[13] The PheRS used for this

study was a previously characterized mutant with relaxed substrate specificity.[13] Proteins were expressed in a Phe-auxotrophic *E. coli* strain grown in cultures supplemented with *p*N$_3$Phe and purified by taking advantage of the temperature-dependent phase behavior of proteins with elastin-like repeats.[14] Incorporation efficiency was determined by integration of the aromatic proton signals in the ^{1}H NMR spectra of the purified proteins (Figure A.4); the extent of Phe replacement varied from 13% to 53%, depending on the concentration of *p*N$_3$Phe in the expression medium (see Methods section below; Figure A.5).

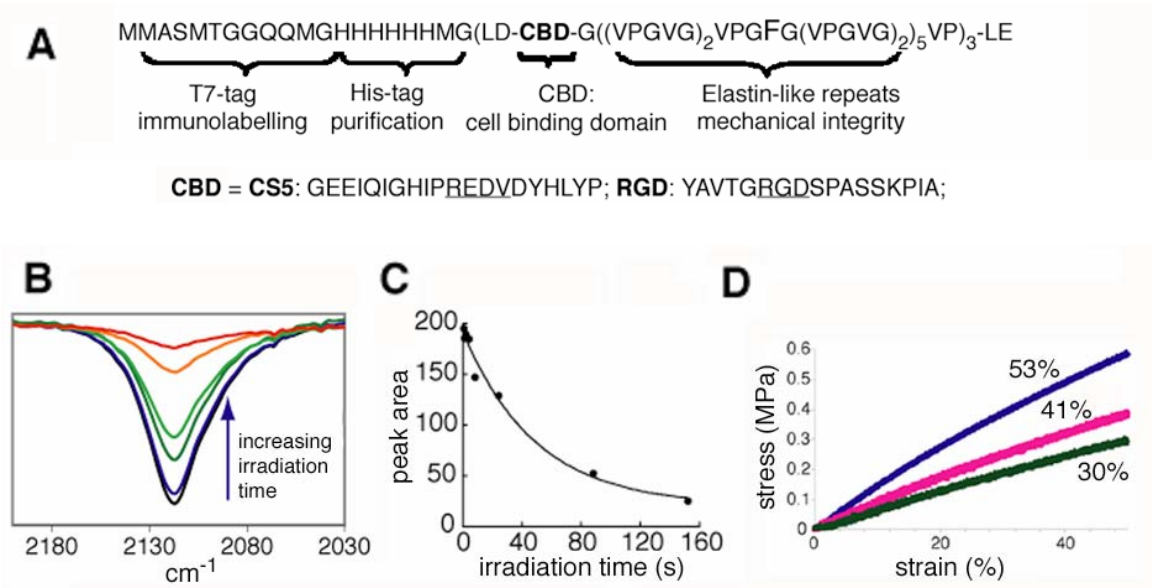

Figure A.1 Response of aE-N$_3$ to irradiation. (A) Primary sequence of aE-N$_3$; the CS5 variant was used in all studies described herein. (B) FTIR demonstrates loss of the characteristic azide asymmetric stretch as a function of time of irradiation of aE-N$_3$ films. (C) Peak area vs. irradiation time yields a first order decay with $t_{1/2}$=34 sec. (D) Uniaxial tensile testing of irradiated mold-cast films of aE-N$_3$ with differing *p*N$_3$Phe contents; modulus increases with increasing concentration of photoreactive side chains.

Understanding the response of the photoreactive protein to irradiation is crucial for high-resolution pattern formation. We measured the rate of azide decomposition under irradiation by monitoring loss of the characteristic infrared (IR) asymmetric stretch at 2130 cm^{-1} (Figure A.1B).[15] Measurements were performed on thin films of aE-N_3 spin coated directly onto zinc selenide wafers and irradiated using a Karl Suss contact aligner filtered to 365 nm in constant intensity (7 mW/cm^2) mode, with a quartz wafer in place of the mask. Azide loss under these conditions was rapid, following first-order kinetics with a half-life of 34 seconds (Figure A.1C). It is noteworthy that none of the other infrared bands were noticeably altered, indicating that irradiation under the conditions used here activates the aryl azide without substantial modification of any of the canonical amino acids. This is as expected given that none of the natural 20 amino acids absorb above 310 nm.[16]

Elastic moduli of irradiated aE-N_3 films were determined by uniaxial tensile testing under simulated physiological conditions (Figure A.1D). As expected, the elastic modulus correlated with the extent of *p*N_3Phe incorporation. Irradiated aE-N_3 films in which 30, 41, or 53% of the encoded Phe residues were replaced by *p*N_3Phe yielded elastic moduli of 0.53 ± 0.10, 0.94 ± 0.09, and 1.39 ± 0.09 MPa, respectively, which are in the range of native elastin (0.3 – 0.6 MPa). Replacement of less than 20% of the encoded Phe residues gave films that were too weak to test, and films made without *p*N_3Phe yielded no evidence of crosslinking. The fact that modulus can be controlled simply by changing the *p*N_3Phe concentration in the expression medium is an attractive feature of the

method, as recent work has highlighted the role of mechanical transduction mechanisms in mediating the physiology of adherent cells.[17,18]

To investigate the potential of photoreactive proteins as substrates for studies of cell adhesion and growth, we created patterns of adherent endothelial cells on proteins patterned by photolithography. Protein films created by spin coating 10% solutions of protein in dimethylsulfoxide directly on poly(ethylene glycol) (PEG)-coated glass coverslips were clear and homogeneous by optical microscopy. Protein films were dried at 50°C for 5 minutes and subsequently irradiated for 30 seconds at 365 nm through a chrome-on-quartz mask using a Karl Suss contact aligner. Efficient stripping of the masked areas was accomplished by washing in mild aqueous detergent (0.05% aqueous sodium dodecylsulfate).

Fluorescence immunolabeling with anti-T7-tag antibody showed that the aE-N_3 protein was localized only within the irradiated areas of the pattern (Figure A.6). Films prepared from the protein lacking *p*N_3Phe formed no detectable patterns even after prolonged exposure times. Non-contact atomic force microscopy (AFM) of dried aE-N_3 patterns demonstrated uniform features (Figure A.7), which varied in height depending on the conditions used for spin coating. Films spun at 1400 and 2000 rpm were 84 and 4 nm thick. Protein patterns stored either dry or in aqueous solutions were stable for weeks.

To create cell arrays, human umbilical vein endothelial cells (HUVEC) were plated on aE-N_3 patterns in the absence of serum. After six hours of incubation, the medium was supplemented with 5% serum. After 24 hours of incubation,

HUVEC exhibited well-spread morphologies and had proliferated to confluence exclusively within the patterned areas (Figure A.2). HUVEC monolayers in the interior of the patterned regions were indistinguishable from monolayers grown on homogenous fibronectin coatings; however, cells positioned along the aE-N_3 pattern edges were elongated and oriented parallel to the pattern border, consistent with previous studies.[19]

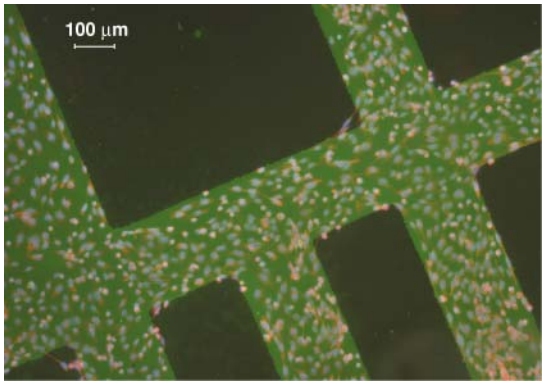

Figure A.2 Fluorescence microscopy of HUVEC attached to photopatterned aE-N_3. Immunostaining with anti-T7 (green) demonstrates colocalization of aE-N_3 protein and cells stained with nuclear stain (blue) and cytoskeletal stain (red).

HUVEC patterns were stable in serum for 48 hours after reaching confluence, consistent with known behavior of PEG coatings as cell-resistant backgrounds.[20] At longer times, cells began growing beyond the protein pattern at sites where the protein pattern formed right angles, presumably in concert with cellular synthesis and secretion of extracellular matrix proteins.

To establish the specificity of the observed adhesion, aE-N_3 proteins with sequence-scrambled CS5 and RGD cell binding domains were created, in which

the positions of just two adjacent amino acids were swapped. HUVEC spread well on uniformly photocrosslinked aE-N_3 films with RGD (RGD-N_3) but not on the scrambled version (RDG-N_3), seen in Figure A.3 below.

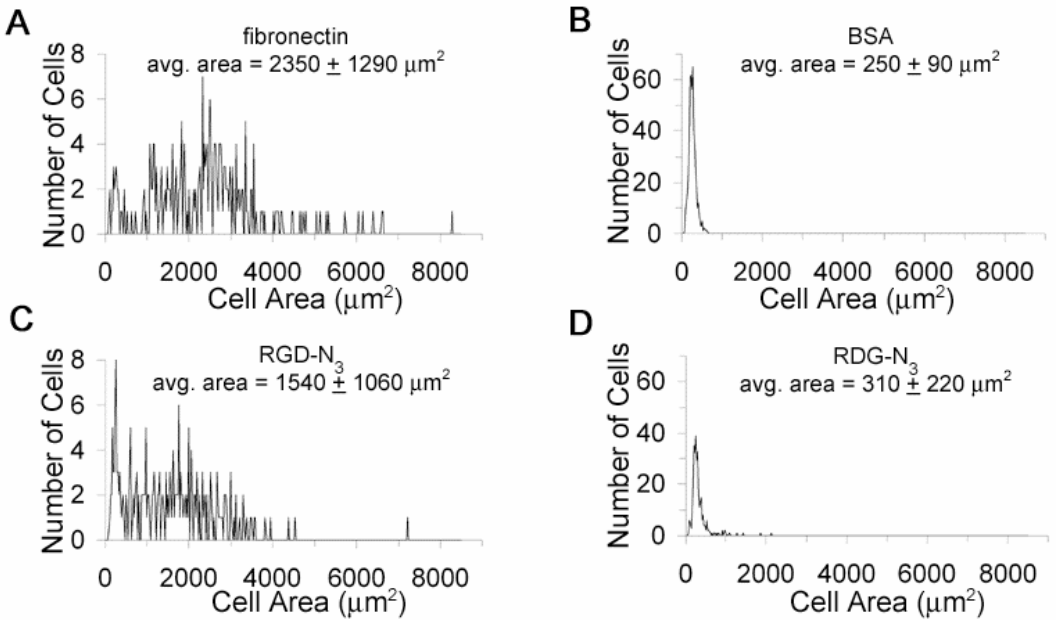

Figure A.3 HUVEC spread areas on (A) fibronectin (positive control), (B) BSA (negative control), (C) RGD-N_3, and (D) RDG-N_3 demonstrate the sequence-specificity of cell spreading.

The availability of intrinsically photoreactive proteins enables a facile new method for patterning of proteins. The technical simplicity of the method allows rapid production of samples with a wide variety of feature shapes and sizes, while permitting straightforward engineering of the elastic modulus of the crosslinked protein. The method is a promising approach to the study of adherent cells, providing control over mechanical properties, ligand-receptor inter-actions, and geometric shape. Applications in medical devices, tissue engineering, and array technologies are readily imagined.

A.3 Methods and additional figures

A.3.1 Cloning of aE protein constructs.

Synthetic oligonucleotides encoding the CS5 and RGD cell-binding domains, and their sequence-scrambled analogs "SC5" and "RDG", were annealed, phosphorylated, and ligated into pEC2[21] to produce pEC2-CS5, pEC2-SC5, pEC2-RGD, and pEC2-RDG. An oligonucleotide encoding the elastin-like repeat $(VPGVG)_2VPGFG(VPGVG)_2$ was similarly ligated into pUC19 (New England Biolabs) between *Eco*R1 and *Bam*H1. The elastin-like insert was cut out using *Ban*1 and self-ligated to form multimers. The multimerization mixture was ligated with *Ban1*-linearized pEC2-CS5, pEC2-SC5, pEC2-RGD, or pEC2-RDG. Transformants with the pentamer insert were selected, digested at *Xho*1 and *Sal*1, and ligated into a modified pET28a (Novagen). This step was repeated twice to obtain the final $[CBD(ELF)_5]_3$ construct under control of the T7 promoter. Finally, the *pheS** gene encoding the alpha subunit of the A294G mutant of *E. coli* phenylalanyl-tRNA synthetase was subcloned into the *Sph*I site from the pKSS vector kindly provided by Dr. Peter Kast[22] to produce pNS-CS5-ELF[23], pSM-SC5-ELF, pSM-RGD-ELF, and pSM-RDG-ELF.

A.3.2 Protein expression and purification.

The target protein was expressed using a phenylalanine auxotrophic derivative of *E. coli* strain designated AF-IQ[24] harboring either pNS-CS5-ELF, pSM-SC5-ELF, pSM-RGD-ELF, or pSM-RDG-ELF. To express proteins from

these strains, a culture was grown overnight in 2xYT medium and used to inoculate 1 L of M9AA medium supplemented with the antibiotics chloramphenicol and kanamycin. At an OD_{600} of 1.0, expression of target protein and T7 RNA polymerase was induced by adding 1 mM IPTG. After 10 additional minutes of growth, the cells were washed twice with 0.9% NaCl and resuspended in M9 medium containing 19 amino acids (excluding phenylalanine) to a final volume of 1 L. The cultures were supplemented with either 25 mg/L phenylalanine (positive control) or up to 250 mg solid *p*N_3Phe and grown for 4 h. Protein expression was monitored by SDS-PAGE and Western blotting with anti-T7 tag-horseradish peroxidase conjugate antibody (Amersham). Cell pellets, produced by spinning down (10,000×g, 10 min, 25°C) 1L of expression culture, were resuspended in 20 mL of TEN buffer (10 mM Tris, 1 mM EDTA, 0.1 M NaCl) by sonication and frozen. Frozen lysate was treated with 1 mM PMSF, and 10 μg/mL each of DNase and RNase was added. This mixture was agitated for 4 h at 37°C and centrifuged at a temperature above the expected LCST of the protein (22000×g, 60 min, 25°C). The target protein was extracted from the pellet into 4 M urea at 4°C. This suspension was clarified by centrifugation below the LCST (22000×g, 60 min, 2°C). The resulting supernatant was exhaustively dialyzed in cold (4°C) distilled water and subsequently lyophilized. Typical experiments yielded 40 mg of protein per liter of culture.

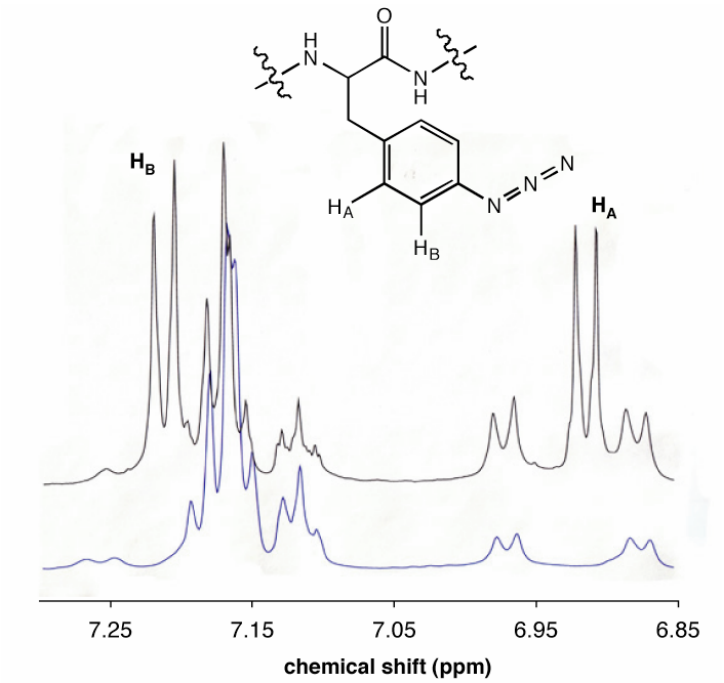

Figure A.4 ^{1}H NMR spectrum of aE-N$_3$ expressed in media supplemented with phenylalanine (bottom spectrum) or with 250 mg/L *p*N$_3$Phe (top spectrum). Spectra are identical except for two additional doublets in the top spectrum resulting from the aromatic protons of *p*N$_3$Phe; integration indicates 53% *p*N$_3$Phe incorporation. 600 MHz spectra were taken on 1 mM samples in DMSO-d$_6$ at 23°C.

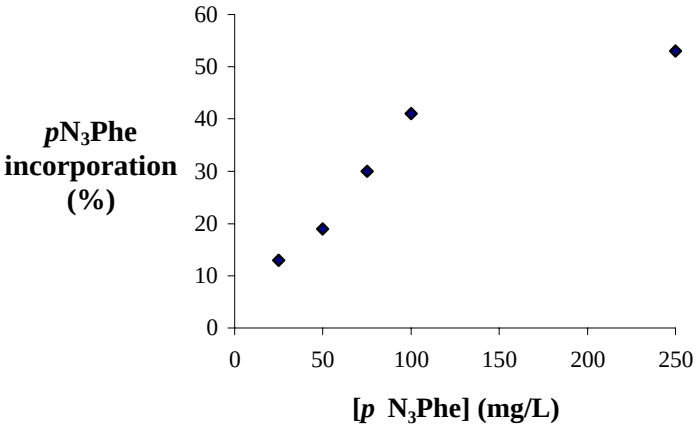

Figure A.5 Incorporation of *p*N$_3$Phe into aE-N$_3$ as a function of concentration in the expression medium.

A.3.4 Mechanical testing.

Samples were created in polytetrafluoroethylene molds by drying 10% aE-N_3 solutions in DMSO overnight at 50°C and were irradiated with a 100 W mercury lamp for 30 minutes. Samples were removed from the mold, swollen in 4°C water overnight to fully hydrate, cut into testing strips, and finally equilibrated in PBS at 37°C. Films were approximately 3 mm x 10 mm. Uniaxial tensile testing of equilibrated films was performed at 37°C in phosphate buffered saline at pH = 7.4 on an Instron Universal Testing Machine model 5542 with a 5 N load cell. Films were extended at a rate of 10% length/minute. Each protein sample was tested 3 to 6 times.

A.3.5 Photolithographic patterning of aE-N_3.

Glass coverslips (12 mm circles) were sonicated for 15 min in a saturated solution of potassium hydroxide in ethanol. Clean coverslips were rinsed under a stream of filtered (0.2 μm) doubly distilled water followed by a stream of filtered ethanol and dried briefly with canned air. Dried coverslips were immersed for 30 min in a freshly prepared solution of 1 mL 3-(trimethoxysilylpropyl)-diethylenetriamine (DETA), 2.5 mL acetic acid, and 46.5 mL methanol (2 % DETA). Aminated coverslips were rinsed under streams of water and then ethanol, dried with canned air, and cured for 4 h at 50°C. Cured coverslips were placed in a covered dish containing a reservoir of pyridine and were covered dropwise with a 100 mM solution in pyridine of mPEG-SPA-2000 (Nektar Therapeutics, MW = 2000 Da). After 12 h, the PEGylated coverslips were

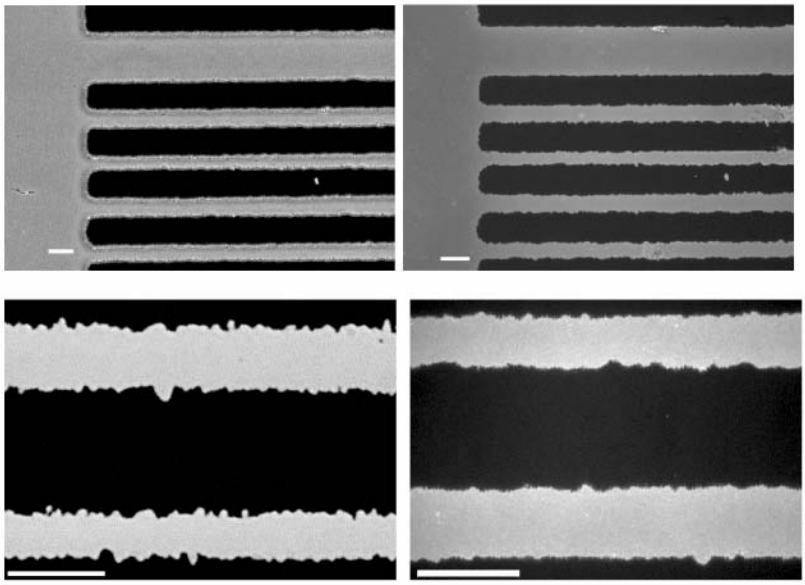

Figure A.6 Phase contrast microscopy images of the chrome mask used in photopatterning (left panels) compared with fluorescence microscopy images of aE-N_3 patterns (right panels). Scale bars represent 50 μm. In the top panels (lower magnification), the protein pattern could be visually matched to precisely the region on the mask that created it. The bottom panels (higher magnification) show two separate regions with features of similar sizes.

rinsed under streams of water and then ethanol, dried with canned air, and used immediately. PEGylated coverslips were covered dropwise with 8 μL of a 12.5 mg/mL solution of aE-N_3 in DMSO that had been centrifuged for 1 min at 14000 rpm to remove particulates. Coverslips were spun for 100 s at 1400 rpm on a Specialty Coating Systems model P-6000 spin coater. Protein-coated slides were dried at 50°C for 30 min. Exposure of protein to sunlight was avoided until protein photolithography was complete. Protein-coated slides were exposed for 30 s in a Karl Suss mask aligner (365 nm) under a chrome-on-quartz mask prepared by Dr. Michael Diehl by chrome deposition and stripping from a 3000 dpi transparency. Irradiated coverslips were washed overnight in 0.05% sodium

dodecyl sulfate to remove soluble protein from the masked regions and then rinsed for 6 h in filtered water.

A.3.6 Atomic force microscopy.

Topographical scans of aE-N_3 protein patterns on PEGylated coverslips were obtained with an AutoProbe M5 atomic force microscope (Park Scientific Instruments) in constant-force contact mode, using pyramidal tips (0.58 N/m, Veeco DNP-S). Imaging was performed in water: a glass slide was affixed to the back of the cantilever mount in the path of the laser, and the space between the sample and the slide was filled with water to provide a smooth and constant optical interface.

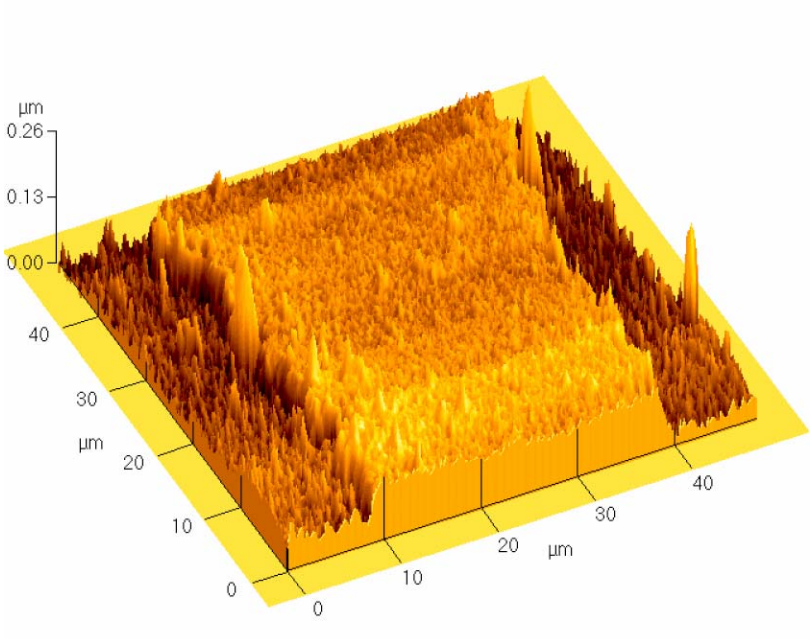

Figure A.7 AFM image of patterned aE-N_3. Full width of pattern feature (30 µm) is visible.

A.3.7 Cell culture.

Human umbilical vein endothelial cells (HUVEC) were purchased from Clonetics and maintained in endothelial growth medium-2 (EGM-2, 2% serum, Clonetics, Walkersville, MD). Cells were kept in a humidified, 5% CO_2 environment at 37°C and passaged non-enzymatically using a 0.61 mM EDTA solution (Gibco, Grand Island, NY). Cells between passages 2 and 9 were used for all experiments.

A.3.8 Cell patterning.

Patterned coverslips were placed in a 24-well plate, and HUVEC were added at density of 2.0×10^5 cells/cm^2 in a total volume of 1 mL of endothelial cell serum-free defined medium (Cell Applications, San Diego, CA). Phase contrast pictures were taken on a Nikon Eclipse TE 300 microscope. Fluorescence pictures were taken on a Zeiss Axioplan II fluorescence microscope equipped with a monochrome Axiocam. To fix and fluorescently label cell patterns, the coverslips were placed in the wells of a 24-well plate, and each well was washed 3 times with 1 mL phosphate-buffered saline (PBS) before 0.5 mL ice-cold acetone was applied for exactly 1 min. The wells were again washed 3 times with 1 mL PBS before 0.5 mL of a 10% BSA solution was applied for 30 min at room temperature. After blocking, 0.25 μL of anti-T7 primary antibody (Novagen) was added and allowed to incubate at room temperature for at least 6 h. The wells were then washed three times with 1 mL of water for 5 min without agitation. A secondary antibody/phalloidin solution composed of 425 μL PBS, 50 μL

secondary antibody (Cy2-labeled anti-mouse, 0.5 mg/mL, Chemicon), and 25 μL Alexa Fluor 546 phalloidin (Molecular Probes) was incubated with the samples in the dark for 1 h. Labeled samples were washed with 1 mL of water for 10 minutes with agitation followed by 1 mL of water for 5 minutes without agitation. The samples were then incubated with 1 mL of DAPI solution (0.3 μM in PBS) for 5 minutes at room temperature. Samples were rinsed 3 times with 1 mL of water and mounted to a glass slide using filtered mounting solution of 1:1 PBS:glycerol and clear fingernail polish as sealant.

A.3.9 Cell spreading.

mPEG-SPA-5000 (100 mg) was dissolved in an excess of propargylamine (1 mL) and stirred overnight. The reaction mixture was poured into 200 mL ether, and the precipitate, alkynyl-mPEG-5000, was collected by centrifugation. ^{1}H-NMR ($CDCl_3$, 300 MHz): 2.21 (t, J = 2.54 Hz, $\underline{H}$-≡), 2.50 (t, J = 5.60, -O-CH_2-$C\underline{H}_2$-C(O)-), 3.36 (s, $C\underline{H}_3$-O-), 3.73 (t, J = 5.60, -O-$C\underline{H}_2$-CH_2-C(O)-), 4.03 (dd, J = 2.54, 2.85, -$C\underline{H}_2$-≡) yield: 50%, conversion: quantitative. RGD-N_3 and RDG-N_3 films were sub-quantitatively photocrosslinked for 60 s using an unfiltered Oriel 100W medium pressure mercury lamp. These films were immediately reacted with alkynyl-mPEG-SPA-5000 in a Cu(I)-catalyzed azide-alkyne [3+2] cycloaddition reaction in PBS buffer at pH 7.5 (200 μM $CuSO_4$, 400 μM tris(2-carboxyethyl)phosphine hydrochloride, 200 μM tris-triazole ligand, 200 μM alkynyl-mPEG-5000)[25]. PEGylated films were rinsed for 1 h in 1 mM EDTA, overnight in 0.05 % SDS, and for 2 h in distilled water. XPS data indicate the

average addition of 1 – 2 PEG molecules per protein chain (by comparing the C/N ratio before and after reaction).

For the fibronectin positive control, 1 mL of a 10 μg/mL fibronectin solution in PBS was adsorbed overnight in a 6-well plate at 4 °C. The wells were rinsed three times, blocked with a 0.2% BSA solution for 30 minutes at room temperature, and again rinsed three times. Coverslips with PEGylated aE-N_3 were adhered to the bottom of a BSA-blocked well by applying sterilized vacuum grease around the edge of the coverslip. Cells were resuspended in endothelial basal medium-2 (EBM-2, Clonetics) and seeded in a total volume of 3 mL per well at a density of 5.0 x 10^3 cells/cm^2. For quantification of spread area, pictures were obtained on a Nikon Eclipse TE 300 microscope. Cell areas were manually traced using ImageJ v. 1.33q (National Institutes of Health, Bethesda, MD). For each substrate, at least 200 cells total were examined in at least 4 independent experiments.

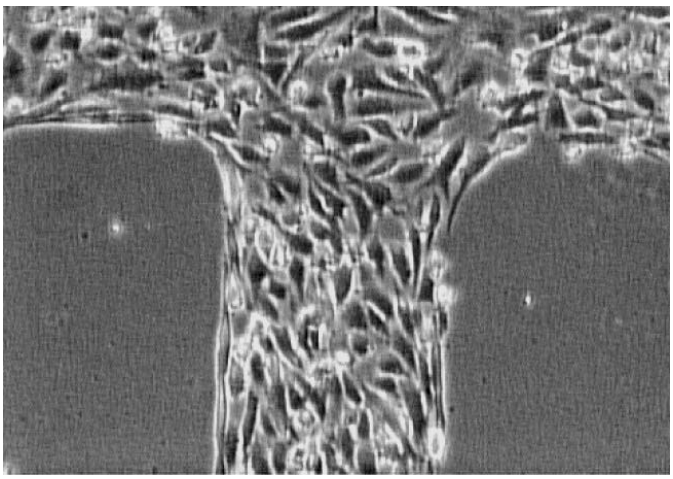

Figure A.8 Phase contrast microscopy of HUVEC attached to photo-patterned aE-N_3 (RGD variant).

Acknowledgements. We thank Michael Diehl, Alireza Ghaffari, and Nandita Sharma for helpful discussion. Supported by the NSF Center for the Science and Engineering of Materials at Caltech and by NIH HL 59987.

A.4 References

(1) Templin, M. F.; Stoll, D.; Schrenk, M.; Traub, P. C.; Vohringer, C. F.; Joos, T. O. *Trends in Biotechnology* **2002**, *20*, 160-166.

(2) Ekins, R. P. *Journal of Pharmaceutical and Biomedical Analysis* **1989**, *7*, 155-168.

(3) Tan, W.; Desai, T. A. *Biomaterials* **2004**, *25*, 1355-1364.

(4) Voldman, J. *Nat. Mater.* **2003**, *2*, 433-434.

(5) Shim, J.; Bersano-Begey, T. F.; Zhu, X. Y.; Tkaczyk, A. H.; Linderman, J. J.; Takayama, S. *Curr. Top. Med. Chem.* **2003**, *3*, 687-703.

(6) Corey, J. M.; Feldman, E. L. *Exp. Neurol.* **2003**, *184*, S89-S96.

(7) Blawas, A. S.; Reichert, W. M. *Biomaterials* **1998**, *19*, 595-609.

(8) Chin, J. W.; Santoro, S. W.; Martin, A. B.; King, D. S.; Wang, L.; Schultz, P. G. *J. Am. Chem. Soc.* **2002**, *124*, 9026-9027.

(9) Chin, J. W.; Martin, A. B.; King, D. S.; Wang, L.; Schultz, P. G. *Proc. Natl. Acad. Sci. U. S. A.* **2002**, *99*, 11020-11024.

(10) Kirshenbaum, K.; Carrico, I. S.; Tirrell, D. A. *Chembiochem* **2002**, *3*, 235-237.

(11) Di Zio, K.; Tirrell, D. A. *Macromolecules* **2003**, *36*, 1553-1558.

(12) Heilshorn, S. C.; Di Zio, K. A.; Welsh, E. R.; Tirrell, D. A. *Biomaterials* **2003**, *24*, 4245-4252.

(13) Ibba, M.; Soll, D. *Annual Review of Biochemistry* **2000**, *69*, 617-650.

(14) Welsh, E. R.; Tirrell, D. A. *Biomacromolecules* **2000**, *1*, 23-30.

(15) Pretsch, E.; Simon, W.; Seibl, J.; Clerc, T. In *Spectral Data for Structure Determination of Organic Compounds*; Fresenius, W., Huber, J. F. K., Pungor, E., Rechnitz, G. A., West, T., Eds.; Springer-Verlag: New York, **1989**, p I80.

(16) Wetlaufer, D. B. In *Advances in Protein Chemistry*; Anfinsen, C. B., Bailey, K., Anson, M. L., Edsall, J. T., Eds.; Academic Press: New York, **1962**; Vol. 17, pp 303-390.

(17) Engler, A.; Bacakova, L.; Newman, C.; Hategan, A.; Griffin, M.; Discher, D. *Biophysical Journal* **2004**, *86*, 617-628.

(18) Ingber, D. E. *Proc. Natl. Acad. Sci. U. S. A.* **2003**, *100*, 1472-1474.

(19) Zhang, S. G.; Yan, L.; Altman, M.; Lassle, M.; Nugent, H.; Frankel, F.; Lauffenburger, D. A.; Whitesides, G. M.; Rich, A. *Biomaterials* **1999**, *20*, 1213-1220.

(20) Mrksich, M.; Dike, L. E.; Tien, J.; Ingber, D. E.; Whitesides, G. M. *Experimental Cell Research* **1997**, *235*, 305-313.

(21) Cantor, E. J. Ph.D. Dissertation, University of Massachusetts, Amherst, MA, **1997**.

(22) Kast, P. *Gene* **1994**, *138*, 109-114.

(23) Sharma, N. Ph.D. Dissertation, University of Massachusetts, Amherst, MA, **2001**.

(24) Yoshikawa, E.; Fournier, M. J.; Mason, T. L.; Tirrell, D. A. *Macromolecules* **1994**, *27*, 5471-5475.

(25) Wang, Q.; Chan, T. R.; Hilgraf, R.; Fokin, V. V.; Sharpless, K. B.; Finn, M. G. *J. Am. Chem. Soc.* **2003**, *125*, 3192-3193.